CHAPTER 4
THERMAL EVALUATION

Table of Contents

4. **THERMAL EVALUATION** 4-1

4.1 Discussion 4-1

4.2 Summary of Thermal Properties of Materials 4-3

4.3 Thermal Evaluation for Normal and Off-Normal Conditions 4-9

4.3.1 Thermal Models for Normal and Off-Normal Conditions 4-9

4.3.2 Maximum Temperatures for Normal and Off-Normal Conditions 4-19

4.3.3 Minimum Temperatures for Normal and Off-Normal Conditions 4-20

4.3.4 Maximum Internal Pressures for Normal and Off-Normal Conditions 4-20

4.3.5 Maximum Thermal Stresses for Normal and Off-Normal Conditions 4-20

4.3.6 Evaluation of Thermal Performance for Normal and Off-Normal Conditions 4-20

4.4 Thermal Evaluation for Accident Conditions 4-22

4.4.1 Thermal Models for Accident Conditions 4-22

4.4.2 Maximum Temperatures for Accident Conditions 4-27

4.4.3 Maximum Internal Pressures for Accident Conditions 4-28

4.4.4 Maximum Thermal Stresses for Accident Conditions 4-28

4.4.5 Evaluation of Thermal Performance for Accident Conditions 4-28

4.5 Thermal Evaluation for Loading and Unloading Conditions 4-29

4.5.1 Vacuum Drying 4-29

4.5.2 Reflooding 4-34

4.6 Maximum Internal Pressure 4-36

4.6.1 Average Gas Temperature 4-36

4.6.2 Amount of Initial Helium Backfill 4-37

4.6.3 Free Gas within Fuel Assemblies / BPRA 4-38

4.6.4 Total Amount of Gases within DSC 4-38

4.6.5 Maximum DSC Internal Pressures 4-38

4.6.6 Maximum Pressure in Annulus 4-39

4.7 Axial Decay Heat Profile 4-40

4.8 Effective Fuel Properties 4-43

4.8.1 Discussion 4-43

4.8.2 Summary of Material Properties 4-43

4.8.3 Effective Fuel Conductivity 4-45

4.8.4 Effective Fuel Density and Specific Heat 4-46

4.8.5 Conclusion 4-47

4.9 Effective Conductivity of Fluids in the Transfer Cask 4-48

4.9.1 Effective Conductivity in the Shielding Panel 4-48

4.9.2 Effective Water Conductivity in Annulus between TC and DSC 4-50

4.10 Justification of the Assumed Hot Gap Sizes 4-52

4.10.1 Radial Gap between Basket Rails and DSC shell 4-52

4.10.2 Radial Gap between Lead and the Cask Structural Shell 4-53

4.11 Heat Transfer Coefficients 4-55
4.11.1 Total heat Transfer Coefficient to Ambient 4-55
4.11.2 Free Convection Coefficients 4-55
4.12 Effective Conductivity of Air in Closed Cavity of HSM-H 4-63
4.13 Thermal-Hydraulic Equations for the HSM-H 4-65
4.14 Thermal Evaluation of DSC Containing Damaged Fuel 4-68
4.14.1 Normal / Off-Normal Conditions 4-68
4.14.2 Accident Conditions 4-68
4.14.3 Effective Properties of Damaged Fuel 4-70
4.14.4 Evaluation of DSC Thermal Performance with Damaged Fuel 4-71
4.15 References 4-73
4.16 Appendices 4-75

LIST OF TABLES

4-1 Maximum Component Temperatures during Transfer Operations at 115°F ambient
4-2 Maximum Component Temperatures for Storage Conditions at 115°F ambient
4-3 Maximum Component Temperatures during Transfer Operations at -20°F ambient
4-4 Maximum Component Temperatures for Storage Conditions at -20°F ambient
4-5 Maximum Component Temperatures for Fire Accident Case
4-6 Maximum Component Temperatures for Blocked Vent Accident Case
4-7 Heat up Rates
4-8 Resultant Temperatures during Vacuum Drying Process
4-9 Maximum decay heat load without time limitation for Vacuum Drying
4-10 DSC Internal Pressure
4-11 Average Peaking Factors
4-12 Characteristics of Fuel Assemblies
4-13 Effective Fuel Properties
4-14 Effective Conductivity of Liquid Neutron Shielding
4-15 Verification of the Calculated Effective Conductivities for Liquid Neutron Shielding
4-16 Effective Conductivity of Liquid Neutron Shield during Burning Period
4-17 Effective Conductivity of Air within Shielding Panel during Cool Down Period
4-18 Verification of the selected k_{eff} value for Water in the Annulus
4-19 Total Heat Transfer Coefficient during Fire
4-20 Effective Conductivity of Air in the Closed HSM-H Cavity
4-21 Summary of the Energy-Hydraulic Calculation Results for 34.8 kW
4-22 Summary of the Energy-Hydraulic Calculation Results for 32.0 kW
4-23 Summary of the Energy-Hydraulic Calculation Results for 26.1 kW
4-24 Minimum Height of the Fuel Rubble
4-25 Transverse Effective Fuel Conductivity at Various Fuel Rod Pitches
4-26 Transverse Effective Conductivity of Damaged Fuel
4-27 Maximum Component Temperatures in DSC containing 16 Damaged Fuel Assemblies
4-28 Internal DSC Pressure during Transferring of Damaged Fuel

LIST OF FIGURES

4-1 Position of the DSC in the Transfer Cask
4-2 Finite element Model of Transfer Cask OS187H
4-3 FEM of Transfer Cask OS187H, Details
4-4 Top and Bottom Sub-Models of Transfer Cask OS187H
4-5 Typical Boundary Conditions on the TC Model
4-6 Finite Element Model of HSM-H
4-7 FEM of HSM-H, Concrete Structure
4-8 FEM of HSM-H, DSC and Support Rails
4-9 DSC Circumferential Convection Regions in the HSM-H Model
4-10 Typical Convection Boundary Conditions in the HSM_H Model
4-11 Typical Heat Flux and Fixed Temperature Boundary Conditions for HSM-H Model
4-12 Finite Element Model of the DSC
4-13 FEM of DSC Basket, Details
4-14 FEM of DSC Rails, Details
4-15 Thermally Bounding Loading Configurations Considered in the DSC Model
4-16 Typical Boundary Conditions in the DSC Model
4-17 Transfer Cask Temperature Distributions, 115°F Ambient
4-18 Temperature Distributions in Transfer Cask Sub-Models
4-19 DSC Temperature Distribution during Transfer Operation Basket Type I, Loading Configuration 1, 115°F Ambient
4-20 Temperature Distribution of DSC and Fuel Assemblies during Transfer Operations, 115°F Ambient
4-21 HSM-H Temperature Distribution 115°F Ambient with Fins on the Aluminum Side Heat Shields
4-22 HSM-H Temperature Distribution 115°F Ambient without Fins on the Side Heat Shields
4-23 DSC Temperature Distribution during Storage – 115°F Ambient
4-24 Temperature Distributions during Transfer Operations, Ambient -20°F
4-25 Temperature Distributions during Storage, Ambient -20°F
4-26 FEM of Transfer Cask for Fire Accident Case
4-27 Basket Model for Calculation of Effective Conductivities (HSM-H Model Blocked Vent Accident Case)
4-28 Temperature Distribution on TC Slice Model for Fire Accident Case
4-29 Time-History of TC Component Temperatures for the Fire Accident Case
4-30 Temperature Distribution for HSM-H with Finned Aluminum Side Heat - 34 hours after Blockage of the Vents
4-31 Temperature Distribution for HSM-H with Finned Aluminum Side Heat - 48 hours after Blockage of the Vents
4-32 Temperature Distribution of DSC Model for Blocked Vents Accident Case
4-33 Temperature-Time History of HSM-H Components for Blocked Vents Accident Case
4-34 Temperature Distribution at the End of Vacuum Drying Process
4-35 Time-Temperature History for Vacuum Drying Procedure A
4-36 Time-Temperature History for Vacuum Drying Procedure B
4-37 Time-Temperature History for Vacuum Drying Procedure C

4-38 Total Free Gas Volume verses Burnup Rate
4-39 Comparison of the Axial Heat Profiles in the FE Model and in Ref. [4]
4-40 Finite Element Model of Fuel Assembly WE17x17 standard
4-41 Effective Transverse Fuel Conductivity in Helium
4-42 Effective Transverse Fuel Conductivity for Vacuum Conditions
4-43 Effective Axial Fuel Conductivity
4-44 Schematic Flow Paths through HSM-H
4-45 Temperature Regions around DSC in the HSM-H Cavity
4-46 Location of the Damaged Fuel Assemblies in the Basket
4-47 Typical FE Models of Damaged (Reconfigured) Fuel WE17x17OFA
4-48 Transverse Effective Fuel Conductivity verses Pitch Size
4-49 Effective Transverse Conductivity of Damaged (Reconfigured) Fuel
4-50 Temperature Distributions in the DSC containing 16 Damaged Fuel Assemblies for Normal / Off-Normal Transfer Conditions
4-51 Temperature Distributions in the DSC containing 16 Damaged Fuel Assemblies for Accident Conditions

4. THERMAL EVALUATION

4.1 Discussion

The NUHOMS®-32PTH DSC is designed to passively reject decay heat during storage and transfer for normal, off-normal, and accident conditions while maintaining temperatures and pressures within specified limits. Objectives of the thermal analyses performed for this evaluation include:

- Determination of maximum and minimum temperatures with respect to material limits to ensure components perform their intended safety functions,
- Determination of temperature distributions to support the calculation of thermal stresses,
- Determination of maximum DSC internal pressures for normal, off-normal, and accident conditions, and
- Determination of the maximum fuel cladding temperature, and to confirm that this temperature will remain sufficiently low to prevent unacceptable degradation of the fuel during storage.

To establish the heat removal capability, several thermal design criteria are established for the System. These are:

- Maximum temperatures of the containment structural components must not adversely affect the containment function.
- To maintain the stability of the neutron shield resin in the transfer cask (TC) during normal transfer conditions, a maximum allowable average temperature of 320°F is set for the neutron shield material [1].
- A maximum fuel cladding temperature limit of 400°C (752°F) has been established for normal conditions of storage and for short-term storage operations such as transfer and vacuum drying [2]. During off-normal storage and accident conditions, the fuel cladding temperature limit is 570°C (1058°F) [2].
- A maximum temperature limit of 327°C (620°F) is considered for the lead in the transfer cask, corresponding to the melting point [3].

- The ambient temperature range for normal operation is 0 to 100°F (-18 to 38°C). The minimum and maximum off-normal ambient temperatures are -20°F (-29 °C) and 115°F (46°C) respectively. In general, all the thermal criteria are associated with maximum temperature limits and not minimum temperatures. All materials can be subjected to a minimum environment temperature of -20°F (-29 °C) without adverse effects.

- The maximum DSC internal pressure during normal and off-normal conditions must be below the design pressures of 15 psig and 20 psig respectively. For accident cases, the maximum DSC internal pressure must be lower than 70 psig during storage and lower than 120 psig during transfer operation.

The NUHOMS®-32PTH DSC is analyzed based on a maximum heat load of 34.8 kW from 32 fuel assemblies with a maximum heat load of 1.5 kW per assembly. The loading requiremenst described in Section 4.3.1.3 are used to develop the bounding load configurations.

A description of the detailed analyses performed for normal/off-normal conditions is provided in Section 4.3, and accident conditions in Section 4.4. The thermal analyses performed for the loading and unloading conditions are described in Section 4.5. DSC internal pressures are discussed in Section 4.6.

The analyses consider the effect of the decay heat flux varying axially along a fuel assembly. The axial decay heat profile for a PWR fuel assembly is based on [4]. Section 4.7 describes the calculated peaking factors and the methodology to apply the axial heat profile in the model.

Fuel assemblies are considered as homogenized materials in the fuel compartments. The effective thermal conductivity of the fuel assemblies used in the thermal analysis is based on the conservative assumption that heat transfer within the fuel region occurs only by conduction and radiation where any convection heat transfer is neglected. The lowest effective properties among the applicable fuel assemblies are selected to perform the thermal analysis. Section 4.8 presents the calculation that determines the bounding effective thermal properties of the applicable fuel assemblies.

The thermal evaluation concludes that with a design basis heat load of 34.8 kW and the loading requiremenst described in Section 4.3.1.3, all design criteria are satisfied.

4.2 Summary of Thermal Properties of Materials

The analyses use interpolated values when appropriate for intermediate temperatures where the temperature dependency of a specific parameter is deemed significant. The interpolation assumes a linear relationship between the reported values.

1. Homogenized PWR Fuel with Helium Backfill [1]

Temp	Transverse conductivity in Helium
(°F)	(Btu/hr-in-°F)
137	0.0188
231	0.0221
327	0.0258
423	0.0304
520	0.0350
617	0.0406
715	0.0468
813	0.0542
1010	0.0684

Temp	Axial Conductivity
(°F)	(Btu/hr-in-°F)
212	0.0576
392	0.0606
572	0.0644
752	0.0695
932	0.0763
1112	0.0852

Temp	$C_{p,\,eff}$
(°F)	(Btu/lbm-°F)
80	0.0593
260	0.0654
692	0.0726
1502	0.0779

ρ_{eff}
(lbm/in^3)
0.1248

2. PWR Fuel with Air Backfill at low pressures for vacuum drying conditions

Temp	Transverse Conductivity for Vacuum Conditions
(°F)	(Btu/hr-in-°F)
188	0.0079
270	0.0099
355	0.0126
444	0.0157
535	0.0197
629	0.0242
723	0.0300
819	0.0363

3. Helium [5]

Temperature		Conductivity	
(K)	(°F)	(W/m-K)	(Btu/hr-in-°F)
200	-100	0.1151	0.0055
250	-10	0.1338	0.0064
300	80	0.1500	0.0072
400	260	0.1800	0.0087
500	440	0.2110	0.0102
600	620	0.2470	0.0119
800	980	0.3070	0.0148
1000	1340	0.3630	0.0175

Density and specific heat of helium is set to zero for transient runs.

[1] See Section 4.8 for calculation of the effective fuel properties

4. Air [5]

Temperature	Conductivity	v	Prandtl No.	Dyn. Visc.
(K)	(W/m-K)	(m^3/kg)	(---)	(Pa-s)
100	0.0093	---	---	---
200	0.0180	0.573	0.740	1.33E-05
300	0.0263	0.861	0.708	1.85E-05
400	0.0336	1.148	0.694	2.30E-05
500	0.0403	1.436	0.688	2.70E-05
600	0.0466	1.723	0.690	3.06E-05
800	0.0577	2.298	0.705	3.70E-05
1000	0.0681	2.872	0.707	4.24E-05

Temperature	Conductivity	ρ	Prandtl No.	Kin. Visc.
(°F)	(Btu/hr-in-°F)	(lbm/ft^3)	(---)	(ft^2/hr)
-280	0.0004	---	---	
-100	0.0009	0.109	0.740	0.2953
80	0.0013	0.073	0.708	0.6172
260	0.0016	0.054	0.694	1.0232
440	0.0019	0.043	0.688	1.5024
620	0.0022	0.036	0.690	2.0430
980	0.0028	0.027	0.705	3.2948
1340	0.0033	0.022	0.707	4.7187

Density and specific heat of air is set to zero for transient runs. Prandtl number, kinematic viscosity, and density of air are used to calculate the convection coefficients in Section 4.11.

5. Solid Neutron Shield [1]

Temp	k	Temp	k_{min}
(°C)	(W/m-K)	(°F)	(Btu/hr-in-°F)
20	0.815	68	0.039
50	0.806	122	0.039
75	0.823	167	0.040
100	0.852	212	0.041
125	0.858	257	0.041
150	0.828	302	0.040
170	0.815	338	0.039

Specific gravity = 1.8 (0.07 lbm/in^3)

Temp	Cp	Temp	Cp
(°C)	(J/g-K)	(°F)	(Btu/lbm-°F)
40	1.07	104	0.256
50	1.07	122	0.256
60	1.09	140	0.260
70	1.14	158	0.272
80	1.18	176	0.282
90	1.22	194	0.291
100	1.26	212	0.301
110	1.33	230	0.318
120	1.37	248	0.327
130	1.43	266	0.342
140	1.5	284	0.358
150	1.55	302	0.370
160	1.59	320	0.380
170	1.62	338	0.387
180	1.65	356	0.394

6. SA-240, Type 304 Stainless Steel

Temperature (°F)	Conductivity (Btu/hr-ft-°F) [6]	Conductivity (Btu/hr-in-°F)	Diffusivity (ft^2/hr) [6]	Specific Heat (Btu/lbm-°F)[2]	Density (lbm/in^3) [3]
70	8.6	0.717	0.151	0.117	0.29
100	8.7	0.725	0.152	0.117	
150	9.0	0.750	0.154	0.120	
200	9.3	0.775	0.156	0.122	
250	9.6	0.800	0.158	0.125	
300	9.8	0.817	0.160	0.126	
350	10.1	0.842	0.162	0.128	
400	10.4	0.867	0.165	0.129	
450	10.6	0.883	0.167	0.130	
500	10.9	0.908	0.170	0.131	
550	11.1	0.925	0.172	0.132	
600	11.3	0.942	0.174	0.133	
650	11.6	0.967	0.177	0.134	
700	11.8	0.983	0.179	0.135	
750	12.0	1.000	0.181	0.136	
800	12.2	1.017	0.184	0.136	

7. Aluminum Alloy 1100

Temperature (°F)	Conductivity (Btu/hr-ft-°F) [6]	Conductivity (Btu/hr-in-°F)	Diffusivity (ft^2/hr) [6]	Specific Heat (Btu/lbm-°F)[2]	Density (lbm/in^3) [6]
70	133.1	11.092	3.67	0.214	0.098
100	131.8	10.983	3.61	0.216	
150	130.0	10.833	3.50	0.219	
200	128.5	10.708	3.42	0.222	
250	127.3	10.608	3.35	0.224	
300	126.2	10.517	3.28	0.227	
350	125.3	10.442	3.23	0.229	
400	124.5	10.375	3.17	0.232	

8. Lead

Temperature (K)	Conductivity (W/m-K) [5]	Temperature (°F)	Conductivity (Btu/hr-ft-°F)	Specific Heat (Btu/lbm-°F) [3]	Density (lbm/in^3) [3]
200	-100	36.7	1.767	0.03	0.393
250	10	36.0	1.733		
300	80	35.3	1.700		
400	260	34.0	1.637		
500	440	32.8	1.579		
600	620	31.4	1.512		

[2] Thermal diffusivity is $\alpha = \frac{k}{\rho c_p}$, this equation is used to calculate the specific heat.

9. Poison Plates

Neutron poison plates in the basket type I are borated aluminum alloy or MMC. The minimum conductivity of the borated material must be equal or larger than the 145 W/m-K at 100°C. It is assumed that the conductivity of the borated aluminum alloy/MMC remains unchanged at higher temperatures. The measured conductivities of the available borated aluminum alloys for the entire range of 20°C to 400°C are much higher than the above requirement [7 and 8].

Basket type II is designed to use Boral® absorber as neutron poison plate. The Boral® absorber possesses orthotropic thermal conductivity. To avoid any uncertainty, conductivity values of Boral® are set conservatively to zero. An equivalent conductivity is calculated for a pair of Boral® and aluminum-1100 plates in thermal analyses. For calculation of the equivalent conductivity, the paired plates are considered as parallel thermal resistances. Since the temperature gradients along the plates are much higher than the temperature gradients across the plates, this assumption is reasonable. The following equation is used to calculate the equivalent thermal conductivity of paired plates.

$$k_{eq} = \frac{k_{Al}\, t_{Al} + k_p\, t_p}{t_{total}} = \frac{k_{Al}\, t_{Al}}{t_{total}}$$

t_{total} = Total thickness of the basket plate = 0.5"
k_{Al} = Thermal conductivity of aluminum plate (Al 1100)
t_{Al} = Thickness of the aluminum plate (t_{total} - t_p-tolerance)
t_p = Thickness of the Boarl plate = 0.075"

Temp (°F)	k - Al-1100 [6] (Btu/hr-ft-°F)	k_{eq} for Basket Type II (Btu/hr-in-°F)
70	133.1	9.34
100	131.8	9.25
150	130.0	9.12
200	128.5	9.02
250	127.3	8.93
300	126.2	8.86
350	125.3	8.79
400	124.5	8.74
650	121.3[3]	8.51

Basket type II contains Boral® plates with a nominal core thickness of 0.05 in.

Total Boral® plate thickness is 0.075±0.004 in. from reference [9]

The minimum thickness of the Al-1100 plate (0.421") is considered to calculate the equivalent conductivity.

The minimum required thermal conductivities of the paired aluminum and poison plates will be verified via testing as described in Chapter 9.

To minimize the thermal resistance of the basket during fire period, the conductivity of poison plate is considered to be equal to the aluminum conductivity. Conductivity of the poison plate is set equal to the minimum value of 145 W/m-K (6.98 Btu/hr-in-°F) during the cool down period to maximize the thermal resistance. Specific heat and density of poison plate is set equal to those of aluminum for transient runs.

[3] Extrapolated from the values in [ASME]

10. Water [5]

Temp	v	μ	k	β	ν	Pr
(K)	(m^3/kg)	(N.s/m^2)	(W/m-K)	(1/K)	(m^2/s)	(---)
275	1.000E-03	1.65E-03	0.574	1.196E-04	1.652E-06	12.22
300	1.003E-03	8.55E-04	0.613	1.200E-04	8.576E-07	5.83
325	1.013E-03	5.28E-04	0.645	3.988E-04	5.349E-07	3.42
350	1.027E-03	3.65E-04	0.668	5.528E-04	3.749E-07	2.29
375	1.045E-03	2.74E-04	0.681	7.011E-04	2.863E-07	1.70
400	1.067E-03	2.17E-04	0.688	8.421E-04	2.315E-07	1.34
420	1.088E-03	1.85E-04	0.688	9.841E-04	2.013E-07	1.16
450	1.123E-03	1.52E-04	0.678	1.072E-03	1.707E-07	0.99
480	1.167E-03	1.29E-04	0.660	1.306E-03	1.505E-07	0.89
500	1.203E-03	1.18E-04	0.642	1.542E-03	1.420E-07	0.86

The expansion coefficient is defined as: $$\beta = \frac{-1}{\rho}\left(\frac{\partial \rho}{\partial T}\right)_p$$

For the thermal analyses, the expansion coefficient is calculated for each interval given in the above table as:

$$\beta = \frac{-1}{\rho}\left(\frac{\rho_2 - \rho_1}{T_2 - T_1}\right)$$

Thermal properties of water are used to calculate the effective conductivity of water in shielding panel of the transfer cask. Section 4.9 describes the methodology to calculate the effective conductivity of the fluids in the shielding panel.

11. Concrete

The thermal conductivity of normal, saturated concrete varies from 1.2 to 2.0 Btu/ft-hr-°F at temperature ranging from 50 to 150°F [10]. The conductivity of concrete decreases rapidly with the rise in temperature and assumes, at 750°C (1382°F) a conductivity value equal approximately to 50 percent of that of normal temperature [10]. For the thermal analyses a thermal conductivity of 1.15 Btu/hr-ft-°F (0.0958 Btu/hr-in-°F) is considered for concrete at 70°F. This conductivity is reduced by half to a value of 0.0479 Btu/hr-in-°F at 1382°F.

The density of concrete is considered to be 145 lbm/ft^3 (0.084 ibm/in^3). The nominal density of the concrete for the HSM-H is 150 lbm/ft^3. Practical thermal conductivity of concrete in this density range is 10.0 to 16.5 Btu/hr-ft^2-(°F/in) (0.0694 to 0.1145 Btu/hr-in-°F) [11]. This shows that the assumed concrete conductivity is within this range and therefore acceptable.

The specific heat of concrete is considered to be 0.22 Btu/lbm-°F in the thermal analyses [11].

12. Soil

The following properties are considered for soil from reference [12]:
Thermal conductivity = 0.3 W/m-K (0.0144 Btu/hr-in-°F)
Density = 1600 kg/m3 (0.0578 lbm/in^3)
Specific heat = 800 J/kg-°C (0.191 Btu/lbm-°F)

13. Emissivities and Absorptivities

Reference [13] gives an emissivity between 0.92 to 0.96 and a solar absorptivity between 0.09 to 0.23 for white paints. To account for dust and dirt and to bound the problem, the thermal analysis uses a solar absorptivity of 0.3 and an emissivity of 0.9 for white painted surfaces.

The unpainted surfaces are weathered stainless steel. The measured emissivity of stainless steel is 0.46 [14]. It is assumed that the absorptivity and the emissivity of stainless steel are equal. Solar absorptivity and emissivity of 0.46 are applied in the thermal analysis for the stainless steel surfaces exposed to ambient. The emissivity value of 0.46 is also considered for radiation exchange between the DSC shell and the transfer cask inner shell. For conservatism, an emissivity of 0.3 is considered for the fuel compartments in calculation of the transverse effective fuel conductivity in Section 4.8.

The emissivity of the TC surface is set to 0.8 as required in [22] during the fire burning time. It is assumed that the cask surface is covered with soot after the fire. The solar absorptivity of soot is 0.95 [13]. To bound the problem, the thermal analysis uses a solar absorptivity of 1.0 and an emissivity of 0.9 for TC surfaces during the cool down period.

Emissivity of concrete is reportedly 0.9 to 0.94 [12 and 13]. An emissivity of 0.90 is considered for concrete surfaces in the analyses. The absorptivity of the concrete surface is 0.73 - 0.91 at 300K [13]. For conservatism a solar absorptivity of 1.0 is considered for concrete surface.

Emissivity of anodized aluminum is reported to be 0.88 to 0.94 [13 and 15] at moderate temperatures and decreases rapidly at high temperatures. An emissivity of 0.80 is considered for anodized aluminum surfaces in the thermal analyses of the HSM-H to cover the expected temperature range. Emissivity of non-anodized aluminum surfaces is set to 0.1 [3].

References [5] and [13] report emissivities of 0.21 to 0.28 for galvanized steel in a temperature range from 68°F to 200°F. To bound the concrete temperature, an emissivity of 0.3 is considered for the galvanized steel in the HSM-H.

4.3 Thermal Evaluation for Normal and Off-Normal Conditions

4.3.1 Thermal Models for Normal and Off-Normal Conditions

The finite element models are developed using the ANSYS computer code [16]. ANSYS is a comprehensive thermal, structural, and fluid flow analysis package. It is a finite element analysis code capable of solving steady-state and transient thermal analysis problems in one, two, and three dimensions. Heat transfer via a combination of conduction, radiation, and convection can be modeled by ANSYS.

Three finite element models are used for evaluation of the normal and off-normal storage and transfer conditions:

- A transfer cask model (OS-187H) to determine temperature distributions within the cask body and neutron shielding. This model also includes the DSC shell and the helium gap between the DSC and the cask inner surface.
- A DSC model including the basket and the homogenized fuel assemblies to determine temperature distributions within the DSC and its contents.
- A HSM-H model including the DSC shell and shield plugs to determine temperature distribution in the HSM-H concrete structure, the supporting rails, and the DSC shell.

The analysis starts first with evaluating the transfer cask or the HSM-H model. The resultant temperatures of the DSC shell are then applied as boundary conditions to the exterior nodes of the DSC model. This approach allows modeling of sufficient detail within the DSC while keeping the overall size of the individual models reasonable.

Ambient temperatures between 0 and 100°F are considered as normal, long-term transfer and storage conditions. Minimum and maximum off-normal ambient temperatures are -20°F and 115°F. Should these extreme temperatures ever occur, they would be expected to last for a short period of time. Nevertheless, these ambient temperatures are conservatively assumed to occur for a significant duration to result in a steady-state temperature distribution in the NUHOMS®-32PTH system components.

Since the normal conditions are bounded by the off-normal conditions, the finite element models are evaluated only for off-normal conditions. The thermal stresses and the DSC internal pressures for the normal conditions are therefore conservatively calculated based on the resultant temperatures for the off-normal conditions.

4.3.1.1 Steady State Transfer Cask Model (OS187H)

OS187H transfer cask is designed to provide structural and radiological protection for the DSC during transfer operation while providing passive heat removal for the canisterized spent fuel. The three-dimensional finite element model of the OS187H transfer cask represents a 180° symmetric section of the TC and includes the geometry and material properties of the DSC shell and shield plugs, inner shell, gamma shell (lead), and structural shell of the transfer cask, as well as the shielding panel, cask lid, cask bottom plate, and the solid neutron shields. Properties of pure water are assumed for the liquid neutron shield contained in the shielding panel.

The neutron shield panel consists of a cylindrical shell welded to the cask structural shell and supported by 17 rings. Each of the 15 inner supporting rings has four holes to allow filling and draining of water in or out of the panel. The water in the neutron shield panel is modeled as 16 individual, cylindrical segments using SOLID70 elements. Effective conductivities are calculated for individual segments in Section 4.9 to model the combination of the conduction and convection heat transfer through the water contained in the shielding panel.

Radiation between the DSC outer shell and the cask inner shell is modeled using radiation LINK31 elements. The LINK elements connect the outermost nodes of the DSC shell to the inner most nodes of the transfer cask in the radial and axial directions. A macro[4] is written to retrieve the average surface area of the elements attached to each LINK31 element and apply it as a real constant to the corresponding LINK31 element.

Since the outer diameter of DSC is very close to the inner diameter of the cask, the radiating surfaces of the DSC and cask can be considered as parallel planes. The effective emissivity for the radiation exchange between the parallel planes is calculated as follows and applied as real constant to radiation LINK31 elements.

$$\varepsilon_{eff} = \frac{1}{\left(\frac{1}{\varepsilon_1} + \frac{1}{\varepsilon_2} - 1\right)} = 0.2987$$

A surface emissivity of 0.46 for stainless steel (see Section 4.2) is used for ε_1, ε_2 in the above equation to calculate the real constant of ε_{eff}. The value of ε_{eff} remains unchanged for all the radiation LINK elements.

Following assumptions are considered in developing the model:

a) DSC in centered axially in the transfer cask. This assumption reduces the axial heat transfer and hence maximizes the DSC shell temperature, which in turn results in higher fuel cladding temperature in the DSC model.
b) The total decay heat load (34.8 kW) is considered evenly distributed over the radial inner surface of the DSC cavity. The applied heat flux is:

$$\text{Decay heat flux} = \frac{Q}{\pi D_i L} = 3.3422 \quad \text{Btu/hr-in}^2$$

where,
Q = total decay heat load = 34.8 kW = 118,748 Btu/hr

[4] See Appendix 4.16.1 for macros

Di = inner DSC diameter = 68.75"
L = DSC cavity length = 164.5"

c) The view factor of the radiation LINK elements is set to one, which implies that each node on the DSC outer surface views only one node on the inner surface of the transfer cask. This assumption reduces the distribution effect of radiation heat transfer slightly but it simplifies the modeling efforts enormously. This assumption is justified since the gap between the transfer cask and the DSC is very small.

d) Since the transfer operation occurs in horizontal position, the lower halves of the cask cylindrical surfaces are in shade. No solar radiation is considered over these surfaces. To remove any uncertainty about the solar impact on the vertical surfaces, the entire surface area of vertical plates is considered for application of the solar heat flux.

Although assumption "a" is conservative regarding the fuel cladding temperature, it is less conservative for calculating the maximum temperatures for the seals and the solid neutron shield at the top and bottom of the TC. Therefore, two sub-models of the TC are developed, in which the DSC is touching either the cask bottom plate or the cask lid with a maximum gap of 0.01". Heat flux to the top and bottom surfaces of the DSC shield plugs in the sub-models are considered to be 5% of the maximum decay heat load distributed evenly over the corresponding surface (1.60 Btu/hr-in^2). The remaining heat load is distributed over the radial inner surface of the DSC. The sub-models calculate conservative temperatures for the seals and solid neutron shield.

The DSC shell rests on four rails in the transfer cask during the transfer operation. These rails are flat stainless steel plates welded to the inner shell of the transfer cask. The thickness of these rails is 0.12". Considering the rail configuration shown in Figure 4-1, the gap between the DSC shell and cask inner shell is calculated. The nodes of the DSC shell and the cask inner shell are coupled only at the location of the two middle rails to represent the contact area at these locations.

The following gaps are considered between components in the model at thermal equilibrium:

- 0.01" axial air gaps are considered on both sides of solid neutron shielding to simulate the contact resistance.
- 0.03" radial air gap is considered between the gamma shell (lead) and the structural shell to take account for the difference in thermal expansion behavior of stainless steel and lead. See Section 4.10 for justification.
- 0.01" axial and radial gap between the cask lid and the cask body
- 0.01" axial gap between the bottom cover plate and the ram access penetration ring

Details of the OS187H transfer cask finite element model and sub-models are shown in Figures 4-2 to 4-4.

Steady State Boundary Conditions for the Transfer Cask Model

Ambient temperature of 115°F is considered for both normal and off-normal conditions. The minimum ambient temperature of -20°F is considered to maximize the temperature gradients.

Convection and radiation to the ambient are combined together to form a total heat transfer coefficient, which is defined as a temperature dependent material property in the model. The total heat transfer coefficient is used to apply the boundary conditions on the outer surface of the cask. Section 4.11 describes the correlations to calculate the total heat transfer coefficients applied on the outer surface of the transfer cask.

Solar radiation is considered as a constant heat flux applied on the SURF152 elements overlaid on the outer surface of the transfer cask. Reference [17] reports the total values for insolance over a 12-hour solar day. These values are used to calculate the solar heat flux on the outer surface of the transfer cask. Although NUREG 1536 [22] allows averageing the insolance over a 24 hour period, it is not considered in the transfer cask thermal model for conservatism.

The outer surface of the shielding panel is painted white. The other surfaces are considered unpainted. The insolance values from [17] are considered as the maximum amount of solar radiation that is available for absorption on any surface. These values are multiplied by the absorptivity factor of each surface to calculate the amount of solar heat flux that each surface absorbs. The resultant value is applied as a constant heat flux to the corresponding surface.

Surface shape	Insolance [17] (gcal/cm^2)	Total solar heat flux average over 12 h (Btu/hr-in^2)	Absorptivity [5]	Solar heat flux in the model (Btu/hr-in^2)
Curved, Painted	400	0.853	0.3	0.256
Curved, Unpainted	400	0.853	0.46	0.392
Flat, Vertical, Painted	200	0.427	0.3	0.128
Flat, Vertical, Unpainted	200	0.427	0.46	0.196

Solar radiation is only considered for the maximum normal and off-normal conditions with ambient temperature of 115°F.

Typical boundary conditions for the transfer cask model are shown in Figure 4-5.

[5] See Section 4.2 for discussion

4.3.1.2 Steady State HSM-H Model

Horizontal Storage Module, type H (HSM-H) is designed to provide an independent, passive system with substantial structural capacity to ensure safe storage of spent fuel assemblies in NUHOMS®-32PTH canisters. The decay heat load from stored canisters is removed via radiation, free convection and conduction. Natural draft of air within the HSM-H cavity is created by the temperature difference between ambient and the DSC surface, and the height difference between the HSM-H vents. Ambient air enters the HSM-H through the inlet openings in the lower part of the HSM-H side walls and circulates around the DSC and the side heat shields. Warm air passes through the top heat shield and exits the HSM-H through the outlet openings in the upper part of the HSM-H side walls.

Decay heat is rejected from the DSC to the HSM-H air space by convection and then is removed from the HSM-H by natural air circulation. Heat is also radiated from the DSC surface to the heat shields and HSM-H walls, where again natural air circulation and conduction through the walls remove the heat. Typical flow paths are shown in Figure 4-44.

A half symmetric, three dimensional, finite element model of the HSM-H is developed using ANSYS [16]. The model represents one module among adjacent HSM-H's containing DSCs with the maximum heat load of 34.8kW. Therefore, adiabatic boundary conditions are applied over the outer surfaces of the HSM-H side walls and back wall. The HSM-H model includes the DSC shell and shield plugs, the concrete structure, and the heat shields. The DSC content is not considered for the steady state runs. The basket and its content are homogenized for the transient runs. The homogenized basket properties are discussed in Section 4.4.1.1.

Conduction through components is modeled using SOLID70 elements. Conduction through air within the HSM-H cavity is not considered for the steady state runs. Radiation between the DSC shell, heat shields, and HSM-H walls is modeled using /AUX12 methodology. SHELL57 elements were superimposed on radiating surfaces to create the Super-element MATRIX50. The SHELL57 elements were unselected prior to solving the model. The finite element model of HSM-H is shown in Figures 4-6 to 4-8.

For the design basis heat load, 34.8 kW, the side heat shields are equipped with fins on the surface facing the DSC. In this case, the fins and the surface facing the DSC are anodized. The side shields are modeled as flat plates with a thickness of 0.3125" at the position of shield base plate. Convection from the fins attached to the side shields is modeled using equivalent convection coefficient. Calculation of the effective convection coefficients is discussed in Section 4.11. Optionally, for lower DSC heat loads, side heat shields without the fins may be utilized. For this unfinned configuration, the convection coefficient for a flat, vertical plate replaces the effective convection coefficient over the fins. Flat side heat shields may be made of aluminum or galvanized steel. If aluminum is used, the surface of the side heat shield facing the DSC is anodized.

The top heat shield is a louver plate attached to the ceiling. The louvered heat shield is also modeled as a flat plate with effective convection coefficients discussed in Section 4.11.

Steady State Boundary conditions for the HSM-H Model

Ambient temperatures between 0 and 100°F are considered as normal storage conditions. The maximum day temperature of 115°F and the minimum temperature of -20°F are considered as the maximum and minimum off-normal storage condition respectively.

Because of the large thermal inertia, the temperature responses of the HSM-H and DSC to maximum day temperature are relatively slow. Therefore, considering an average maximum temperature over a 24 hour period is reasonable to calculate the maximum component temperatures during storage using steady state boundary conditions.

In order to calculate a daily average temperature given a maximum day temperature, a minimum daily range must be specified. Reference [18] shows that the minimum daily range in the contiguous United States is 27°F for a maximum summer ambient above 110°F. the hourly temperature is defined in [18] as:

$T_{hour} = T_{max}$ – (percentage of the daily range) x (min daily range)

The percentages of the daily range are shown as a function of day time in [18]. The average of the hourly temperatures over the 24 hour period gives the daily average temperature. The following table shows the calculated daily average temperature for a maximum day temperature of 115°F and a daily minimum range of 27°F.

Maximum day temperature = 115°F
Minimum daily range = 27°F

Time, hr	% daily range [16]	T_{hour} (°F)		Time, hr	% daily range 16]	T_{hour} (°F)
1	87	91.5		13	11	112.0
2	92	90.2		14	3	114.2
3	96	89.1		15	0	115.0
4	99	88.3		16	3	114.2
5	100	88.0		17	10	112.3
6	98	88.5		18	21	109.3
7	93	89.9		19	34	105.8
8	84	92.3		20	47	102.3
9	71	95.8		21	58	99.3
10	56	99.9		22	68	96.6
11	39	104.5		23	76	94.5
12	23	108.8		24	82	92.9

Daily average temperature = 100°F

A daily average temperature 105°F is used in this analysis to bound the maximum temperatures for normal and off-normal storage conditions. To maximize the temperature gradients in the HSM-H concrete structure, only the off-normal storage condition of -20°F ambient is considered for the evaluation.

The circumference of the DSC model is divided into eight regions with linearly progressive bulk temperatures. The first region covers the area between the supporting rails from an angle of -90° to -64.2°. The second region begins from the center line of the supporting beam at -60° to -45°. The surface of the DSC shell from -64.2° to -60° is located above the upper edge of the slots in the slotted plate. The free convection is therefore restricted over this area. For conservatism, this area is considered as a dead zone with no free convection. The other circumferential regions are equal in size and each covers 22.5° of the DSC shell. Figure 4-9 shows the regions of the DSC lower half. Correlation of free convection over horizontal cylinder is considered to calculate the convection coefficients for circumferential DSC regions.

Similar to the DSC circumference, the cross section of the HSM-H cavity is divided into different regions to apply the convection boundary conditions. Energy and hydraulic equations are combined to calculate the bulk air temperatures for various ambient temperatures. Section 4.13 shows the regions and describes briefly the methodology to calculate the bulk air temperatures in the HSM-H cavity.

Convection on HSM-H end walls is calculated using free convection correlations for vertical surfaces at HSM-H average bulk air temperature (T_s). Convection on the lower part of the side wall, below the side heat shield, is determined using free convection correlation for vertical surfaces at cold region temperature (T_0). For the space between the side wall and the side heat shield, free convection correlation for a narrow channel is used to determine the free convection coefficient. For the HSM-H ceiling and the HSM-H basemat, correlations for flat horizontal surfaces are used to determine free convection coefficients. Air temperatures for the convection on the basemat and ceiling are cold region temperature (T_0) and exit air temperature (T_{exit}) respectively. The calculation methods of free convection coefficients are discussed in detail in Section 4.11. Figure 4-10 shows the convection boundary conditions applied in the HSM-H model.

Insolance is applied as a constant heat flux on the roof and front wall of the HSM-H, which are exposed to the ambient. The value of the solar heat flux is taken from [17] averaged over a 24 hour period. The insolance is applied as a constant heat flux over the SURF152 elements superimposed on the SOLID70 elements on the HSM-H roof and front wall. A solar absorptivity of 1.0 is assumed for the concrete surface. The values of the applied heat fluxes are listed below:

Shape	Insolance [17] (gcal/cm^2)	Averaged over 24 hr (Btu/hr-in^2)
HSM roof	800	0.8537
HSM front wall	200	0.2134

Insolance is not considered for the minimum ambient temperature of -20°F.

Convection and radiation from the roof and the front wall are combined together as a total convection coefficient. The calculation of the total convection coefficient is discussed in Section 4.11.

The decay heat load is considered to be distributed evenly on the radial inner surface of the DSC for the steady state runs in this analysis. The applied decay heat flux is:

$$Decay\ heat\ flux = \frac{Q}{\pi D_i L} = 3.3422 \quad \text{Btu/hr-in}^2$$

where,

Q = total decay heat load = 34.8 kW = 118748 Btu/hr
Di = inner DSC diameter = 68.75"
L = DSC cavity length = 164.5"

In the event that the side heat shields are not equipped with fins, applying the maximum decay heat load of 34.8 kW increases the maximum component temperatures within the HSM-H. In order to limit the maximum concrete temperature below the values considered for the structural analyses in Chapter 3, the maximum decay heat load is decreased for the HSM-H modules without fins on the side heat shields. The maximum decay heat load for the HSM-H modules with unfinned aluminum side heat shields is 32.0 kW, which gives a uniform heat flux of 3.0733 Btu/hr-in^2.

$$Decay\ heat\ flux = \frac{Q_1}{\pi D_i L} = 3.0733 \quad \text{Btu/hr-in}^2 \quad \text{for HSM-H with unfinned aluminum side heat shields}$$

Q_1 = 32.0 kW = 109193.6 Btu/hr

For the HSM-H modules with galvanized side heat shields, the maximum decay heat load is limited to 26.1 kW.

$$Decay\ heat\ flux = \frac{Q_2}{\pi D_i L} = 2.5067 \quad \text{Btu/hr-in}^2 \quad \text{for HSM-H with galvanized steel side heat shields}$$

Q_2 = 26.1 kW = 89061.0 Btu/hr

It is assumed that soil has a temperature of 70°F at 10' below the HSM-H basemat for hot conditions. The soil temperature for cold condition (-20°F) is assumed to be 45°F. These assumptions are consistent with the assumptions in the thermal analysis of the standardized HSM design [19]. The HSM-H basemat is considered to be a 4' thick concrete slab. Due to low conductivity of concrete and soil, the model is insensitive to the thickness of the basemat / soil and the soil temperature. The heat flux and fixed temperature boundary conditions applied in the model are shown in Figure 4-11.

4.3.1.3 Steady State 32PTH DSC Model

The 32PTH DSC is a high integrity stainless steel welded pressure vessel that provides confinement of radioactive material, encapsulates the fuel in a helium atmosphere, and when placed in the transfer cask, provides radiological shielding.

A three dimensional finite element model of the 32PTH DSC is developed using ANSYS [16] to determine the maximum fuel cladding temperature. The DSC model includes the DSC shell, shield plugs, basket rails, basket, and fuel assemblies. The fuel assemblies are modeled as homogenized regions within the fuel compartments. The effective thermal properties for the homogenized fuel are calculated in Section 4.8.

The following conservative assumptions are considered in developing the finite element model to maximize the fuel cladding temperature:

- No convection occurs within the DSC cavity,
- The basket containing the fuel assemblies is centered axially in the DSC cavity,
- Heat transfer across the contact gaps within the basket occurs only by gasous conduction.

The following gaps are considered between components in the model at thermal equilibrium:

- 0.010" gap between each two adjacent basket plates except for the following cases:
  - between the aluminum inserts and the stainless steel rails – this gap is considered to be at least 0.020"
  - between the aluminum and the poison plates, when applicable. The aluminum plate and the poison plate are sandwiched between fuel compartments. For ease of modeling the 0.010" gaps are placed on both sides of the paired plates. No gap is considered between the paired aluminum and poison plates.
- 0.010" gap between the basket plates and aluminum rails
- 0.100" radial gap between rails and inner shell (see Section 4.11 for justification)

The axial cold gap of 0.07" between the stainless steel support plates and the aluminum plates is divided into a 0.01" axial gap at the bottom and a 0.060" axial gap at the top of the stainless steel plate. All dimensions of the canister are at nominal values. Details of the finite element model are shown in Figures 4-12 to 4-14.

Five basket types in two categories are designed for NUHOMS-32PTH DSC. Relevant characteristics of these basket types are listed below.

Basket type	I	II
A	Boron Aluminum, or Metal Matrix Composites (MMC) Maximum thickness 0.187"	Boral® Maximum thickness 0.075"
B		
C		
D		Not applicable
E		Not applicable

Aluminum plates are to be paired with the poison plates to make a nominal thickness of 0.5". The conductivity of the borated aluminum/MMC plate depends on the boron content and the fabrication procedure. To bound the maximum component temperature, the maximum thickness of the boron containing plate (0.1875") is considered in the model for basket type I.

Paired Boral®/ aluminum plates are used in basket type II. An effective conductivity is calculated for the paired Boral® / aluminum plates, as discussed in Section 4.2. Other combination of aluminum and poison plates that satisfies the conductivity requirements in Chapter 9 can be used in the basket.

Heat transfer from the fuel regions occurs only by conduction through the basket plates and the rails. Conduction and radiation heat transfer are considered between the rails and the DSC shell. Conduction through components is modeled using SOLID70 elements.

Radiation between the rails and the DSC shell is modeled using radiation LINK31 elements using the same methodology as described in Section 4.3.1.1. Axial radiation is also considered between the top and bottom surfaces of the fuel assemblies to the shield plugs. The emissivity of the heavily oxidized top and bottom surfaces of the fuel assemblies are considered to be 0.9.

Steady State Boundary conditions for the DSC Model

The nodal temperatures of the DSC shell are retrieved from the transfer cask or HSM-H models described in Sections 4.3.1.1 and 4.3.1.2, and applied to the corresponding nodes in the DSC model via a macro described in Appendix 4.16.1.

The SOLID70 elements representing the homogenized fuel are given heat generating boundary conditions in the region of the active fuel length. Active fuel length is considered to be 144" [20] beginning at approximately 4.0" above the bottom of the fuel assembly [20]. Fuel assembly has a total length of 162" in the model. Peaking factors to apply the axial decay heat profile for the homogenized fuel region are calculated in Section 4.7.

The maximum heat load per canister is 34.8 kW. The maximum decay heat per assembly is 1.5 kW. Heat load zoning, as illustrated below, is used to maximize the number of higher heat load assemblies per DSC. The loading requirements are as follows.

- Q_{zi} is the maximum decay heat per assembly in zone i
- Total Decay Heat ≤ 34.8 kW
- 4 fuel assemblies in zone 1 with
  - total decay heat ≤ 3.2 kW
  - $Q_{z1a} \leq 1.05$ kW in the lower compartments
  - $Q_{z1b} \leq 0.8$ kW in the upper compartments
- 20 fuel assemblies in zone 2 with $Q_{z2} \leq 1.1$ kW
- 8 fuel assemblies in zone 3 with $Q_{z3} \leq 1.5$ kW
- $Q_{z1} \leq Q_{z2} \leq Q_{z3}$

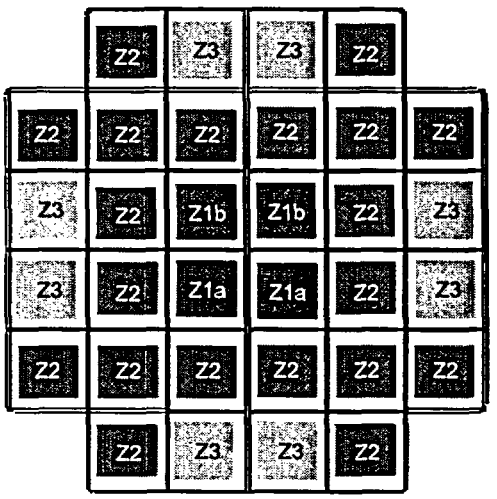

Heat generation rates as a function of spent fuel parameters are calculated in Appendix 4.16.2. Five extreme loading configurations are considered to bound the maximum component temperatures. The loading configurations are shown in Figure 4-15. In the first configuration, the heat load in the core compartments is maximized, so that zone 1 has a uniform heat load of 0.8 kW per assembly and zone 2 has a heat load of 1.1 kW per assembly. Since the total heat load is limited to 34.8 kW, the heat load of zone 3 is 1.2 kW per assembly.

The heat load in the peripheral compartments is maximized in loading configuration 2, so that zone 3 has a heat load of 1.5 kW per assembly and zone 2 has a heat load of 1.1 kW per assembly. Since the total heat load is limited to 34.8 kW, the heat load of zone 1 is 0.2 kW per assembly. A heat load of 0.2 kW per assembly for a fuel assembly in zone 1 is rather unrealistic.

To have a more realistic estimation of maximum component temperatures loading configuration 3 is considered, in which zone 1 has a heat load of 0.55 kW per assembly and zone 3 has a heat load of 1.5 kW per assembly. Zone 2 is divided into two subdivisions. The first subdivision includes the fuel assemblies around the central assemblies with a heat load of 0.925 kW per assembly and the second subdivision located at the periphery has a heat load of 1.1 kW per assembly.

In loading configuration 4, the heal load in zone 1 and zone 3 are maximized, so that the central and peripheral compartments have maximum heat load. The heat load is 1.5 kW per assembly in zone 3 and 0.8 kW per assembly in zone 1. The remaining heat load is divided uniformly over assemblies in zone 2, which gives a heat load of 0.98 kW per assembly.

To investigate the effect of non-uniform loading in zone 1, loading configuration 5 is considered, in which the two lower compartments in zone 1 have a heat load of 1.05 kW per assembly. It gives a heat load of 0.55 kW per assembly for the two upper compartments in zone 1 based on the loading restrictions.

The five loading configurations discussed above are considered only for the maximum ambient temperature of 115°F during transfer operation. For the other conditions loading configuration 1 is evaluated, which gives the maximum DSC component temperatures for high enriched fuel assemblies in basket type I.

Heat generating rate for each segment of the active fuel region is calculated as follows:

$$\dot{q}''' = \frac{\left(\frac{Q}{a^2 L_a} \times PF\right)}{0.984}$$

where

Q = Heat load per assembly defined for each loading zone
a = Width of the modeled fuel assembly = 8.7"
L_a =Active fuel length = 144"
PF = Peaking Factor from Section 4.7

The area beneath the peaking factor curve shown in Section 4.7 is 0.984. The heat generating value is divided by this factor to avoid any reduction of the total heat load in the model. The total heat load applied in the model is verified by retrieving the reaction solution from the solved model and comparing it to the 34.8 kW maximum heat load value. Typical applied boundary conditions are shown in Figure 4-16.

4.3.2 Maximum Temperatures for Normal and Off-Normal Conditions

Steady state thermal analyses are performed using the maximum decay heat load of 34.8 kW per canister, 115°F ambient temperature, and the maximum insolation per reference [17]. Insolation is averaged over a 12 hour period for transfer conditions and over a 24 hour period for storage conditions.

The temperature distributions within the TC, the HSM-H, and the DSC models are shown in Figures 4-17 to 4-23. Summaries of the maximum component temperatures are listed in Tables 4-1 and 4-2.

The maximum temperatures calculated for off-normal conditions bound the values for the normal conditions. Therefore, thermal stress and DSC internal pressures for both normal and off-normal conditions are calculated based on the temperatures resulted from the maximum off-normal conditions (115°F ambient) for conservatism.

4.3.3 Minimum Temperatures for Normal and Off-Normal Conditions

Temperature distributions under the minimum ambient temperatures of –20°F with no insolation and the maximum design heat load are determined under steady state conditions to maximize the temperature gradients in the TC, the HSM-H and the DSC. Figures 4-24 and 4-25 show the temperature distributions for transfer operations and storage conditions at -20°F respectively. Tables 4-3 and 4-4 summarize the results of these analyses.

The resultant DSC and transfer cask temperatures for the -20°F ambient during transfer and storage are used to calculate the thermal stresses for the normal conditions at 0°F ambient.

4.3.4 Maximum Internal Pressures for Normal and Off-Normal Conditions

Maximum internal pressure within the NUHOMS®-32PTH DSC is calculated in section 4.6.

4.3.5 Maximum Thermal Stresses for Normal and Off-Normal Conditions

Maximum thermal stresses during normal and off-normal conditions of storage and transfer are calculated in Chapter 3.

4.3.6 Evaluation of Thermal Performance for Normal and Off-Normal Conditions

The thermal analysis for normal and off-normal conditions of transfer and storage concludes that the NUHOMS®-32PTH System design meets all applicable requirements.

The maximum component temperatures calculated using conservative assumptions are lower than the allowable limits. The maximum TC seal temperature (255°F / 124°C) during off-normal transfer conditions is well below the 400°F long-term limit specified for continued seal function. The maximum solid neutron shield temperature (265°F / 129°C) is below allowable limit of 320°F (160°C) and no degradation of the solid neutron shielding material is expected. The maximum pressure within the neutron shielding panel (38.5 psia / 23.8 psig) corresponding to the average temperature of the liquid neutron shield (265°F / 129°C) is below the set point of the pressure relief valve (54.7 psia / 40 psig).

If the side heat shield is equipped with fins, the maximum local temperature of the HSM-H concrete structure is lower than 200°F as required in [21]. If the side heat shields are not equipped with fins, the maximum local temperature of concrete is slightly above 200°F but does not exceed 225°F. The concrete structure of the HSM-H is made using Type II cement with fine aggregates satisfying ASTM C33 or equivalents as defined in NUREG-1536 [22], when the side heat shields are not equipped with the fins.

The calculated maximum fuel cladding temperature is lower than the temperature limit of 752°F (400°C) considered for normal conditions of storage and short-term operations in [2]. The comparison of the resultant maximum temperatures with the allowable limits is listed below:

Component	Transfer Conditions [6]	Allowable / Design Limit
Cask Lid Seal	205°F	400°F
Cask Bottom Plate Seal	190°F	400°F
Lead	337°F	621°F
Liquid Neutron Shield (Temp / Press)	265°F / 23.8 psig	45 psig
Solid Neutron Shield	213°F	320°F
Fuel Cladding	723°F	752°F

Component	Storage Conditions [6]	Allowable / Design Limit
Concrete in module with finned aluminum side heat shields @ 34.8 kW	190°F	200°F
Concrete in module with unfinned aluminum side heat shields @ 32.0 kW	202°F	225°F
Concrete in module with unfinned galvanized steel side heat shields @ 26.1 kW	201°F	225°F
Fuel Cladding @ 34.8 kW	684°F	752°F for normal conditions / 1058°F for off-normal conditions

The maximum DSC internal pressures for normal and off-normal storage conditions are 5.9 and 10.7 psig respectively. The maximum DSC internal pressure for normal transfer conditions is 6.4 psig and for off-normal transfer conditions is 11.2 psig. The DSC internal pressures are lower than the design pressure limits of 15 psig for normal and 20 psig for off-normal storage and transfer conditions.

[6] The TC and HSM-H models are run only with off-normal conditions at 115°F ambient. The resultant temperatures are used to evaluate the thermal performance for both normal and off-normal conditions. The fuel cladding temperature remains in all cases below the normal allowable limit of 752°F.

4.4 Thermal Evaluation for Accident Conditions

Three hypothetical accident cases during transfer operation are relevant for thermal evaluation:

- Loss of the TC liquid neutron shield due to damages on the shielding panel
- Loss of helium gas in annulus between the DSC and the TC
- Postulated fire engulfing the TC

It is considered in all the above cases that the transfer cask contains a fully loaded DSC. The fire accident is postulated in which maximum amount of 300 gallons of diesel fuel is spilled onto the ground in such a way as to completely engulf the transfer cask. Subsequent to the fire accident, it is assumed that the seals for the TC lid and the bottom cover plate will burn, and the liquid neutron shield will be released and evaporates completely. Therefore, the fire accident scenario bounds the loss of liquid neutron shield and the loss of helium gas in the accident cases. The fire accident case is analyzed to give the bounding fuel cladding temperature for the transfer accident cases.

Since the HSM-H is located outdoors, there is a remote probability that the air inlet and outlet openings will become blocked by snow or by debris from events such as flooding, high wind, and tornados. The perimeter security fence around ISFSI and the location of the air inlet and outlet openings reduces the probability of such an event. Nevertheless, it is conservatively considered in this analysis that all the inlet and outlet openings become blocked.

The thermal mass of the HSM-H, the construction of the vent openings, and the location of the fuel on the transfer vehicle limit the effect of a fire accident for the HSM-H. Therefore, the worst case fire accident is bounded by the fire accident case during transfer operation.

A new model is developed to evaluate the fire accident case during transfer operation. The HSM-H model described in Section 4.3 is slightly modified to evaluate the blocked vent accident case during storage. The DSC model is unchanged for this evaluation. Details of the models are discussed in section 4.4.1.

4.4.1 Thermal Models for Accident Conditions

4.4.1.1 Transient Transfer Cask Model

To determine the temperature distribution in the transfer cask and the DSC for fire accident case, a three dimensional model is developed using ANSYS [16]. This model is created by selecting the nodes and elements of the DSC model described in Section 4.3 at z-axis from 56.06" to 86.07". The shells of TC including the annulus are then modeled around the DSC using SOLID70 elements. LINK31 elements are created using the same methodology as described in Section 4.3.1.1 to simulate the radiation between the DSC shell and the TC inner shell. The three dimensional model represents a slice of the DSC within the transfer cask. The TC slice model is shown in Figure 4-26. Axial length of the slice model is 30".

It is assumed that the helium gas in the annulus will remain in place during the burning period to maximize the heat input from fire into the transfer cask. For the same reason, all the air gaps in the transfer cask were removed during the burning period. To eliminate the uncertainties about the maximum poison plate conductivity, the conductivity of poison plate is set equal to that of aluminum 1100 during the fire.

The effective conductivity of liquid neutron shield (water) is calculated using the methodology discussed in Section 4.9. The liquid neutron shield (water) will be released at high temperatures (~ 417°F) when its saturation pressure exceeds the set point of the pressure relief value (40 psig). The average temperature of liquid neutron shield drops to 212°F (boiling point of water) when the pressure relief valve opens. After this point, the energy of fire will be consumed to evaporate the liquid neutron shield and the temperatures remain constant until the liquid shield is evaporated completely. Nevertheless, an effective conductivity of 2.25 Btu/hr-in-°F is considered for the liquid neutron shield to bound the problem and to maximize the heat input from the fire into the transfer cask. The selected value (2.25 Btu/hr-in-°F) is higher than the effective conductivity values calculated for the liquid neutron shield during fire in Section 4.9.

During the cool down period all the air gaps are replaced. Subsequent to the fire, it is assumed that the TC seals are burned and air has replaced water in the shielding panel. The properties of air are therefore given to the elements in the shielding panel and to the elements in the annulus between the DSC and the transfer cask during the cool down period. Convection and radiation through the air in the shielding panel are combined together in form of an effective conductivity. Section 4.9 describes the calculation of the effective conductivity for the air within the shielding panel. Convection is not considered for the air in the annulus. As mentioned in Section 4.3.1.1, radiation in annulus is modeled using LINK31 elements.

Boundary Conditions for the Fire Accident Case

Initial temperatures for the transfer cask slice model are transferred from the steady-state models at 115°F ambient conditions.

Fire is assumed to have an average flame temperature of 1475°F and an emissivity of 0.9. The cask surface emissivity is set to 0.8 during the fire. These assumptions are in compliance with 10CFR71.73 [17].

It is assumed that the diesel fuel creates a pool diameter of about 200 inches, which is the approximate length of the transfer cask. Considering a volume of 300 gallons and a minimum burning rate of 0.15 in/min [23] give a burning time of 14.5 minutes for diesel fuel. A burning time of 15 minutes is considered conservatively for analytical purposes.

A forced convection value of 4.5 Btu/hr-ft^2-F is considered during the burning time as concluded in [23]. The calculation of the heat transfer coefficients on the transfer cask during fire accident are described in Section 4.11.1.

Heat generation corresponding to loading configuration 1 is considered for the solid elements representing the homogenized fuel during the burning time and the cool down period.

A peaking factor of 1.1 is considered for this evaluation. Adiabatic boundary conditions are applied over the vertical end surfaces of the slice model. This model is conservative regarding the fuel cladding temperature since the axial heat transfer is restricted and the maximum peaking factor is applied to the heat generating rate.

4.4.1.2 Transient HSM-H Model

A slightly modified HSM-H model discussed in Section 4.3.1 is used to determine the temperature distribution in the HSM-H and the 32PTH DSC shell for the blocked vent accident case. The basket and its content including the fuel assemblies are homogenized for the transient run required for the blocked vent analysis. The effective thermal properties of the homogenized DSC content are calculated as follows.

Effective Properties of the Homogenized Basket

Volume and weight of the basket components are calculated in chapter 3. The relevant values are listed below for calculation of the effective basket properties.

	Volume	Weight	C_p	C_p x M
Component	in^3	lbm	Btu/lbm-°F	Btu/°F
Fuel Assemblies	148488	50720	0.068	3449
Basket, Stainless Steel	75928	22019	0.116	2554
Basket, Aluminum	79952	7835	0.218	1708
Total	304368	80574	---	7711

The equations for calculating the average basket density and heat capacity are:

$$\bar{\rho} = \frac{basket\ weight + fuel\ assemblies\ weight}{total\ cavity\ volume}$$

$$\bar{C}_p = \frac{weight\ of\ SS \times C_{p,ss} + weight\ of\ Al \times C_{p,ss} + weight\ of\ fuel \times C_{p,fuel}}{basket\ weight + fuel\ assemblies\ weight}$$

total cavity volume = $\pi/4 \times D_i^2 \times L$
D_i = DSC inner diameter = 68.75"
L = cavity length = 164.5"
$C_{p,ss}$ = 0.114 Btu/lbm-°F @ 100°F [6]
$C_{p,Al}$ = 0.216 Btu/lbm-°F @ 100°F [6]
$C_{p,fuel}$ = 0.068 Btu/lbm-°F @ 400°F [Section 4.8]

Specific heat capacities of stainless steel and aluminum increase at higher temperatures as shown in Section 4.2. Initial basket temperature for blocked vent case is higher than 100°F. Selecting lower heat capacity values for stainless steel and aluminum at 100°F is conservative since it reduces the amount of stored heat in the basket and results in a higher fuel cladding temperature.

The heat capacity of the fuel assembly is selected at 400°F, which is lower than the average off-normal temperature of the fuel assemblies in the 32PTH DSC model. Similar to stainless steel and aluminum, selecting lower heat capacity values for fuel assemblies is conservative.

The resultant effective density and specific heat capacity of the basket are:

$\bar{\rho} = 0.132$ lbm/in^3

$\bar{C}_p = 0.095$ Btu/lbm-°F

To calculate the axial and the transverse effective conductivities of the basket a 15" long slice of the basket is created by selecting the nodes and elements of the 32PTH DSC shell and basket from the finite element model described in section 4.3.1.3. DSC shell elements are unselected prior to run the slice model. The basket slice model is shown in Figure 4-27.

To calculate the axial effective conductivity of the basket, constant temperature boundary conditions are applied at the top and bottom of the slice model. No heat generation is considered for the fuel elements in this case. The axial effective conductivity is calculated using the following equation:

$$k_{eff,axl} = \frac{Q \times L}{A \times \Delta T}$$

where,

Q = Amount of heat leaving the upper face of the slice model – reaction solution of the uppermost nodes (Btu/hr)

L = Length of the model = 15"

A = Surface area of the upper (or bottom) face of the model = $\pi/2 \times r_i^2 = 1856$ in^2

r_i = Inner radius of the DSC shell = 34.375"

$\Delta T = (T_1 - T_2)$ =Temperature difference between upper and lower faces of the model (°F)

T_1 = Constant temperature applied on the lower face of the model (°F)

T_2 = Constant temperature applied on the upper face of the model (°F)

In determining the temperature dependent axial effective conductivities an average temperature, equal to $(T_1 + T_2)/2$, is used for the basket temperature. The resulting axial effective conductivities of the basket are listed below.

T_1 (°F)	T_2 (°F)	T_{avg} (°F)	$Q_{reaction}$ (Btu/hr)	$k_{eff,axl}$ (Btu/hr-in-°F)
300	400	350	12380	1.0005
400	500	450	12533	1.0128
500	600	550	12734	1.0291
600	700	650	12928	1.0448
700	800	750	13096	1.0583
800	900	850	13280	1.0732
900	1000	950	13449	1.0869
1000	1100	1050	13627	1.1013
1100	1200	1150	13762	1.1122

To calculate the transverse effective conductivity of the basket, constant temperature boundary conditions are applied on the outermost nodes of the slice model and heat generating conditions

are applied on the fuel elements. The heat generation rates are calculated based on the loading configuration 1 shown in Figure 4-15 with a peaking factor of 1.1.

The following equation from [15] determines the maximum temperature for long solid cylinders with uniformly distributed heat sources.

$$T = T_o + \frac{\dot{q}\, r_o^{\,2}}{4k}\left[1 - \left(\frac{r}{r_o}\right)^2\right]$$

with T_o = Temperature at the outer surface of the cylinder (°F)
T = Maximum temperature of cylinder (°F)
$\dot{q}$ = Heat generation rate (Btu/hr-in^3)
r_o = Outer radius =34.375"
r = Inner radius = 0 for slice model
k = Conductivity (Btu/hr-in-°F)

The above equation is rearranged to calculate the transverse effective conductivity of the basket.

$$\dot{q} = \frac{Q}{V} = \frac{Q}{\frac{\pi r_o^{\,2}}{2} L} \quad \rightarrow \quad k_{eff,rad} = \frac{2Q}{4\pi L \Delta T}$$

with Q = Amount of heat leaving the periphery of the slice model – reaction solution of the outermost nodes (Btu/hr)
L = length of the model = 15"
$\Delta T = (T - T_o)$ = Difference between maximum and the outer surface temperatures in (°F)

Since the surface area of the fuel assemblies at the basket cross section is much larger than the other components, assuming a uniform heat generation is a reasonable approximation to calculate the radial, effective conductivity. In determining the temperature dependent transverse effective conductivities an average temperature, equal to $(T_{max} + T_o)/2$, is used for the basket temperature. The resulting transverse effective conductivities of the basket are listed below.

T_o (°F)	T_{max} (°F)	T_{avg} (°F)	$Q_{reaction}$ (Btu/hr)	$k_{eff,rad}$ (Btu/hr-in-°F)
100	491	296	6914	0.1876
200	568	384	6914	0.1993
300	647	474	6914	0.2114
400	728	564	6914	0.2237
500	810	655	6914	0.2366
600	894	747	6914	0.2495
700	980	840	6914	0.2620
800	1068	934	6914	0.2737
900	1160	1030	6914	0.2821
1000	1254	1127	6914	0.2888

Boundary Conditions for the Blocked Vent Case

The initial temperatures for the HSM-H model are calculated using the same convection and radiation boundary conditions as described in Section 4.3.1.2 for the maximum ambient temperature of 115°F (105°F daily average temperature).

The insolence on the HSM-H surfaces exposed to the ambient and the soil temperature are applied also in the same way as described in Section 4.3.1.2. Uniform heat generating boundary conditions are applied over the elements representing the homogenized basket. The heat generating rate for the basket elements is calculated as follows.

$$Heat\ generating\ rate = \frac{Q}{\left(\frac{\pi}{4} D_i^2 L\right)} = 0.1945 \quad \text{Btu/hr-in}^3$$

where,

Q = total decay heat load = 34.8 kW = 118748 Btu/hr
Di = inner DSC diameter = 68.75"
L = DSC cavity length = 164.5"

Elements representing air in the HSM-H cavity are given the air conductivity to ease the transient run. During the blockage of the vents, all convection boundary conditions within the HSM-H cavity are removed and natural convection in closed cavity is considered for the air trapped within the HSM-H cavity. The natural convection in closed cavity is applied as an effective conductivity to the air elements within the HSM-H cavity. The calculation of the effective conductivity is discussed in Section 4.12.

The DSC shell temperatures are retrieved from the transient HSM-H model and applied as steady-state boundary conditions to the 32PTH DSC model. This methodology over-predicts the fuel cladding temperature since the fuel assemblies heat up faster than the DSC shell. The heat generating rates and peaking factors for the homogenized fuel regions in the DSC model are calculated in the same way as described in 4.3.1.3. The maximum decay heat load of 34.8 kW and loading configuration 1 (Figure 4-15) are considered for this evaluation. The DSC temperatures for 34.8 kW decay heat load bound the temperatures for lower decay heat loads of 32.0 and 26.1 kW cases.

4.4.2 Maximum Temperatures for Accident Conditions

The maximum component temperatures resulted from the transient run of the transfer cask model are listed in Table 4-5. Figure 4-28 shows the temperature distributions for the transfer cask fire accident. The temperature-time histories of major components in the transfer cask OS187H during fire accident are shown in Figure 4-29.

The transient model of the HSM-H simulates 48 hours of the blocked vents accident case. 34 hours after complete blockage of the inlet and outlet vents, the temperature of the sidewall rises to 347°F for the HSM-H equipped with finned aluminum side heat shields. Since lower heat loads are specified for the HSM-H with unfinned side heat shields (aluminum or galvanized steel), it takes longer than 34 hours of vent blockage until the maximum concrete temperature of these modules reaches the allowable temperature of 350°F. Typical temperature distributions for the HSM-H model during blockage of the vents are shown in Figures 4-30 and 4-31.

The DSC shell temperatures at the specific times, such as 48 hours after blockage of the vents are retrieved from the transient model and applied as steady-state boundary conditions to the DSC model. The typical resultant temperature distributions are shown in Figure 4-32.

The maximum component temperatures for the blocked vent cases are listed in Table 4-6. Figure 4-33 shows the temperature-time history of major components in the HSM-H during blockage of the vents.

4.4.3 Maximum Internal Pressures for Accident Conditions

Maximum internal pressure within the NUHOMS®-32PTH DSC is calculated in section 4.6.

4.4.4 Maximum Thermal Stresses for Accident Conditions

Maximum thermal stresses during accident conditions of storage and transfer are calculated in Chapter 3.

4.4.5 Evaluation of Thermal Performance for Accident Conditions

The thermal analysis for the accident conditions during storage or transfer operation concludes that the NUHOMS®-32PTH System design meets all applicable requirements.

The conservative model of the transfer cask for the fire accident case shows that the maximum fuel cladding temperature does not exceed 1036°F. This maximum temperature is lower than the allowable limit of 1058°F.

The maximum fuel cladding temperature after blockage of the vents for 48 hours is 796°F in the HSM-H with finned aluminum side heat shields at the design basis heat load of 34.8 kW. This temperature is well below the maximum allowable limit of 1058°F set for fuel cladding in accident conditions.

For the design basis heat load, 34.8 kW, the maximum local temperature of the HSM-H concrete structure is lower than 350°F after 34 hours blockage of the vents, when aluminum side heat shields are equipped with fins. This time limit is adequate for a combination of inspection and reaction times to remove any vent blockage. In the event that longer inspection/reaction time is requested, the strength of the concrete structure shall be verified at the maximum predictable temperature based on the corresponding concrete curve from Figure 4-33 and the guidelines established in NUREG 1536 [22].

The maximum DSC internal pressure 48 hours after blockage of the HSM-H vents is 13.7 psig, which is lower than the design pressure of 70 psig. The maximum DSC internal pressure for fire accident case during transfer operation is 91.0 psig, which is well below 120 psig design pressure considered for the transfer accident cases.

4.5 Thermal Evaluation for Loading and Unloading Conditions

Fuel loading and unloading operations occur in the fuel handling building. During loading operation fuel assemblies are submerged in pool water permitting heat dissipation. After fuel loading is complete, the TC and 32PTH DSC are removed from the pool and the DSC is drained, dried, backfilled with helium and sealed. The TC will be sealed and backfilled with helium after sealing the DSC.

4.5.1 Vacuum Drying

The loading condition evaluated is the heatup of the DSC before transfer to the storage site. The 32PTH DSC heatup occurs during draining, vacuum drying, backfilling, and sealing of the DSC, when the DSC is contained in the TC in the vertical position inside the fuel handling building. At the design basis heat load, the water in the annulus between the DSC and the transfer cask could boil between the time the canister is drained, and the time it is backfilled with helium. There are two methods that may be utilized to prevent this; one is to monitor the temperature of the annulus water and if required, circulate or introduce fresh water to maintain the temperature below 180°F, the other is to simply drain the annulus water when it exceeds this temperature limit. In any of these methods, the DSC may be backfilled with helium after complete drainage of the water.

It is assumed in this evaluation that the complete drainage of water from the 32PTH DSC cavity may occur either before or after welding the DSC top shield plug. Partial drainage of water from the DSC cavity and from the annulus between the DSC and the transfer cask is required to perform the welding.

Fuel cladding temperature must be maintained below 752°F as required in [2]. The following procedures are considered for limitation of fuel temperature between the time of complete drain and helium backfill of the 32PTH DSC.

A. Annulus water temperature remains below 180°F by water flow or circulation in the annulus between the DSC and the TC, as required, for the entire vacuum drying process. A time limit is calculated for this procedure which includes all the activities after complete DSC drainage until DSC backfilling starts.

B. Water neither flows nor circulates in the annulus between the DSC and the TC. The water in the annulus will be drained as soon as its temperature exceeds 180°F. Two time limits are calculated for this procedure. Similar to procedure A, the first time limit starts after complete DSC drainage. The second time limit includes the activities after drainage of the annulus water to the point that DSC backfilling starts

C. This procedure is the same as procedure B except that the DSC will be backfilled with helium after drainage of the DSC water. To consider the worst case, it is assumed that backfilling of the DSC starts not immediately after drainage of the DSC water, but occurs after drainage of the annulus water. The two time limits described above for procedure B are also calculated for procedure C.

If one chooses to follow procedure A and backfill the DSC with helium after drainage of water, there is no time limit for completion of the vacuum drying process. The reason is the DSC shell temperature is maintained at temperatures lower than the values calculated for the storage conditions. With helium in the DSC cavity, the fuel cladding temperature is well below the values calculated for the off-normal storage conditions in Section 4.3.6, and would never approach the allowable limit of 752°F.

After completion of the vacuum drying, the DSC must be sealed, the annulus between the DSC and the transfer cask must be drained (if not already drained), the cask must be sealed and backfilled with helium. To ensure the integrity of the fuel cladding, a time limit is considered for performing the activities after vacuum drying until backfilling of the transfer cask starts. This time limit is calculated for procedure B, which has the shortest time limits of all three procedures. For the other procedures, specifically procedure A, the time limit to seal and backfill the transfer cask is significantly longer.

Parts of the above procedures might be combined together to build a new procedure. The time limit for the new procedure can be calculated from appropriate combination of the resultant transient curves discussed in Section 4.5.1.4.

Transient thermal analyses are performed to determine the component temperatures at the end of each procedure separately. A bounding initial average temperature is considered to start the transient analysis.

The three-dimensional model of the 32PTH DSC within the TC described in Section 4.4.1.1 is slightly modified to analyze the vacuum drying procedures. The model contains a half slice of the 32PTH DSC within the TC. The modifications are:

- The DSC is centered in the transfer cask cavity
- The effective conductivity of fuel assemblies are changed to the values reported for vacuum conditions in Section 4.2
- Air conductivity is given to the elements representing the gas and gaps within the basket
- It is considered that the annulus between the DSC and the TC is initially filled with water
- Radiation is not considered between the basket rails and the DSC shell

All the other material properties remain unchanged.

Free convection and radiation are combined together to calculate the total heat transfer coefficient from the TC outer surface to the ambient. Due to the large outer diameter of the TC, the free convection coefficient approaches that for a vertical flat plate. The correlations to calculate the free convection coefficient on vertical plates are discussed in Section 4.11. Following inputs are considered to calculate the total heat transfer coefficient on the outer surface of the transfer cask in this evaluation.

- Ambient temperature in the fuel handling building is 100°F.
- Height of the cylinder is 173", which is approximately the length of the neutron shield panel

- Surface emissivity of the transfer cask is 0.9 (see Section 4.2 for painted surfaces)

A decay heat load of 34.8 kW is considered for all the transient runs. The decay heat is applied as heat generating boundary conditions on the elements representing the homogenized fuel assemblies with a peaking factor of 1.1. Loading configuration 1 is considered for this purpose. Adiabatic boundary conditions are applied on the top and bottom faces of the slice model for conservatism. The other boundary conditions are discussed separately for each procedure in Sections 4.5.1.1 to 4.5.1.3.

An average, initial temperature at the beginning of the transient runs is calculated for the 32PTH DSC and transfer cask as follows.

Initial Temperature 1 = initial pool temperature +
average heat up rate with water in DSC × duration of lifting +
average heat up rate without water in DSC × duration of drainage
when water from the DSC cavity is drained completely before the welding process

and

Initial Temperature 2 = initial pool temperature +
average heat up rate with water in DSC × duration of lifting +
average heat up rate with water in DSC × duration of welding
when water from the DSC cavity is drained completely after the welding process

Following assumptions are considered to calculate the initial temperature:

- Initial pool temperature is 115°F
- No heat dissipation occurs from the transfer cask outer surface
- All the decay heat is used to heat up the transfer cask and its content
- Lifting the transfer cask from the pool to the fuel handling building and performing the required inspections take 2 hours
- Drainage (pumping) of water from the DSC takes 4 hours
-

The average heat up rate is defined as:

$$heat\ up\ rate = \frac{Q}{M\,\overline{C}_p}$$

Q = total decay heat load = 34.8 kW (118748 Btu/hr)
M = total weight (lbm)
$\overline{C}_p$ = average specific heat (Btu/lbm-°F)

The average specific heat is the mass average specific heat of all of the components.

$$\overline{C}_p = \frac{\sum m_i\, C_{p,i}}{M}$$

The components volumes and weights are taken from Chapter 3. Specific heat values increase generally at higher temperatures. Specific heats of the components are taken at about 100°F, which results in higher initial temperature and increases the conservatism in the model. A summary of the heat up rate calculation is shown in Table 4-7. The initial average temperature of the transfer cask and its content is then:

Initial average temp 1 = 115 + 3.2 × 2 + 4.5 × 4 = 139.4°F
with initial pool temperature =115°F
average heat up rate during lifting = 3.2°F /hr (see Table 1)
duration of lifting = 2 hrs
average heat up rate after drainage of DSC = 4.5 °F /hr (see Table 1)
duration of draining water from DSC = 4 hrs

Initial average temp 2 = 115 + 3.2 × 2 + 3.2 × 10 = 153.4°F
with initial pool temperature =115°F
average heat up rate during lifting = 3.2°F /hr (see Table 1)
duration of lifting = 2 hrs
average heat up rate before drainage of DSC = 3.2°F /hr (see Table 1)
duration of welding the DSC shield plug = 10 hrs

For conservatism, an initial temperature of 160°F is considered for the TC and its content at the start of the transient runs.

4.5.1.1 Boundary Conditions for Procedure A

Adequate water should flow or circulated in the 32PTH DSC/TC annulus to prevent water from boiling. In this case the maximum surface temperature of the DSC shell does not exceed the boiling point of water. To simulate procedure A, it is assumed conservatively that the DSC shell temperature remains at 215°F during the entire vacuum drying process. The start time of simulation is after complete drainage of the DSC water.

Temperature gradient through the TC is determined by applying constant temperature of 215°F at the inner shell of the TC. Free convection and radiation boundary conditions are applied on the outer surface of the TC using the total heat transfer coefficient described in Section 4.11.

4.5.1.2 Boundary Conditions for Procedure B

Conduction and free convection heat transfer are combined together to calculate an effective conductivity for the water in the annulus. The calculation of the effective conductivity for the water in the annulus is discussed in detail in Section 4.9.

After draining the water from the annulus, thermal properties of air (conduction only) are considered for the elements in the annulus between the 32PTH DSC and the TC. Free convection and radiation boundary conditions are applied on the outer surface of the TC using the total heat transfer coefficient described in Section 4.11.

Procedure B is also considered to calculate the time limit to backfill the transfer cask with helium after completion of the vacuum drying. For this purpose, the properties of the DSC backfill gas is changed to that of helium, and the fuel effective conductivities are changed to those calculated for helium atmosphere. Time of this change is 28 hours after complete drainage of DSC water or 14 hours after drainage of the annulus water. Other boundary conditions remain unchanged.

4.5.1.3 Boundary Conditions for Procedure C

The same boundary conditions as those described for procedure B are considered for Procedure C except that the 32PTH DSC is backfilled with helium after drainage of the annulus water. It is considered that it takes three hours until the helium replaces the air and water vapor within the DSC cavity completely. Before helium backfill, the model considers air conductivity for the DSC back fill gas. After the three hour period, the conductivity of back fill gas is changed to that of helium, and the fuel effective conductivities are changed to those calculated for helium atmosphere.

4.5.1.4 Evaluation of Vacuum Drying Procedure

Transient simulation of vacuum drying procedures gives the time-temperature history of the fuel assemblies with the maximum decay heat load of 34.8 kW. Duration of the vacuum process is limited to the time at which the maximum temperature of the fuel assemblies is close to the allowable limit of 752°F (400°C) [2]. A margin of about 20°F is considered for conservatism in determining the time limit. The maximum fuel cladding temperatures are summarized in Table 4-8. Typical temperature distributions at the end of vacuum drying process are shown in Figure 4-34. Histories of the maximum component temperatures are shown in Figures 4-35 to 4-37.

As Table 4-8 shows, the vacuum drying can proceed up to 36 hours, if procedure A is followed. For procedure B, the time limit to complete the vacuum drying is 14 hours after drainage of the annulus water or 28 hours after complete drainage of DSC water, whichever is the limiting time.

Backfilling the transfer cask must start within12 hours after completion of the vacuum drying, if one chooses to follow procedure B. The time limit to start backfilling the transfer cask with helium is significantly longer, if procedure A is followed. For procedure C, backfilling of the transfer cask with helium must start within 42 hours after complete DSC drainage or 28 hours after drainage of the annulus water based on the time-temperature history curve shown in Figure 4-37.

Should the decay heat load be lower than 34.8 kW, the time frame will increase for completion of the vacuum drying process. At some decay heat load, the maximum fuel cladding temperature remains always below the allowable limit regardless of the vacuum drying duration. To determine the decay heat load at which the time limitation is not required, models of procedure A to C are investigated separately assuming steady state conditions. Uniform heat generating boundary conditions are applied on the fuel assemblies in the steady state analysis. The results summarized in Table 4-9 show that the fuel cladding temperature remains always below the allowable limit for 23.2 kW decay heat load using procedure A. Similarly, there is no time limit for vacuum drying with 16.0 kW and 22.4 kW using procedures B and C respectively.

Vacuum drying procedures A to C preclude any thermal cycling of fuel cladding. Backfilling the DSC with helium gas causes a one time temperature drop, which is not considered as a repeated thermal cycling. Re-evacuation of the DSC under helium atmosphere does not reduce the pressure sufficiently to decrease the thermal conductivity of helium. Therefore, evacuation and re-pressurizing the DSC under helium atmosphere proceed on a descending curve to the minimum steady state temperatures, and does not include any thermal cycling. It concludes that the limit of 65°C (118°F) considered for thermal cycling is not applicable for NUHOMS®-32PTH system.

4.5.2 Reflooding

For unloading operations, the DSC will be filled with the spend fuel pool water through the siphon port. During this filling, the DSC vent port is maintained open with effluents routed to the plant's off-gas monitoring system.

When the pool water is added to a DSC cavity containing hot fuel and basket components, some of the water will flash to steam causing internal cavity pressure to rise. The steam pressure is released through the vent port. The initial flow rate of the reflood water must be controlled such that the internal pressure in the DSC cavity does not exceed 20 psig. This is assured by monitoring the maximum internal pressure in the DSC cavity during reflood event. The reflood of the DSC is considered as a "Service Level D" event and the design pressure of the DSC is 120 psig. Therefore, there is sufficient margin in the DSC internal pressure during the reflooding event to ensure that the DSC will not be over pressurized.

The maximum fuel cladding temperature during reflooding process is significantly less than the vacuum drying condition owing to the presence of water/steam in the DSC cavity. Hence, the peak cladding temperature during the reflooding operation will be less than 734°F calculated for procedure A in Section 4.5.1 when water circulates in the annulus between the DSC and transfer cask.

To evaluate the effects of the thermal loads on the fuel cladding during reflooding operations, a conservative high fuel rod temperature of 750°F and a conservative low quench water temperature of 50°F are used.

The following material properties, corresponding to 750°F, are used in the evaluation.

Modulus of elasticity, $E = 10.4 \times 10^6$ psi $= 7.17 \times 10^{10}$	(Pa)	[26]
Modulus of rigidity, $G = 2.47 \times 10^{10}$	(Pa)	[25]
Thermal expansion coefficient, $\alpha = 6.72 \times 10^{-6}$	(1/K)	[25]
Yield stress, Sy = 80,500 psi $= 5.55 \times 10^8$	(Pa)	[26]
Poisson's ratio, $\upsilon = \frac{E}{2G} - 1$		[27]

The fuel cladding stress is evaluated as a hollow cylinder with an outer surface temperature of T (50°F), and the inner surface temperature of T+ΔT (750°F) using the following equations from [27].

Maximum circumferential stresses are:

$$\text{(outer surface)}\quad \sigma_{to} = \frac{\Delta T \cdot \alpha \cdot E}{2(1-\upsilon)\ln(r_o / r_i)}\left(1 - \frac{2 r_i^2}{(r_o^2 - r_i^2)}\ln(\frac{r_o}{r_i})\right) \qquad \text{tension}$$

$$\text{(inner surface)}\quad \sigma_{ti} = \frac{\Delta T \cdot \alpha \cdot E}{2(1-\upsilon)\ln(r_o / r_i)}\left(1 - \frac{2 r_o^2}{(r_o^2 - r_i^2)}\ln(\frac{r_o}{r_i})\right) \qquad \text{compression}$$

The longitudinal stresses are equal to the tangential stresses [27]. The maximum stresses calculated for the fuel assembly types to be stored in the NUHOMS-32PTH are summarized in the following table.

	WE15x15	WE17x17Std	17x17MkBW	WE17x17OFA
OD fuel rod (in)	0.422	0.374	0.374	0.360
Clad thickness (in)	0.0243	0.0225	0.0240	0.0225
ID Clad (in)	0.3734	0.3290	0.3260	0.3150
σ_{to} max (Pa)	1.64E+08	1.64E+08	1.63E+08	1.63E+08
σ_{to} max (psi)	23,768	23,719	23,644	23,676
σ_{ti} max (Pa)	1.78E+08	1.78E+08	1.79E+08	1.78E+08
σ_{ti} max (psi)	25,787	25,835	25,910	25,879

σ_max (psi) = 25,910

The maximum stress is 25,910 psi. The calculated maximum stress is much less than the yield stress of 80,500 psi. Therefore, cladding integrity is maintained during reflooding operation.

4.6 Maximum Internal Pressure

The following methodology is used to determine the maximum pressures within the 32PTH DSC during storage and transfer conditions:

- Average cavity gas temperatures are derived from component temperatures.
- The amount of helium present within the canister after the initial backfilling is determined via the ideal gas law.
- The total amount of free gas within the fuel assemblies, including both fill and fission gases, is calculated based on data reported in [28].
- The amount of released gas from the fuel rods into the DSC cavity is determined based on the maximum fraction of the ruptured fuel rods considered in NUREG 1536 [22].
- The amount of helium gas is added to the amount of released gases to make the total amount of gases in the 32PTH DSC cavity.
- Finally, the maximum cavity pressures are determined via the ideal gas law.

The design pressures for the NUHOMS®-32PTH DSC are summarized in the following table.

Condition	Maximum Allowable Pressure For Storage (psig)	Maximum Allowable Pressure for Transfer (psig)
Normal	15	15
Off-Normal	20	20
Accident	70	120

Based on the ideal gas law, the internal pressure of the DSC increases as the average gas temperature increases. Since the DSC normal operating temperatures are bounded by the off-normal temperatures, the maximum internal pressure of the DSC is conservatively calculated based on the off-normal temperatures for both the normal and the off-normal conditions. The average cavity gas temperatures are calculated for loading configuration 1 and HSM-H with unfinned side heat shields at 34.8 kW, which give the maximum component temperatures.

The maximum fractions of the fuel rods that can rupture and release their free gases to DSC cavity for normal, off-normal, and accident cases are 1, 10, and 100% respectively as considered in NUREG 1536 [22].

4.6.1 Average Gas Temperature

To determine the average gas temperature, volume average temperatures of the elements representing the helium gaps (T_{void}) and the homogenized fuel assemblies (T_{fuel}) are calculated discretely from the thermal models. Although the average temperature of the homogenized fuel elements includes the fuel rods and the helium gas between them, this average temperature is considered as the average gas temperature within fuel compartments. The following volumes are considered to calculate the gas average temperature:

Gas volume in the fuel compartments = Volume of the fuel compartments – Volume of the fuel rods
Volume of the fuel compartment = 8.7 x 8.7 x 162 x 32 = 392,377 in^3
Volume of the fuel rods = 148,488 in^3 [Chapter 3]
Gas volume in the fuel compartments ($V_{He,comp}$) = 243,889 in^3

Gas volume in the void space of DSC = Total DSC cavity volume – Gas volume in the fuel compartments
Total DSC cavity volume (V_{cavity}) = 308,146 in^3 [Chapter 3]
Gas volume in fuel compartments = 243,889 in^3
Gas volume in void space of DSC (V_{void}) = 64,257 in^3

The average gas temperature in the 32PTH DSC is calculated as follows:

$$\overline{T}_{DSC} = \frac{T_{avg,fuel} \times V_{He,comp} - T_{avg,void} \times V_{void}}{V_{cavity}}$$

For an average gas temperature, the mass and volume average temperatures are equal. The results are summarized below.

Operating Condition		$\overline{T}_{DSC}$ (°F)
Storage	Normal	515
	Off-Normal	515
	Accident [7]	631
Transfer	Normal	537
	Off-Normal	537
	Accident [8]	961

4.6.2 Amount of Initial Helium Backfill

The initial helium fill pressure within the canister is 2.5±1.0 psig after vacuum drying. An initial pressure of 3.5 psig (18.2 psia) is considered here to maximize the amount of helium gas. The finite element model developed to analyze the vacuum drying process (Section 4.5.1) is run for steady state conditions with helium atmosphere to consider the minimum initial DSC temperature before backfillig, which gives the maximize amount of initial helium gas. Procedure A for vacuum drying (circulation of cool water around DSC) is considered in this run to have the lowest DSC temperature after vacuum drying. The average gas temperature is then calculated using the same methodology described in section 4.6.1. The initial temperature of the backfill gas within the canister is 469°F.

From the backfill pressure and initial backfill gas temperature, the amount of helium backfill gas can be calculated using the ideal gas law.

$$n = \frac{PV}{RT}$$

P = maximum initial canister fill pressure = 18.2 psia
V = DSC cavity volume (loaded) = 308,146 in^3 = 178.3 ft^3 [Chapter 3]
T = initial fill temperature = 469°F = 929 R
R = universal gas constant = 10.730 psia-ft^3/lbmoles-R [3]

n_{back} = 0.326 lb-moles

[7] After 48 hours of vent blockage
[8] At the end of cool down period, 120 hours after beginning of the fire

4.6.3 Free Gas within Fuel Assemblies / BPRA

Maximum volume of free gas per assembly is bounded by WE 15x15 fuel assembly with 204 fuel rods for burnup rates from 35,000 to 55,000 MWd/MTU as concluded in [28]. The reported total free gas volumes from reference [28] are extrapolated to evaluate the free gas volume at the maximum design burnup rate of to 60,000 MWd/MTU. Figure 4-38 illustrates this extrapolation. Based on extrapolation results, the total free gas volume at 60,000 MWd/MTU burnup rate is 1123 cc per fuel rod at standard pressure and temperature (0°C and 760 mmHg). The amount of free gases in the fuel rods based on the ideal gas law is then:

n_{fuel} = (204 rods/assy)(32 assy)[(760 x 1123/1000)/ (62.361 x 273.15)] (2.2046E-3 lbm/g)
= 0.721 lbmoles

with R = 62.361 (mmHg-lit/gmoles-K)

Customer supplied data [29] states that the Westinghouse BPRA has the largest displacement volume and the most amount of free gas among the applicable BPRA types. The amount of free gas in each BPRA rod is 2.0E-4 lbmoles per reference [29].

The amount of free gases in the BPRA rods is:

n_{BPRA} = (2.0E4 lbmole/rod)(20 rod/assy)(32 assy)
= 0.128 lbmoles

Total amount of free gases is:

$$n_{free} = n_{fuel} + n_{BPRA}$$

4.6.4 Total Amount of Gases within DSC

The total amount of gas within the DSC is equal to the amount of the initial helium backfill gas plus any free gases within the ruptures fuel assembly rods or BPRA. All free gases within the ruptured fuel rods/BPRAs will be released into the canister. It is assumed that the fractions of the ruptured BPRA rods are the same as those considered for the fuel rods, i.e., 1, 10, and 100% for normal, off-normal, and accident case respectively.

Total amount of free gas released to the DSC cavity is:

$$n_{total} = n_{back} + f_B (n_{free})$$

n_{total} = total amount of gases (lbmoles)
f_B = fraction of the ruptured fuel rods

4.6.5 Maximum DSC Internal Pressures

Displacement volume of the BPRA is 480 in^3 per reference [29]. Maximum DSC internal pressures are determined via the ideal gas law:

$$P = \left(n_{total}\ R\bar{T}_{DSC}\right)/V$$

P = pressure (psia)
V = Cavity volume =178.3(ft^3) without BPRAs
V = Cavity volume – BPRA volume = (308,146 – 32*480)/12^3 = 169.4 (ft^3) with BPRAs
R = universal gas constant = 10.73 (psia-ft^3/lbmoles-R)

The results are summarized in Table 4-10.

4.6.6 Maximum Pressure in Annulus

The pressure in the annulus between the transfer cask and the DSC is calculated using the ideal gas law:

$$P_{ann} = P_{init}\frac{T}{T_{init}}$$

P_{ann} = Annulus pressure (psia)
P_{init} = initial pressure = 3.0 psig = 16.7 psia
T = annulus average temperature (R)
T_{init} = annulus initial temperature = 70°F = 530 R

Average annulus temperature is the volume average temperature of the annulus elements retrieved from the transfer cask model. The results are summarized below.

Transfer Condition	$\bar{T}_{ann}$	P_{ann}	P_{ann}
	(°F)	(psia)	(psig)
Normal and Off-Normal	349	27.0	12.3
Accident	682	38.1	23.4

4.7 Axial Decay Heat Profile

The normalized axial burnup profile for typical PWR fuels with burnups higher than 30 GWd/MTU from Reference [4] is shown below. An active fuel length of 144" is considered for the evaluation.

% of Core Height	Corresponding Length from Bottom of Active Fuel (in)	Peaking Factor	Area under the Profile
0.00	0.00	0	
2.78	4.00	0.652	1.31
8.33	12.00	0.967	6.47
13.89	20.00	1.074	8.17
19.44	27.99	1.103	8.70
25.00	36.00	1.108	8.85
30.56	44.01	1.106	8.86
36.11	52.00	1.102	8.82
41.67	60.00	1.097	8.80
47.22	68.00	1.094	8.76
52.78	76.00	1.094	8.76
58.33	84.00	1.095	8.75
63.89	92.00	1.096	8.77
69.44	99.99	1.095	8.76
75.00	108.00	1.086	8.73
80.56	116.01	1.059	8.59
86.11	124.00	0.971	8.11
91.67	132.00	0.738	6.84
97.22	140.00	0.462	4.80
100.00	144.00	0	0.92
Sum			141.76
Average			0.984

The average value in the above table is the total area under the axial decay heat profile divided by the active fuel length. This value must be equal to 1. Since it differs from one, a correction factor of 1/0.984 is multiplied by the heat generating rate to avoid any degradation of the applied heat in the model.

14 axial fuel regions are defined for the fuel assembly in the finite element model. An average peaking factor is calculated for each region so that the resultant axial profile is identical to the profile resulted from the above table.

The average peaking factor of each fuel region is set equal to the area underneath the peaking factor curve divided by the height of the corresponding region. The area underneath the peaking factor curve is calculated as follows.

$$A_j = \sum_{1}^{n} \frac{(P_{i+1} + P_i)}{2(l_{i+1} - l_i)}$$

Where,

A_j = area underneath the profile in fuel region j
P_i = Local peaking factors at location i in fuel region j
l_i= Corresponding length to the local peaking factor P_i

Average peaking factor is:

$$P_j = \frac{A_j}{H_j}$$

P_j = Average peaking factors of fuel region j
H_j= Height of fuel region i

The following Figure depicts this methodology. The resultant average peaking factors for active fuel length of 144" are listed in Table 4-11.

Calculation of the Average Peaking Factor

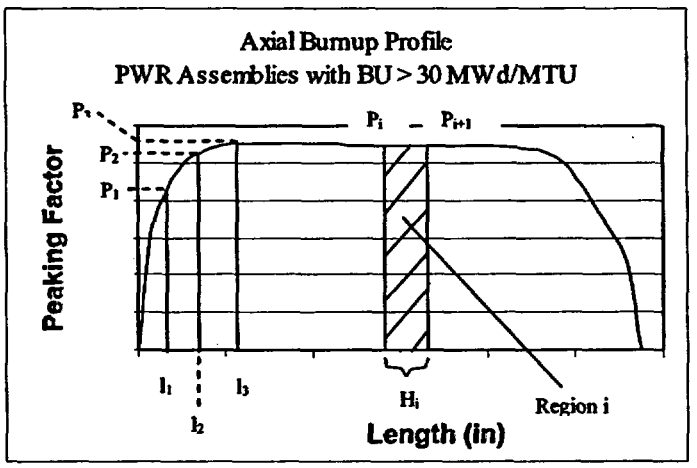

The height of each region is converted to the corresponding local coordination in the finite element model to apply the peaking factors in the model. The peaking factors applied in the model are listed below.

Region No.	Height from bottom of active fuel		Z-axis in FEM		Peaking Factor
	from	To	from	to	
1	0	1.32	4	5.32	0.107
2	1.32	7.0675	5.32	11.0675	0.582
3	7.0675	14.5	11.0675	18.5	0.908
4	14.5	22.0675	18.5	26.0675	1.048
5	22.0675	37.0675	26.0675	41.0675	1.100
6	37.0675	57.69	41.0675	61.69	1.104
7	57.69	66.9425	61.69	70.9425	1.096
8	66.9425	82.0675	70.9425	86.0675	1.094
9	82.0675	97.0675	86.0675	101.0675	1.095
10	97.0675	111.9425	101.0675	115.9425	1.088
11	111.9425	121.26	115.9425	125.26	1.046
12	121.26	127.0675	125.26	131.0675	0.955
13	127.0675	136.26	131.0675	140.26	0.743
14	136.26	144	140.26	148	0.374

A comparison between the axial burnup profile from Reference [4] and the axial burnup profile used in the finite element model is shown in the Figure 4-39.

Figure 4-39 shows that the calculated axial profile perfectly matches the data from reference [4] except for the very ends of the active fuel. The small discrepancy at the very ends is due to the size of the regions and has a minimum effect on the thermal evaluation.

4.8 Effective Fuel Properties

4.8.1 Discussion

The NUHOMS®-32PTH DSC finite element models simulate the effective thermal properties of the fuel with a homogenized material occupying the volume within the basket where the fuel assemblies are stored. Effective values for density, specific heat, and conductivity are determined for this homogenized material for use in the finite element models.

The 32PTH DSC is capable of handling a variety of spent PWR fuel assemblies. In order to determine conservative thermal properties of the homogenized fuel assembly, all of the PWR fuel assemblies types to be stored in the 32PTH DSC are studied. The lowest effective thermal conductivity, density, and specific heat of the studied fuel assemblies are selected to apply in the finite element model. Use of these properties would conservatively predict bounding maximum temperatures for the components of the NUHOMS®-32PTH DSC.

The characteristics of the fuel assemblies to be stored in the 32PTH DSC are listed in Table 4-12.

4.8.2 Summary of Material Properties

1. UO_2, Fuel Pellets

Conductivity and specific heat for fuel pellets are taken from [30] and listed below.

Temperature (°C)	k (cal/s-cm-°C) [30]	Temperature (°F)	k (Btu/hr-in-°F)
25	0.025	77	0.503
100	0.021	212	0.423
200	0.018	392	0.362
300	0.015	572	0.302
500	0.0132	932	0.266
700	0.0123	1292	0.248
800	0.0124	1472	0.250

Temperature (°C)	C_p (cal/g-°C) [30]	Temperature (°F)	C_p (Btu/lbm-°F)
0	0.056	32	0.056
100	0.063	212	0.063
200	0.0675	392	0.068
400	0.0722	752	0.072
1200	0.079	2192	0.079

The density of fuel pellets (UO_2) is 10.96 g/cc = 0.396 lbm/in^3 [30].

2. Zircaloy-4, Cladding

Table B-2.I of Reference [31] lists measured and calculated values of thermal conductivity for zircaloy-4 at various temperatures. The measured values used in this calculation are listed below.

Temperature (K)	k (W/m-K) [31]	Temperature (°F)	k (Btu/hr-in-°F)
373.2	13.6	212	0.655
473.2	14.3	392	0.689
573.2	15.2	572	0.732
673.2	16.4	752	0.790
773.2	18.0	932	0.867
873.2	20.1	1112	0.968

Table B-1.1 of [31] lists specific heat values for Zircaloy as a function of temperature.

Temperature (K)	C_p (J/kg-K) [31]	Temperature (°F)	C_p (Btu/lbm-°F)
300	281	80	0.067
400	302	260	0.072
640	331	692	0.079
1090	375	1502	0.090

The density of Zircaloy is 6.56 g/cm3 = 0.237 lbm/in3, as defined in [30].

Table B-3.11 of [31] lists the measured emissivity values for fuel cladding. For ease of calculation a temperature independent emissivity of 0.8 is set for zircaloy4 in this calculation.

$\varepsilon zirc = 0.80$

3. Helium

Temperature (K)	Conductivity [5] (W/m-k)	Temperature (°F)	Conductivity (Btu/hr-in-°F)
200	0.1151	-100	0.0055
250	0.1338	-10	0.0064
300	0.150	80	0.0072
400	0.180	260	0.0087
500	0.211	440	0.0102
600	0.247	620	0.0119
800	0.307	980	0.0148
1000	0.363	1340	0.0175

4. Air at low pressure (0.1 bar)

Temperature (K)	Conductivity [5] (W/m-k)	Temperature (°F)	Conductivity (Btu/hr-in-°F)
200	0.0180	-100	0.0009
300	0.0263	80	0.0013
400	0.0336	260	0.0016
500	0.0403	440	0.0019
600	0.0466	620	0.0022
800	0.0577	980	0.0028
1000	0.0681	1340	0.0033

The air conductivity at low pressure is used to calculate the effective transverse conductivity for vacuum drying conditions.

5. Stainless Steel SA-240, Type 304

A stainless steel emissivity of 0.3, a value lower than the measured values from Reference [14], is used in the analysis for conservatism.

4.8.3 Effective Fuel Conductivity

4.8.3.1 Transverse Effective Conductivity

The purpose of the effective conductivity in the transverse direction of a fuel assembly is to relate the temperature drop of a homogeneous heat generating square to the temperature drop across an actual assembly cross section for a given heat load. This relationship is established by the following equation obtained from Reference [32]:

$$k_{eff} = \frac{Q}{4L_a(T_o - T_s)}(0.29468) = \frac{Q_{react}}{(T_c - T_o)}(0.29468)$$

where:

k_{eff} = Effective thermal conductivity (Btu/hr-in.-°F)
Q = Assembly head generation (Btu/hr)
Q_{react} = Reaction solution retrieved from quarter model (Btu/hr)

$$Q = 4 \times Q_{react} \times L_a$$

L_a = Assembly active length (in.)
T_o = Maximum temperature (°F)
T_s = Surface temperature (°F)

Discrete finite element models of the fuel assemblies to be stored in the NUHOMS®-32PTH DSC are developed using the ANSYS computer code [16]. These two-dimensional models simulate heat transfer by radiation and convection and include the geometry of the fuel rods and fuel pellets. Helium or air properties are used as the fill gas in the fuel assembly. A fuel assembly decay heat load of 0.8 kW [9] is used for heat generation. An active length of 144" is assumed.

[9] 0.8 kW is the maximum decay heat load for the fuel assemblies in the center of the basket.

The finite element models are used to calculate the maximum radial temperature difference with isothermal boundary conditions. All components are modeled using 2-D PLANE55 thermal solid elements. LINK32 elements are placed on the exteriors of the fuel assembly components to set up the creation of the radiation super-element. The compartment wall is modeled using LINK32 elements and used only to set up the surrounding surface for the creation of the radiation matrix super-element using the /AUX12 processor in ANSYS. All LINK32 elements are unselected prior to solution of the thermal problem. The thermal properties used in the model are described in Section 4.8.2, and the fuel assembly geometries are shown in Table 4-12. A typical ANSYS finite element model of fuel assemblies is shown in Figures 4-40 on hand fuel assembly WE 17x17.

Several computational runs were made for each model using isothermal boundary temperatures ranging from 100 to 1000°F. In determining the temperature dependent effective conductivities of the fuel assemblies an average temperature, equal to $(T_o + T_s)/2$, is used for the fuel temperature. The transverse effective conductivity is calculated in helium for storage and transfer conditions. For vacuum drying conditions, the conductivity of helium is replaced by air conductivity at low pressure. The vacuum drying of the DSC generally does not reduce the pressure sufficiently to reduce the thermal conductivity of the water vapor and air in the DSC cavity [33]. Therefore, air conductivity at low pressures is assumed for the backfill gas for vacuum drying conditions and the effect of water vapor conductivity is neglected.

4.8.3.2 Axial Effective Conductivity

The backfill gas, fuel pellets, and zircaloy behave like resistors in parallel. However, due to the small conductivity of the fill gas and the axial gaps between fuel pellets, credit is only taken for the zircaloy in the determination of the axial effective conductivities.

$$kaxial = \frac{cladding\ area}{4a^2} \times cladding\ conductivity$$

with a = half of compartment width = 8.7"/2 = 4.35"

4.8.4 Effective Fuel Density and Specific Heat

Volume average density and weight average specific heat are calculated to determine the effective density and specific heat for each fuel assembly type separately. The equations to determine the effective density and specific heat are shown below.

$$\rho_{eff} = \frac{\sum \rho_i V_i}{V_{assembly}} = \frac{\rho_{UO2}\ V_{UO2} + \rho_{Zr4}\ V_{Zr4}}{4a^2 L_a}$$

$$C_{p,eff} = \frac{\sum \rho_i V_i C_{Pi}}{\sum \rho_i V_i} = \frac{\rho_{UO2}\ V_{UO2}\ C_{P,UO2} + \rho_{Zr4}\ V_{Zr4}\ C_{P,Zr4}}{\rho_{UO2}\ V_{UO2} + \rho_{Zr4}\ V_{Zr4}}$$

4.8.5 Conclusion

The effective transverse conductivity values are plotted in Figure 4-41. As Figure 4-41 shows, fuel type WE17x17 OFA has the lowest conductivity for the range of 100 to 700°F under helium atmosphere. For temperatures higher than 700°F, fuel assembly 17x17 MK BW has the lowest transverse conductivity. To bound the transverse effective conductivity, the lowest effective conductivity value in each temperature range is selected to apply in the thermal analysis.

The calculated transverse effective conductivties for vacuum drying conditions are plotted in Figure 4-42. As Figure 4-42 shows, fuel assembly 17x17MK BW has the lowest conductivity for vacuum drying conditions, which are used in thermal analysis for vacuum conditions.

The axial effective conductivity for each fuel type is calculated using the equation from Section 4.8.3.2. The resultant values are listed in Table 4-13 and plotted in Figure 4-43. The lowest axial effective conductivity belongs to fuel type WE 15x15, which is used in the thermal analysis.

Effective density of each fuel type is calculated using the corresponding equation from Section 4.8.4. Since using the lowest density results in the highest cladding temperature for accident conditions, the density of fuel assembly WE 17x17 OFA is the bounding density. The calculated effective density values are listed in Table 4-13.

Effective specific heat values are calculated as a function of temperature using the corresponding equation from Section 4.8.4. Properties of fuel pellets and fuel cladding from Section 4.8.2 are linearly interpolated for this purpose. The lowest specific heat belongs to the fuel type WE15x15. Since the lowest specific heat results in the highest cladding temperature for transient calculations, specific heat of fuel type WE 15x15 is selected for thermal analysis as the bounding property. The calculated effective specific heat values are listed in Table 4-13.

The bounding effective fuel properties used in the finite element models are listed in Section 4.2.

4.9 Effective Conductivity of Fluids in the Transfer Cask

4.9.1 Effective Conductivity in the Shielding Panel

Heat transfer in the shielding panel occurs by conduction and convection through the fluid (water) contained in the shielding. The shielding panel consists of 16 cylindrical segments. Each segment can be considered as two concentric, horizontal cylinders. The following correlation from [5] is used to calculate the free convection coefficient for water within each of the panel segments.

$$k_{con} = Nu \; k_w$$

k_{con} = effective conductivity for conduction and convection from inner to outer cylinder
k_w = conductivity of water

$$Nu = [Nu_{COND}, Nu_l]_{\max}$$

$$N_{COND} = \frac{\ln(D_o / D_i)}{\cosh^{-1}\left[\left(D_o^2 + D_i^2 - 4E^2\right)/2D_oD_i\right]} \qquad \text{conduction}$$

$$Nu_l = 0.603\,\overline{C}_l \frac{(\ln D_o / D_i)\,Ra^{1/4}}{\left[(L/D_i)^{3/5} + (L/D_o)^{3/5}\right]^{5/4}} \qquad \text{laminar flow}$$

where,

$$Ra = \frac{g\beta(T_i - T_o)L^3}{\nu^2} \times \Pr \qquad \text{with} \qquad L = (D_o - D_i)/2 \qquad \text{and}$$

$$\overline{C}_l = \tfrac{4}{3}\frac{0.503}{[1 + (0.492/\Pr)^{9/16}]^{4/9}}$$

All water properties are evaluated at average temperature:

$$T_{avg} = (T_o + T_i)/2$$

T_o = average temperature of the outer cylinder
T_i = average temperature of the inner cylinder

Diameter of the inner cylinder is 81.7", and diameter of outer cylinder is 91.825". The average inner and outer temperatures are initially unknown. Iterative solution of the ANSYS [16] model combined with the above correlations determines the inner and outer temperatures, and the effective conductivity. The iteration continues until the difference between the applied coefficient in the ANSYS model and the calculated coefficient is less than 5% for the off-normal conditions at 115°F ambient. To ease the analysis, this criterion is increased to 10% for the off-normal conditions at -20°F ambient, which is less sensitive for thermal evaluations.

Water properties are reported in Section 4.2. The calculated effective conductivity values and their verifications are shown in the Table 4-14 and 4-15 for normal and off-normal transfer conditions.

The same methodology as described above is used to calculate the effective conductivity of liquid neutron shield during the burning period of fire accident case.

The calculated values are listed in Table 4-16. Theses values are bounded by a value of 2.25 Btu/hr-in-F used in the thermal analysis to maximize the fire heat flux toward the interior of the transfer cask

It is assumed that water in the shielding panel evaporates completely subsequence to the hypothetical fire accident. Heat transfer in the empty (filled with air) shielding panel occurs by conduction, convection, and radiation through air during the cool-down period. Conduction and convection are combined together using the same methodology described above, with the exception that the water properties are replaced with the air properties from Section 4.2.

Radiation between two concentric, horizontal cylinders can be described as follows [5].

$$q_r = \frac{\sigma A_1 (T_1^4 - T_2^4)}{\frac{1}{\varepsilon_1} + \frac{A_1}{A_2}\left(\frac{1}{\varepsilon_2} - 1\right)} \qquad (4.9\text{-}1)$$

Where

q_r = radiation heat transfer rate (Btu/hr)
σ = Stefan-Boltzmann constant =0.1714x10^{-8} (Btu/hr-ft^2-R^4)
A_1 = area of the inner surface = π D_1 L (ft^2)
A_2 = area of the outer surface = π D_2 L (ft^2)
ε_1 = emissivity of the inner surface = 0.46 for stainless steel [section 4.2]
ε_2 = emissivity of the outer surface = 0.46 for stainless steel [section 4.2]
T_1 = temperature of the inner surface (R)
T_2 = temperature of the outer surface (R)

Conduction in cylindrical shells is [5]:

$$q_{cond} = \frac{2\pi k L (T_1 - T_2)}{\ln\left(\frac{D_2}{D_1}\right)} \qquad (4.9\text{-}2)$$

Comparing equation (4.9-1) with equation (4.9-2) gives the equation for effective radiation conductivity:

$$k_r = \frac{\sigma D_1}{2\left[\frac{1}{\varepsilon} + \left(\frac{D_1}{D_2}\right)\left(\frac{1}{\varepsilon} - 1\right)\right]} \cdot \frac{(T_1^4 - T_2^4)}{(T_1 - T_2)} \cdot \ln\left(\frac{D_2}{D_1}\right) \qquad (4.9\text{-}3)$$

Adding k_r to k_{con} results in the total effective conductivity for the air inside the shielding panel. The total effective conductivity values are calculated iteratively using the results of the ANSYS model. The final results are shown in Table 4-17. This table shows that the effective conductivity values applied in the ANSYS model deviates less than 10% from the final calculated values. The applied effective conductivities are lower than the calculated values. The applied effective conductivities are therefore conservative regarding the fuel cladding temperature.

4.9.2 Effective Water Conductivity in Annulus between TC and DSC

At the beginning of the vacuum process, the annulus between the transfer cask and the DSC is filled with fresh water. During vacuum drying, the DSC and the transfer cask remain in vertical position. Due to the large size of the DSC outer diameter and transfer cask inner diameter, the curvature effects are minimal and the convection in the annulus can be approximated as convection in a vertical rectangular cavity. Reference [5] introduces the following correlations to calculate the combination of the convection and conduction heat transfer in vertical rectangular cavities.

For $\Pr \approx 0.7$ (4.9-4)

$$Nu = [Nu_{ct}, Nu_l, Nu_t]_{\max}$$

where

$$Nu_{ct} = \left[1 + \left\{\frac{0.104\, Ra^{0.293}}{1+(6310/Ra)^{1.36}}\right\}^3\right]^{1/3}$$

$$Nu_l = 0.242\left(\frac{Ra\, L}{H}\right)^{0.273}$$

$$Nu_t = 0.0605\, Ra^{1/3}$$

For $\Pr \geq 4$ (4.9-5)

If $Ra\,(H/L)^3 < 4\times10^{12}$ then

$$Nu = \left[1,\ 0.36\,\Pr^{0.051}\left(\frac{L}{H}\right)^{0.36} Ra^{0.25},\ 0.084\,\Pr^{0.051}\left(\frac{L}{H}\right)^{0.1} Ra^{0.3}\right]_{\max}$$

and for $Ra\,(H/L)^3 > 4\times10^{12}$

$$Nu = 0.039\, Ra^{1/3}$$

with

$$Ra = \frac{g\beta(T_h - T_c)}{\nu^2}\Pr$$

Since the Pr number of water in the annulus is between 0.7 and 4.0, the Nu is calculated as the linear interpolation between Nu numbers from correlations (4.9-4) and (4.9-5). The combined convection and conduction heat transfer can be expressed as an effective conductivity as defined in [5]. The effective conductivity of water in annulus is:

$$k_{eff} = Nu\, k_w$$

k_{eff} = effective conductivity of water in the annulus
Nu = calculated Nusselt number
k_w = water conductivity

All water properties are considered at average water temperature. The thermal properties of water are listed in Section 4.2.

The temperature difference between hot and cold surfaces is initially unknown. To bound the problem, a k_{eff} value of 0.055 Btu/hr-in-°F is used in the model. To verify this value, k_{eff} is calculated based on the average hot and cold surface temperatures of the annulus retrieved from the results of the model as shown in the first part of Table 4-18. The selected value of 0.055 Btu/hr-in-°F is lower than all the calculated values except for the first hour of simulation, as shown in the second part of Table 4-18.

The model uses uniform initial temperatures to start the analysis. Therefore, the temperature gradients at the start of the simulation are too small to give realistic convection coefficient. The effects of the uniform initial temperatures are eliminated after the first hour.

Using lower effective conductivities for water in annulus is conservative, since lower effective conductivity values result in higher fuel cladding temperature for the vacuum drying analysis. The selected value of 0.055 Btu/hr-in-°F for effective conductivity of water in annulus (k_{eff}) is therefore acceptable.

4.10 Justification of the Assumed Hot Gap Sizes

4.10.1 Radial Gap between Basket Rails and DSC shell

The radial cold gap between the rails and the 32PTH DSC shell is 0.125". The nominal DSC inner diameter is 68.75". This gives a nominal basket outer diameter of 68.5". The diameters of the basket and the DSC shell can be calculated after the thermal equilibrium using the following equation:

$$D_{hot} = D_{cold}\ (1+\alpha\,(T_{avg} - 70)) \qquad (4.10\text{-}1)$$

α = mean coefficient of thermal expansion
T_{avg} = average component temperature

To calculate the average basket temperature only stainless steel components of the basket are considered. Adequate gaps exist between the aluminum plates and the stainless steel structure of the basket to avoid deformation. The size of the radial, hot gap can be calculated as follows:

$$\text{Hot gap} = (D_{i,\,DSC,\,hot} - D_{o,\,basket,\,hot})/2$$

The maximum and minimum temperatures are taken from result files of the DSC model (Section 4.3) at hottest ($71.067 \le Z \le 86.067$) and coolest ($4.0 \le Z \le 20.32$) sections for 115°F ambient during transfer operation. The calculated hot dimensions are listed below.

Hottest Cross Section	Cold Dimension	T_{max}	T_{min}	T_{avg}	Material	α [10]	Hot Dimension
	(in)	(°F)	(°F)	(°F)	---	(in/in-°F)	(in)
$D_{o,\,basket}$	68.50	693	345	519	SA 240, type 304	9.738×10^{-6}	68.800
$D_{i,\,DSC}$	68.75	474	339	407	SA 240, type 304	9.514×10^{-6}	68.970
Radial Gap	0.125	---	---	---	---	---	0.085

Coolest Cross Section	Cold Dimension	T_{max}	T_{min}	T_{avg}	Material	α [10]	Hot Dimension
	(in)	(°F)	(°F)	(°F)	---	(in/in-°F)	(in)
$D_{o,\,basket}$	68.50	611	303	457	SA 240, type 304	9.614×10^{-6}	68.755
$D_{i,\,DSC}$	68.75	452	271	362	SA 240, type 304	9.224×10^{-6}	68.935
Radial Gap	0.125	---	---	---	---	---	0.090

A radial, hot gap of 0.1" is considered in the model. This assumption is conservative, since the average gaps calculated in the above table are smaller than the assumed gap.

[10] Interpolated from values in Reference [6]

4.10.2 Radial Gap between Lead and the Cask Structural Shell

A 0.030" radial air gap is assumed between the lead and the TC structural shell in the finite element model described in Section 4.3.1.1. This air gap might occur due to different thermal expansion factors of stainless steel lead after the lead is poured.

The following assumptions are made for the verification of the lead gap:

1) The TC body has nominal dimension at 70°F.
2) During the lead pour the cask body and lead are at 620°F.
3) The inner diameter of the gamma shell (lead) is equal to the outer diameter of the inner cask shell at thermal equilibrium.

The average coefficients of thermal expansion for SA-240, type 304 stainless steel are:

Temperature (°F) [6]	α (in/in-°F) [6]
70	8.5×10^{-6}
100	8.6×10^{-6}
150	8.8×10^{-6}
200	8.9×10^{-6}
250	9.1×10^{-6}
300	9.2×10^{-6}
350	9.3×10^{-6}
400	9.5×10^{-6}
450	9.6×10^{-6}
500	9.7×10^{-6}
550	9.8×10^{-6}
600	9.8×10^{-6}
650	9.9×10^{-6}

The density of lead as a function of temperature is found below.

Temperature (K) [5]	Density (kg/m^3) [5]	Temperature (°F)	Density (lbm/in^3)
50	11,570	-370	0.4180
100	11,520	-280	0.4162
150	11,470	-190	0.4144
200	11,430	-100	0.4129
250	11,380	-10	0.4111
300	11,330	80	0.4093
400	11,230	260	0.4057
500	11,130	440	0.4021
600	11,010	620	0.3978

The volume within the "lead cavity" is found by determining the stainless steel body dimensions at 620°F. Since no gaps will be present between the molten lead and the stainless steel body, this volume is equal to the volume of lead at 620°F. The mass of the lead filled the lead cavity at 620°F is then determined.

Maximum cask inner shell temperature is 340°F during normal condition of transfer (see Table 4-1). The dimensions of the "lead cavity" at 340°F are determined using similar equations to equation (4.10-1). From the mass of the lead, the lead volume is determined using the lead density at 340°F. Conservatively assuming the maximum possible axial length for the lead, the lead volume is used to determine the maximum size of the air gap adjacent to the lead.

Determination of Lead Mass

$\alpha = 9.84 \times 10^{-6}$ in/in-°F @ 620 °F (via linear interpolation for SA240, type 304)
R_{in} = inner radius of lead cavity = 35.75"
R_{out} = outer radius of lead cavity = 39.35"
L = length of lead cavity = 179.1"

$R_{in,\,620} = (R_{in})(1+(\alpha)(\Delta T)) = (35.75)(1+(9.84E\text{-}6)(620\text{-}70)) = 35.9438"$
$R_{out,\,620} = (R_{out})(1+(\alpha)(\Delta T)) = (39.35)(1+(9.84E\text{-}6)(620\text{-}70)) = 39.5630"$
$L_{620} = (L)(1+(\alpha)(\Delta T)) = (179.1)(1+(9.84E\text{-}6)(620\text{-}70)) = 180.0693"$

$V_{cavity} = V_{lead} = (\pi)(R_{out,620}^2 - R_{in,620}^2)(L_{620}) = 154{,}603.8\ in^3$
$M_{lead} = (V_{lead})(\rho_{lead}) = (154{,}603.8\ in^3)(0.3978\ lbm/in^3) = 61{,}501.4\ lbm$

Lead gap determination

ρ_{lead} = 0.4037 lbm/in^3 at 340°F, via linear interpolation
$R_{in,\,ss,\,340} = (R_{in})(1+(\alpha)(\Delta T)) = (35.75)(1+(9.28E\text{-}6)(340\text{-}70)) = 35.8396"$
$R_{out,\,ss,\,340} = (R_{out})(1+(\alpha)(\Delta T)) = (39.35)(1+(9.28E\text{-}6)(340\text{-}70)) = 39.4486"$
$L_{ss,\,340} = (L)(1+(\alpha)(\Delta T)) = (179.1)(1+(9.28E\text{-}6)(340\text{-}70)) = 179.5487"$

$V_{lead,\,340} = M_{lead} / \rho_{lead} = 61{,}501.4 / 0.4037 = 152{,}344.3\ in^3$

Since $R_{in,ss,340} = R_{in,lead,340}$, then :

$V_{lead,340} = (\pi)(R_{out,\,lead,340}^2 - R_{in,\,ss,\,340}^2)(L_{ss,\,340})$

It gives:

$R_{out,lead,340} = 39.4279"$

The difference between the cavity outer radius and the lead outer radius gives the maximum radial gap size.

Air gap = $R_{out,ss,340} - R_{out,\,lead,340} = 0.021"$

The assumed air gap of 0.03" is conservative to maximize the DSC shell temperature.

4.11 Heat Transfer Coefficients

4.11.1 Total heat Transfer Coefficient to Ambient

The outer surfaces of the transfer cask or the HSM-H dissipate heat to the ambient via free convection and radiation. Total heat transfer coefficient is defined as:

$$H_t = h_r + h_c$$

where,

h_r = radiation heat transfer coefficient
h_c = free convection heat transfer coefficient

The radiation heat transfer coefficient, h_r, is given by the equation:

$$h_r = \varepsilon F_{12}\left[\frac{\sigma(T_1^4 - T_2^4)}{T_1 - T_2}\right] Btu/hr - ft^2 - {}^oF$$

where,

ε	= surface emissivity
F_{12}	= view factor from surface 1 to ambient
σ	= 0.1714×10^{-8} Btu/hr-ft^2-R^4
T_1	= surface temperature, R
T_2	= ambient temperature, R

The free convection coefficients are calculated based on the surface shape and position in Section 4.11.2. The above correlations are incorporated in ANSYS [16] model via macros "HTOT_VPL.mac" and "HTOT_HCL.mac" for the transfer cask and "HC_ROOF.mac" and "HC_FRONT.mac" for the HSM-H model. Air properties reported in Section 4.2 are used in these macros. The macros are listed in Appendix 4.16.1.

The free convection heat transfer at the outer surface of the transfer cask is replaced with forced convection to analyze the fire accident case. A forced convection value of 4.5 Btu/hr-ft^2-F is considered during the burning time from reference [23]. The calculated total heat transfer coefficients for the outer cask surfaces during the fire are listed in the Table 4-19.

4.11.2 Free Convection Coefficients

The free convection coefficients are calculated based on the shape and position of the convective surface using correlations from Reference [5]. The convection correlations are described in the following sections.

4.11.2.1 Horizontal Cylinder

$$Ra = Gr\,\mathrm{Pr} \quad ; \quad Gr = \frac{g\beta(T_w - T_\infty)D^3}{\nu^2}$$

$$Nu_l = \frac{2f}{\ln(1 + 2f/Nu^T)}$$ Nusselt number for laminar flow with

$Nu^T = 0.772\,\overline{C}_t\,Ra^{1/4}$, $f = 1 - \frac{0.13}{(Nu^T)^{0.16}}$, and $\overline{C}_t = 0.515$ for gases [5]

$Nu_t = \overline{C}_t\,Ra^{1/3}$ Nusselt number for turbulent flow

$\overline{C}_t = 0.103$ for horizontal cylinders [34]

$Nu = \left[(Nu_l)^m + (Nu_t)^m\right]^{1/m}$ *with* $m = 3.3$ *for* $10^{-10} < Ra < 10^{10}$

$h_c = \frac{Nu\,k}{D}$ with

D = diameter of the horizontal cylinder
k = air conductivity

The above correlations are incorporated in ANSYS [16] model via macro "HC_HCL.mac" listed in Appendix 4.16.1.

4.11.2.2 Vertical Flat Plate

$Ra = Gr\ \mathrm{Pr}$; $Gr = \frac{g\beta(T_w - T_\infty)L^3}{\nu^2}$

$Nu_l = \frac{2.8}{\ln(1 + 2.8/Nu^T)}$ Nusselt number for laminar flow with

$Nu^T = \overline{C}_l\,Ra^{1/4}$, $\overline{C}_l = 0.515$ for gases [5]

$Nu_t = C_t^V\,Ra^{1/3}$ Nusselt number for turbulent flow with

$C_t^V = \frac{0.13\,\mathrm{Pr}^{0.22}}{(1 + 0.61\,\mathrm{Pr}^{0.81})^{0.42}}$

$Nu = \left[(Nu_l)^m + (Nu_t)^m\right]^{1/m}$ *with* $m = 6$ *for* $1 < Ra < 10^{12}$

$h_c = \frac{Nu\,k}{L}$ with

L = height of the vertical surface
k = air conductivity

The above correlations are incorporated in ANSYS [16] model via macro "HC_VPL.mac" in Appendix 4.16.1.

4.11.2.3 Horizontal Flat Plate Facing Upwards

$Ra = Gr\ \mathrm{Pr}$; $Gr = \frac{g\beta(T_w - T_\infty)L^3}{\nu^2}$

$Nu_l = \frac{1.4}{\ln(1 + 1.4/Nu^T)}$ Nusselt number for laminar flow with

$Nu^T = 0.835\,\overline{C}_l\,Ra^{1/4}$, and $\overline{C}_l = 0.515$ for gases [5]

$Nu_t = C_t^H\,Ra^{1/3}$ Nusselt number for turbulent flow with

$C_t^H \approx 0.14$ for $Pr < 100$ [5]

$Nu = \left[(Nu_t)^m + (Nu_t)^m\right]^{1/m}$ *with* $m = 10$ *for* $Ra > 1$

$h_c = \dfrac{Nu\,k}{L}$ with

L = A/P
A=surface area of heated surface
P= perimeter of the heated surface
k = air conductivity

The above correlations are incorporated in ANSYS [16] model via macro "HC_HPLU.mac" in Appendix 4.16.1.

4.11.2.4 Horizontal Flat Plate Facing Downwards

$Ra = Gr\,\mathrm{Pr}$; $Gr = \dfrac{g\beta(T_w - T_\infty)L^3}{\nu^2}$

$Nu_l = \dfrac{0.527\,Ra^{1/5}}{[1+(1.9/\mathrm{Pr})^{9/10})^{2/9}}$ for laminar flow

$Nu = Nu_l$

$h_c = \dfrac{Nu\,k}{L}$ with

L = A/P
A=surface area of heated surface
P= perimeter of the heated surface
k = air conductivity

The above correlations are incorporated in ANSYS [16] model via macro "HC_HPLD.mac" in Appendix 4.16.1.

4.11.2.5 Inclined Flat Plate, Positive Angled

Reference[5] gives the following correlations for free convection over inclined flat, plates. The angle of inclined surface is measured from vertical line. The positive or negative sign of the angle is defined in the following figure.

$Ra = Gr\,\mathrm{Pr}$; $Gr = \dfrac{g\beta(T_w - T_\infty)L^3}{\nu^2}\cos\phi$

$Nu_l = \dfrac{2.8}{\ln(1+2.8/Nu^T)}$ Nusselt number for laminar flow with

$$Nu^T = \overline{C}_t\ Ra^{1/4} \qquad , \overline{C}_t = 0.515 \quad \text{for gases [5]}$$

$$Nu_t = C_t\ Ra^{1/3} \qquad \text{Nusselt number for turbulent flow with}$$

$$C_t = C_t^V \cos^{1/3}\phi \qquad \text{for} \qquad -90^\circ \le \phi \le \tan^{-1}\left(\frac{C_t^V}{C_t^H}\right)^3$$

$$C_t = C_t^H \sin^{1/3}\phi \qquad \text{for} \qquad \tan^{-1}\left(\frac{C_t^V}{C_t^H}\right)^3 \le \phi \le 90^\circ$$

with

$$C_t^V \approx \frac{0.13\,\mathrm{Pr}^{0.22}}{(1+0.61\,\mathrm{Pr}^{0.81})^{0.42}}$$

$$C_t^H \approx 0.14 \qquad for \qquad \mathrm{Pr} < 100$$

$$Nu = \left[(Nu_l)^m + (Nu_t)^m\right]^{1/m} \qquad with \quad m = 6 \quad for \quad 1 < Ra < 10^{12}$$

$$h_c = \frac{Nu\ k}{L} \qquad \text{with}$$

L = length of the inclined plate
k = air conductivity

The above correlations are incorporated in ANSYS [16] model via macros "HC_IPLU.mac" and "HCIPLUm.mac" listed in Appendix 4.16.1.

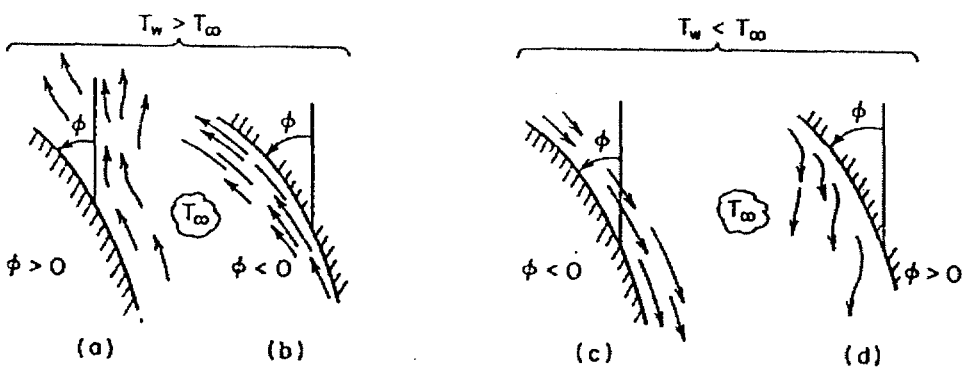

Definition of surface angle ϕ for a heated wall (*a* and *b*), and a cooled wall (*c* and *d*). If the flow is turbulent, *a* and *d* depict detached flow, *b* and *c* attached flow.

4.11.2.6 Inclined Flat Plate, Negative Angled

$$Ra = Gr\ \mathrm{Pr} \quad ; \quad Gr = \frac{g\beta(T_w - T_\infty)L^3}{\nu^2} \times \cos\phi$$

$$Nu_{l,V} = \frac{2.8}{\ln(1 + 2.8/Nu^T)}$$

$$Nu^T = \overline{C}_t\ Ra^{1/4} \qquad , \overline{C}_t = 0.515 \quad \text{for gases [5]}$$

$$Nu_{l,H} = \frac{0.527\,Ra^{1/5}}{[1+(1.9/\mathrm{Pr})^{9/10})^{2/9}}$$

$Nu_l = \max[Nu_{l,V}, Nu_{l,H}]$ Nusselt number for laminar flow

$Nu_t = C_t\ Ra^{1/3}$ Nusselt number for turbulent flow with

$$C_t = C_t^V \cos^{1/3}\phi \quad \text{for} \quad -90^\circ \le \phi \le \tan^{-1}\left(\frac{C_t^V}{C_t^H}\right)^3$$

$$C_t = C_t^H \sin^{1/3}\phi \quad \text{for} \quad \tan^{-1}\left(\frac{C_t^V}{C_t^H}\right)^3 \le \phi \le 90^\circ$$

with $$C_t^V \approx \frac{0.13\,\mathrm{Pr}^{0.22}}{(1+0.61\,\mathrm{Pr}^{0.81})^{0.42}}$$

$C_t^H \approx 0.14$ *for* $\mathrm{Pr} < 100$

$Nu = [(Nu_l)^m + (Nu_t)^m]^{1/m}$ *with* $m = 6$ *for* $1 < Ra < 10^{12}$

$h_c = \frac{Nu\,k}{L}$ with

L = length of the inclined plate
k = air conductivity

The above correlations are incorporated in ANSYS [16] model via macro "HC_IPLD.mac" listed in Appendix 4.16.1.

4.11.2.7 Effective convection Coefficient through Top Heat Shield

Top shield is a louver consists of seven pieces each containing 78 inclined plates. Because of the relative large opening between the plates and the short length of them, the interference of the thermal boundary layers is minimal, so that convection coefficient can be calculated separately for each plate. The total convection from one inclined plate is:

$q_{conv} = (h_{up} + h_{down})A_p(T_p - T_\infty)$

with h_{up} = convection coefficient on upper surface of louver plates (positive angled)
h_{down} = convection coefficient on lower surface of louver plates (negative angled)
plate surface area $Ap = l \times h = 24 \times 2 = 48$ in^2
air temperature $T_\infty = T_g = 178^\circ F$ [see Section 4.13]

h_{up} and h_{down} are calculated using the correlations described above for inclined plates.
The louver is modeled as a flat plat to reduce the number of SHELL57 elements in creation of radiation super-element. To compensate for the reduced area, an effective convection coefficient is calculated for the louver.

$$h_{louver,eff} = (h_{up} + h_{down}) \cdot \frac{A_{\text{louver}}}{A_{\text{model}}}$$

$A_{louver} = n_{louver} \times n_{segments} \times A_p$

n_{louver} = no. of plates in each segment = 78

$n_{segments}$ = no. of segments = 7

$A_{model} = 15'2" \times 6'2" = 14196 \quad in^2$

The above correlations are incorporated in ANSYS [16] model via macro "HC_Louver.mac" listed in Appendix 4.16.1.

4.11.2.8 Effective convection Coefficient for Side Heat Shield with Fins

Cross section of the side heat shield shows that the fin width, W, is much larger than the distance between the parallel fin plates, S. Reference [5] states that when W/S≥5, the convection coefficient through the fins is the same as for the parallel–plate channel shown bellow.

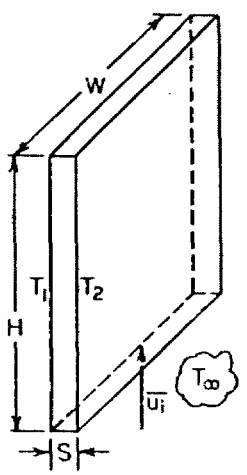

Specified wall temperatures

$$Nu = \frac{qS}{2HW\,(\bar{T}_w - T_\infty)\,k}$$

$$Ra = \frac{g\beta(\bar{T}_w - T_\infty)\,S^3}{\nu a}\,\frac{S}{H}$$

$$Re = \bar{u}_i\,S/\nu$$

$$\bar{T}_w = \frac{1}{2}\,(T_1 + T_2)$$

$$T^* = \frac{T_2 - T_\infty}{T_1 - T_\infty};\ T_1 \geq T_2;\ 0 \leq T^* \leq 1$$

Geometry and nomenclature for natural-convection heat transfer from a wide ($W \gg S$), rectangular cooling slot with temperature-specified conditions on the walls. [5]

The following correlations for parallel-plate channels are specified in Reference [5], when W/S≥5.

W=2.5", S=0.5"

$$Nu \approx \frac{Ra}{24} \qquad \text{for } Ra \leq 10$$

$$Nu = 0.62\,Ra^{1/4} \qquad \text{for } 10 < Ra < 1000$$

$$Nu = \left[\left(\frac{Ra}{24}\right)^m + \left(0.62\,Ra^{1/4}\right)^m\right]^{1/m} \qquad \text{with m=-1.9} \quad \text{for } Ra < 10^5$$

Rayleigh number for the above correlations is defined in above figure. Since the average plate temperature is first unknown, the model is solved iteratively. The final results are:

For off-normal conditions (115°F maximum day temperature):
Average side heat shield temperature = 164°F (retrieved from HSM-H model results)
Average air temperature within HSM = 136°F (Section 4.13)

For off-normal conditions (-20°F minimum temperature):
Average side heat shield temperature = 22°F (retrieved from HSM-H model results)
Average air temperature within the HSM = 3.2°F (Section 4.13)

T_w	T_{amb}	T_{avg}	T_{avg}	k [5]	β	ν [5]	Pr [5]	C_l	Ra	Nu	h_fin
(°F)	(°F)	(°F)	(K)	(W/m-K)	(1/K)	(m^2/s)	(---)	(---)	(---)	(---)	(Btu/hr-in²-°F)
164	136	150	339	0.029	2.95E-03	2.000E-05	0.70	0.514	40.5	1.56	0.0044
22	3.2	13	263	0.023	3.81E-03	1.282E-05	0.72	0.516	87.6	1.90	0.0042

The fins are modeled as a flat plat to reduce the number of SHELL57 elements in creation of radiation super-element. To compensate for the reduced area, an effective convection coefficient is calculated for the fins.

$$h_{fin,eff} = h_{fin} \cdot \frac{A_{fins}}{A_{model}}$$

$$A_{fin} = \left(2\, n_{up} \times 4 + 2 n_{down}\right) H W$$

number of fins at upper half: $n_{up} = (15'2"-4")/(0.5"+0.125") + 1 = 285$ [2]

number of fins at lower half: $n_{down} = (15'2"-44")/(0.5"+0.125") + 1 = 221$ [2]

H= 20"
W = 2.5"

$A_{fin} = 136100$ in²

$A_{model} = [15'2" \times 7'2" + 1'10" \times (15'2" - 2 \times 1'8")] = 18776$ in²

$$h_{fin,eff} = 0.0044 \cdot \frac{136100}{18776} = 0.032$$ Btu/hr-in-°F for 115°F ambient

$$h_{fin,eff} = 0.0042 \cdot \frac{136100}{18776} = 0.031$$ Btu/hr-in-°F for -20°F ambient

The h_{fin} value used in the HSM-H model is 0.030 Btu/hr-in-°F.

Distance between the base plate of the side heat shield and the HSM-H side wall is 2". The base plate and the HSM-H side wall create a narrow channel behind the side heat shield. The convection coefficient for this narrow channel is calculated using the same methodology described above. The dimensions of the narrow channel behind the side heat shield used to calculate the convection coefficient are:

S = 2"
H = 108"
W = 182"

The final surface temperature of the narrow channel is verified after iterative solution of the model. The final results are:

For off-normal conditions (115°F maximum day temperature):
Average nodal temperature of narrow channel = 154°F (retrieved from model results HSM-H)
Entering air temperature into channel = 110°F (Section 4.13)

For off-Normal conditions (-20°F minimum day temperature):
Average nodal temperature of narrow channel = 12.8°F (retrieved from HSM-H model results)
Entering air temperature into channel = -17°F (Section 4.13)

T_w	T_{amb}	T_{avg}	T_{avg}	k [5]	β	ν [5]	Pr [5]	C_l	Ra	Nu	h channel
(°F)	(°F)	(°F)	(K)	(W/m-K)	(1/K)	(m^2/s)	(---)	(---)	(---)	(---)	(Btu/hr-in^2-°F)
154	110	132	329	0.028	3.04E-03	1.90E-05	0.70	0.514	3468	4.75	0.003
12.8	-17	-2	254	0.023	3.93E-03	1.21E-05	0.72	0.516	7600	5.79	0.003

The $h_{channel}$ value used in the HSM-H model is 0.003 Btu/hr-in-°F.

4.12 Effective Conductivity of Air in Closed Cavity of HSM-H

During blockage of the inlet and outlet vents, the air within the HSM-H is trapped. The convection heat transfer under these circumstances reduces to free convection in closed cavities. To simplify the model, an effective conductivity for air is calculated, which includes the conduction and convection heat transfer through the air in the closed cavity of the HSM-H.

Reference [12] introduces the following correlation to calculate the conduction and convection heat transfer in closed cavities for eccentric horizontal cylinders.

$$Nu = [Nu_{COND}, Nu_l]_{max} \qquad (4.12\text{-}1)$$

with q' = heat transfer by conduction and convection from the inner cylinder to the outer one per unit axial length of cylinder

$$Nu_{COND} = \frac{\ln(D_o/D_i)}{\cosh^{-1}[(D_o^2 + D_i^2 - 4E^2)/2D_oD_i]}$$

$$Nu_l = 0.603\,\overline{C}_l \frac{\ln(D_o/D_i)\,Ra^{1/4}}{[(L/D_i)^{3/5} + (L/D_o)^{3/5}]^{5/4}}$$

where $Ra = \frac{g\beta(T_i - T_o)L^3}{\nu^2} \times \Pr$ with $L = (D_o - D_i)/2$ and

$$\overline{C}_l = \tfrac{4}{3}\frac{0.503}{[1 + (0.492/\Pr)^{9/16}]^{4/9}}$$

The geometry and dimensions to use in the correlations are shown in the following figure.

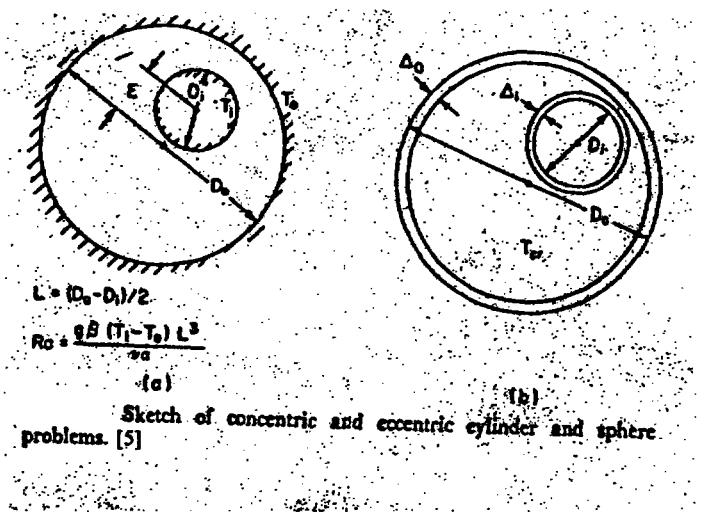

Sketch of concentric and eccentric cylinder and sphere problems. [5]

The Nusselt number (Nu) in correlation (4.12-1) is defined as

$$Nu = \frac{q'\ln(D_o/D_i)}{2\pi(T_i - T_o)k}$$

This implies that the air effective conductivity is equal to the product of Nu and the air conductivity for the closed cavity between cylinders.

$k_{eff} = Nu\ k_w$

k_{eff} = *effective conductivity for conduction and convection from inner to outer cylinder*
k = *conductivity of air*

All air properties are evaluated at average temperature.

$$T_{avg} = (T_o + T_i)/2$$

In order to use the above correlations for the HSM-H cavity, a hydraulic diameter is calculated for the cross section of the HSM-H cavity surrounded by the side and top shields.

$$D_{h,HSM} = \frac{4A}{P} = \frac{4 \times (82.375 \times 168)}{2 \times (82.375 + 168)} = 115"$$

The effective conductivity defined in the above correlations depends on the inner cylinder and outer cylinder temperatures (T_i and T_o) and its gradient. A study of the effect of T_i and T_o on the effective conductivity of air in the closed cavity of the HSM-H is shown in Table 4-20. In the study, the inner temperature T_i varies from 425°F to 825°F, which represents the DSC shell temperature during blockage of the vents. The outer temperature T_o varies from 150°F to 350°F, which represents the heat shield or the concrete temperatures. The gradient between T_i and T_o varies from 275°F to 475°F. As Table 4-20 shows, the effective conductivity of air in the HSM-H closed cavity is relative insensitive to the temperature gradients and its value is about 0.05 Btu/hr-in-°F for all of the studied cases.

The minimum temperature gradient observed in the model occurs between the middle of the side heat shield and the DSC side. The minimum gradient after 48 hour blockage of the vents is:

527 (DSC side-Node # 3929) – 424 (side heat shield-Node # 4038) = 103°F with fins
534 (DSC side-Node # 3929) – 434 (side heat shield-Node # 4038) = 100°F without fins

The maximum temperature gradient occurs between the uncovered top corner of the HSM-H and top of the DSC shell. The maximum gradient after 40 hour blockage of the vents is:

534 (DSC top-Node # 3937) – 265 (HSM corner-Node # 3972) = 269°Fwith fins
541 (DSC side-Node # 3929) – 275 (side heat shield-Node # 4038) = 266°F without fins

The temperature gradients covered in the study are higher than the gradients observed after solving the model. Nonetheless using the calculated value of 0.05 Btu/hr-in-°F for effective air conductivity is acceptable since the concrete temperature is the limiting factor in the blocked vent thermal analysis. Using a higher temperature gradient, which results in a higher air effective conductivity value, increases the heat transfer from the DSC shell to the concrete walls and causes a higher concrete temperature during blockage of the vents.

4.13 Thermal-Hydraulic Equations for the HSM-H

Various bulk temperatures are considered within the HSM-H to apply the convection boundary conditions. Energy and hydraulic equations are combined together to calculate the bulk temperatures in the HSM_H cavity. For this purpose, it is assumed that the total decay heat load will be transferred out of the HSM-H only by free convection to the air flowing through the cavity. Since the thermal conduction through the concrete structure is minimal, this assumption is conservative.

The air flow paths inside the HSM-H are designed, so that the pressure difference due to buoyancy effects is greater than the pressure losses due to friction, area, and flow direction changes. The pressure difference due to buoyancy effect (stack pressure) is driven by the density differences between indoor and outdoor air and is given by:

$$\Delta P_s = (\frac{g}{g_c})(\rho_c - \rho_s)(\Delta h) = (\frac{g}{g_c})(\Delta\rho)(\Delta h)$$

where:

ΔP_s = stack pressure
ρ_c = ambient air density
ρ_s = stack average air density
g = local gravity
g_c = universal gravitational constant
Δh = total height difference between entrance and exhaust vents

The expansion coefficient is defined as follows:

$$\beta = \frac{-1}{\rho}\left(\frac{\partial\rho}{\partial T}\right)_P \qquad \rightarrow \qquad \frac{\Delta\rho}{\rho_s} = \beta \cdot \Delta T_{avg}$$

where:

$\Delta T_{avg} = (T_s - T_c)$
T_c = ambient air temperature (absolute temperature)
T_s = stack average air temperature (absolute temperature)
ρ_s = air density at stack average temperature T_s

Considering air as an ideal gas the expansion coefficient is defined: $\beta = \frac{1}{T}$

Then it follows: $$\frac{\Delta\rho}{\rho_s} = \frac{\Delta T_{avg}}{T_s}$$

Substituting the above equation into stack pressure equation gives:

$$\Delta P_s = \frac{g}{g_c} \cdot \frac{\rho_s}{T_s} \cdot \Delta T_{avg} \cdot \Delta h$$

The dynamic pressure loss is given by:

$$\Delta P_{loss} = \sum(K \cdot \frac{1}{2} \cdot \rho \cdot \frac{V^2}{g_c}) = \sum(K_{Ei} \cdot \frac{1}{2} \cdot \frac{1}{gc \cdot \bar{\rho}} \cdot \frac{\dot{m}_{Ei}^{\ 2}}{A_{Ei}^{\ 2}})$$

where:

ΔP_{loss} = dynamic pressure loss
$\dot{m}_{Ei}$ = air mass flow rate

K_{Ei} = dynamic loss coefficient through a specific flow path

A_{Ei} = cross sectional flow area

$\bar{\rho}$ = average density for the flow path

If the air mass flow rate is equal for all paths, then:

$$\Delta P_{loss} = \frac{\dot{m}_E^{\,2}}{2g_c \cdot \bar{\rho}} \sum \frac{K_{Ei}}{A_{Ei}^{\,2}} \qquad \text{with } \bar{\rho} = (\rho_c + \rho_{exit})/2$$

The energy balance requires:

$$Q = \dot{m}_E \, C_p \, (T_{exit} - T_c) = \dot{m}_E \, C_p \, \Delta T_{HSM}$$

with Q = total decay heat load

Setting ΔP_s equal to ΔP_{loss}, substituting $\dot{m}_E$ from energy balance, and solving for ΔT_{HSM} gives:

$$\Delta T_{HSM} = \left[\frac{T_s \, Q^2}{2\rho_s \, \bar{\rho} \, g \, \Delta h \, C_p^{\,2} \, \Delta T_{avg}} \cdot \sum \frac{K_{Ei}}{A_{Ei}^{\,2}} \right]^{1/2}$$

The dynamic loss coefficients (K_{Ei}) depend on the air velocity (air mass flow rate) and the flow path shape. Iterative solution of the above equation using dynamic loss coefficient correlations gives the ΔT_{HSM} and the T_{exit}. Schematic views of flow paths through the HSM-H module are shown in Figure 4-44.

The stack average air temperature (T_s) in the above equation is considered as the volumetric average temperature within the HSM-H cavity. The HSM-H cavity is divided into eight regions around the DSC circumference for this purpose. These regions are shown in Figure 4-45. The following equation determines the stack average temperature.

$$T_s = \frac{\sum_0^i (T_i * V_i)}{\sum_0^i (V_i)}$$

V_i = Volume of air region i = A_i * L_{DSC}

A_i = Cross sectional are of air region i

= (HSM-H cavity cross sectional area)$_i$ – (DSC cross sectional area)$_i$

For ease of calculation, length of each region is set equal to the overall DSC length (185.25"). Following table show height and area of each air region.

Location	Height	Value (in)	Area	Value (in^2)
Lower part of HSM	L0	71.125	A_0	5859
Region 1	L1	2.655	A_1	171
Region 2	L2	7.560	A_2	323
Region 3	L3	11.314	A_3	276
Region 4	L4	13.346	A_4	192
Region 5	L5	13.346	A_5	192
Region 6	L6	11.314	A_6	276
Region 7	L7	7.560	A_7	323
Region 8	L8	39.780	A_8	3229

It is assumed that the air temperature in region 0 is equal to the average of the ambient temperature and the temperature of the first region. It is also assumed that the temperature rise in region 1 to 8 are equal, so that:

$$T_i = T_{i-1} + (\Delta T_{HSM} / 8)$$

where:

T_i = Temperature of air leaving region i.

The temperature of the air leaving region 8 is equal to the exit air temperature.

The HSM-H is divided into three following sections to calculate the dynamic loss coefficients.

- 1: from air entrance opening to the inlet vent at the lower part of the HSM-H sidewall
- 2: HSM-H cavity from inlet opening to outlet opening
- 3: from outlet opening at the upper part of the HSM-H sidewall to the exhaust opening on the roof.

Each section is divided into subsections. Hydraulic loss coefficients in subsections are calculated using corresponding correlations from [35] and [36]. Serial loss coefficients of subsections are added together to make the equivalent total loss coefficient ($\sum \frac{K_{Ei}}{A_{Ei}^2}$). For calculation of the equivalent loss coefficient for parallel flow paths see footnote on Table 4-21. Table 4-21 summarizes the results for 34.8 kW decay heat load. The results for 32.0 kW and 26.1 kW decay heat loads are listed in Tables 4-22 and 4-23 respectively.

4.14 Thermal Evaluation of DSC Containing Damaged Fuel

Maximum 16 damaged fuel assemblies can be stored in the basket of the NUHOMS®-32PTH DSC. Damaged fuel is defined as fuel assemblies with one or more non-adjacent damaged grid spacer(s) and /or containing fuel rods with known or suspected cladding defects greater than hairline cracks or pinhole leaks. Missing cladding and/or crack size in the fuel pins is to be limited such that a fuel pellet is not able to pass through the gap created by the cladding opening during handling. Retrievability of the damaged fuel must be assured following normal and off-normal conditions.

Location of the damaged fuel assemblies in the 32PTH DSC basket is shown in Figure 4-46. To ensure the retrievibility of the fuels, the maximum cladding temperature of the intact fuel rods must remain below the allowable temperature limits established in [2].

Thermal analyses of the 32PTH DSCfor normal and off-normal conditions (Section 4.3) show that the fuel cladding temperature has the highest value during transfer operation. For the accident conditions also, the maximum fuel temperature is resulted for transfer operation (Section 4.4). Hence, transfer conditions are considered to evaluate the effects of the damaged fuel assemblies on the thermal performance of NUHOMS-32PTH System.

4.14.1 Normal / Off-Normal Conditions

The 32PTH DSC model described in Section 4.3 is used for this evaluation. Loading configuration 1 and maximum heat load of 34.8 kW are considered to analyze the transfer operation with 16 damaged fuel assemblies in the DSC. Identical decay heat profiles from Section 4.7 are considered for both the damaged and the intact fuel assemblies for this analysis. Due to these conditions, the heat flux on the transfer cask inner shell remains unchanged in comparison to values discussed in Section 4.3. Therefore, the DSC shell temperatures resulted from the transfer cask model in Section 4.3 is applicable to the DSC model containing 16 damaged fuel assemblies.

Transverse effective conductivity for the damaged fuel is discussed in Section 4.14.3. To bound the reduction in axial conductivity of damaged fuel due to the cladding defects, the axial effective conductivity of the fuel calculated in Section 4.8 is decreased by 10% to use for the damaged fuel elements. All other material properties remain the same as those described in Section 4.3. The model is run steady state to determine the maximum temperature of the intact fuel.

4.14.2 Accident Conditions

Due to presence of damaged fuel assemblies, an extra hypothetical accident case is considered foe evaluation. Although unlikely, but it is postulated that the defected cladding of damaged fuel assemblies might break entirely in consequence of a drop accident. In that event, the fuel pellets could be released in the compartment space. The end caps will hold the fuel rubble within the compartment volume, though the decay heat profile is changed subsequently.

The concentration of the decay heat for the rubble fuels is maximized, when all the rubble are compressed to a minimum height at one end of the fuel compartment.

To bound the maximum cladding temperature of the intact fuel assemblies, it is assumed that all the 16 damaged fuel assemblies transform to rubble. The cladding is considered as powder but the pellets are assumed to keep their shape in the rubble. An approximate void volume between the pellets can be evaluated considering the area ratio of the pellet cross-section to the square area with a width equal to the pellet outer diameter. The increased volume due to the void spaces between pellets is then:

$$\{(OD_{pellet}^2 - \pi\, OD_{pellet}^2 / 4) / (\pi\, OD_{pellet}^2 / 4)\} \times 100 = (4/\pi - 1) \times 100 = 27.32\ \%$$

The minimum height of the fuel rubble is calculated as follows.

$$H_{min} = \frac{V_{UO2} \times 1.2732 + V_{Zr4}}{A}$$

where

A = cross-sectional area of the fuel compartment = $8.7 \times 8.7 = 75.69$ in^2
V_{UO2} = volume of fuel pellets from Section 4.8
V_{Zr4} = volume of fuel cladding from Section 4.8

Table 4-24 summarizes the calculation of H_{min} for all the fuel types. The shortest height of 61" is considered for the fuel rubble.

Thermal model of the transfer cask described in Section 4.3 is modified for the purpose of the evaluation. It is assumed that the seals of transfer cask and the shielding shell will be damaged in the consequence of the hypothetical drop accident. In this event, the helium in the annulus and the water in the shielding shell will be released to the ambient. To evaluate the thermal effects of this accident, the transfer cask model developed in Section 4.3 is used to determine the DSC shell temperature when the DSC contains fuel rubble. Helium conductivity in the annulus is replaced with air conductivity. The effective conductivity in the shielding panel is also recalculated based on air properties.

To stabilize the ANSYS run and shorten the run time, the LINK31 elements simulating the radiation between the DSC and transfer cask are replaced with equivalent effective conductivity. Calculations of the effective conductivities for air in annulus and in the shielding shell are based on the methodologies described in Section 4.9. The equivalency of the applied effective conductivities to the radiation elements (LINK31) is verified on hand comparison of the maximum temperatures resulted from separate runs of the transfer cask slice model using LINK31 elements and equivalent effective conductivities.

Steady state boundary conditions are considered to run the transfer cask model. Total heat load of 34.8 kW is applied uniformly on the DSC inner radial surface. The resultant DSC shell temperatures are transferred then to the DSC model to determine the maximum fuel temperature for this accident case.

The 32PTH DSC model described in Section 4.3 is also slightly modified to include the fuel rubble. The height of the elements in the core compartments are adjusted, so that a region with the height of 61" (H_{min}) is created. This region is assigned as fuel rubble region. All the elements beyond the fuel rubble region, which previously represented homogenized fuel within the core compartments, are deleted. The decay heat load of the damaged fuel assemblies are applied as a uniform heat generation rate without peaking factor to the elements in the fuel rubble region. Thermal properties of helium are considered for the elements representing the fuel rubble to eliminate the uncertainties regarding the fuel rubble conductivity. The decay heat profile from Section 4.7 is considered for the intact fuels in the peripheral compartments for this analysis. The DSC model is run steady state to determine the maximum component temperatures.

Except for those mentioned above, the geometry and material properties of all the other elements in the DSC and the transfer cask models remain unchanged.

In the drop accident case considered above, it was assumed that the liquid neutron shield and the helium in the transfer cask were lost. Since the 15 min fire has only a short term effect on the neutron shield panel as shown in Figure 4-29, and the transfer cask and the DSC models are run steady state, the drop accident case bounds the fire accident case temperatures.

4.14.3 Effective Properties of Damaged Fuel

Defected spacer or grids might change the fuel rod pitch and hence change the effective fuel conductivity. It is assumed that the fuel rods in the assembly with defected grids can move in axial and in transverse directions. The axial moving of the fuel rods has no impact on the thermal conductivity in either direction. To determine the impact of the transverse moving on the fuel effective conductivity, the fuel assemblies WE 17x17 OFA and Framatome17x17 MK BW are investigated. The reason to investigate these assemblies is that the intact assembly WE 17x17 OFA has the lowest transverse conductivity in temperature range from 100 to 700°F and the intact assembly 17x17 MK BW has the lowest transverse conductivity for temperatures higher than 700°F as shown in Section 4.8.

For the investigation, the effective transverse fuel conductivity is determined using the same methodology described in Section 4.8.

The effect of the transverse moving of the fuel rods is investigated by changing the pitch size of the fuel rods. The pitch size is changed from the minimum closest packed pitch to the maximum most spread out pitch. A 0.01" gap has been added to the minimum and maximum pitch to account for contact resistance. Typical finite element models of reconfigured fuel assemblies are shown in Figure 4-47.

Each pitch is evaluated for two different compartment wall temperatures and then the average conductivity is determined. Compartment wall temperatures of 200°F and 300°F are considered for various pitch sizes of WE 17x17 OFA assembly. For 17x17 MK BW assembly, compartment wall temperatures of 700°F and 800°F are considered. The effective transverse conductivities are interpolated to average temperatures of 300°F for WE 17x17 OFA and 800°F for 17x17 MK BW.

The results of the investigation are summarized in Table 4-25 and plotted in Figure 4-48. As Figure 4-48 shows, the minimum transverse conductivities occur at a pitch sizes of 0.387" for WE 17x17 OFA and 0.402" for 17x17 MK BW.

Finite element models of WE 17x17 OFA and 17x17 MK BW with minimum conductivity pitch sizes are created to determine the minimum effective transverse conductivity of reconfigured fuel for the temperature range of 100 to 1000°F. The results are listed in Table 4-26 and plotted in Figure 4-49. WE 17x17 OFA assembly provides lower transverse conductivities for the entire temperature range. Following values calculated for reconfigured WE 17x17 OFA are used in the model for the effective transverse conductivity of damaged fuel.

Temperature (°F)	Transverse Effective Conductivity (Btu/hr-in-°F)
150	0.0138
243	0.0161
337	0.0187
432	0.0217
527	0.0252
624	0.0290
721	0.0331
818	0.0376
916	0.0426
1014	0.0481

Reconfiguration of the fuel rods as a consequence of damaged grids does not have any impact on the other effective fuel properties such as density, specific heat, and axial conductivity.

4.14.4 Evaluation of DSC Thermal Performance with Damaged Fuel

To establish the heat removal capability and the integrity of the intact fuel cladding, maximum fuel cladding temperature limit of 752°F is considered for normal / off-normal transfer conditions [2]. For the accident conditions, a maximum fuel cladding temperature limit of 1058°F is considered [2].

Temperature distributions for the normal / off-normal, and accident cases are shown in Figures 4-50 and 4-51. A comparison between the maximum component temperatures resulted for a DSC with 32 intact fuel assemblies and a DSC with 16 damaged fuel assemblies are shown in Table 4-27.

As Table 4-27 shows, the maximum fuel cladding temperature remains below the allowable limit for the DSC containing 16 damaged fuel assemblies. The basket temperature increases only by 3°F for this case. Regarding the margin to the allowable limit this temperature increase is not significant. Similar behavior is expected for storage conditions.

The maximum temperature of intact fuels, when the damaged fuel is transformed to rubble in consequence of an accident is lower than the maximum fuel temperature resulted from fire accident case with 32 intact fuel assemblies.

Due to the increased fuel and basket temperatures during transfer of damaged fuel, the inner DSC pressure increases in comparison to transfer of 32 intact fuel assemblies. Using the same methodology as described in section 4.6, the internal pressure of DSC containing damaged fuels is calculated. The results of pressure calculation are shown in Table 4-28. As Table 4-28 shows, the DSC pressure increase due to transfer of damaged fuels is minimal (about 0.1 psi). Similar behavior is expected to occur for the normal / off-normal storage conditions.

Table 4-27 shows that the maximum fuel and basket temperatures drop when the damaged fuel is transformed to rubble in consequence of an accident. Therefore, the 32PTH DSC inner pressure in this case is bounded by the pressure calculated for the fire accident case in Section 4.6.

4.15 References

1. Cogema Logistics, "Qualification du Materiau Vyal B", Rapport d'essaias n° 99 023-1
2. USNRC, SFPO, Interim Staff Guidance – 11, Rev. 3, "Cladding Considerations for the Transportation and Storage of Spend Fuel"
3. Perry, R. H., Chilton, C. H., "Chemical Engineers' Handbook", 5th Edition, 1973
4. USDOE, "Topical Report on Actinide-Only Burnup Credit for PWR Spent Nuclear Fuel Packages", Department of Energy, Report No. DOE / RW0472, Rev. 2, 1998
5. Rohsenow, W. M., Hartnett, J. P., Ganic, E. N. , "Handbook of Heat Transfer Fundamentals", 2nd Edition, 1985
6. ASME Boiler and Pressure Vessel Code, Section II, Part D, "Material Properties", 1998 and 2000 addenda
7. Issard, Herve, "ACL Progress on Boralyn Development", Cogema Logistics presented in "Transnuclear Group Technical Exchange Meeting", October 11, 2002
8. Final Documentation Package TN-68, P.O. # EP-2001-022, Section G, "Thermal Conductivity Measurements of Borated Aluminum Specimens", Rev. 0
9. AAR Brooks & Perkins Advanced Structures Division, "Boral® The Neutron Absorber – Product Performance", Report 624
10. Zoldners, N. G., "Thermal Properties of Concrete under Sustained Elevated Temperatures", ACI Publications, Paper SP 25-1, American Concrete Institute, Detroit, MI, 1970
11. Cavanaugh, Kevin, "Guide to Thermal Properties of Concrete and Masonary Systems", Reported by ACI Committee 122, Report # ACI 122R-02, American Concrete Institute, Detroit, MI, 2002
12. Bentz, D. P., "A Computer Model to Predict the Surface Temperature and Time-of-wetness of Concrete Pavements and Bridge Decks", Report # NISTIR 6551, National Institute of Standards and Technology, 2000
13. Siegel, Robert, Howell, R. H., "Thermal Radiation Heat Transfer", 4th Edition, 2002
14. Azzazy Technology Inc., "Emissivity Measurements of 304 Stainless Steel", Report Number ATI-2000-09-601, 2000
15. Kreith, Frank, "Principles of Heat Transfer", 3rd Edition, 1973
16. ANSYS Computer Code and User's Manuals, Rev. 6.0
17. USNRC, Code of Federal Regulations, Part 71, "Packaging and Transportation of Radioactive Material", 2003
18. "ASHRAE Handbook Fundamentals", 4th Edition, 1983
19. Transnuclear, Inc., "Standardized NUHOMS® Horizontal Modular Storage System for Irradiated Nuclear Fuel", Final Safety Analysis Report, Rev. 7
20. Viebrock, J. M., Douglas, H. M., "Domestic Light Water Reactor Fuel Design Evolution", Vol. III, Nuclear Assurance Corporation, 1981
21. American Concrete Institute, "Code Requirements for Nuclear Safety Related Concrete Structures (ACI-349-01) and Commentary (ACI 349R-01)", 2001
22. USNRC, SFPO, NUREG-1536, "Standard Review Plan for Dry Cask Storage Systems - Final Report", 1997.
23. Gregory, J. J., Mata, R., Keltner, N. R., "Thermal Measurements in a Series of Long Pool Fires", SANDIA Report, SAND 85-0196, TTC-0659,1987
24. Parker O-Ring Handbook, 5700, Y2000 Edition, 1999

25. NUREG/CR-0497, "A Handbook of Materials Properties for Use in the Analysis of Light Water Reactor Fuel Rod Behavior", MATPRO - Version 11, EG&G Idaho, Inc., TREE-1280, 1979
26. Chun, R., Witte, M., Schwartz, M., "Dynamic Impact Effects on Spent Fuel Assemblies", Lawrence Livermore National Laboratory, Report UCID-21246, 1987
27. Young, W. C., "Roark's Formulas for Stress and Strain", 6th Edition, 1989
28. Plannel, et. al., "Extended Fuel Burnup Demonstration Program – Topical Report – Transport Considerations for Transnuclear Casks", DOE/ET 34014-11, TN-E4226, Transnuclear, Inc. 1983
29. Brookmire, et. al., "Storage of Burnable Poison Rod Assemblies and Thimble Plug Devices in Dry Storage Casks Surry ISFSI", NE-1162, Rev. 0, 1998
30. Oak Ridge National Laboratory, RSIC Computer Code Collection, "SCALE, A Modular Code System for Performing Standardized Computer Analysis for Licensing Evaluation for Workstations and Personal Computers", NUREG/CR-0200, Rev. 6, ORNL/NUREG/CSD-2/V3/R6
31. USNRC, SFPO, NUREG/CR-0497, "A Handbook of Materials Properties for Use in the Analysis of Light Water Reactor Fuel Rod Behavior", MATPRO - Version 11, EG&G Idaho, Inc., TREE-1280, 1979
32. SANDIA Report, SAND90-2406, "A Method for Determining the Spent Fuel Contribution to Transport Cask Containment Requirements", 1992.
33. Diament, R.M.E., "Thermal and Acoustic Insulation", 1986
34. Kreith, Frank, "The CRC Handbook of Thermal Engineering", 2000
35. "ASHRAE Handbook, Fundamentals" – SI Edition, 1997
36. I.E. Idelchik, "Handbook of Hydraulic Resistance", 3rd Edition, 1994

4.16 Appendices

The ANSYS [16] macros for

- Calculation of heat transfer coefficients,
- Creation of the radiation LINK31 elements between the DSC shell and the transfer cask inner shell and
- Transferring of the nodal temperatures from the transfer cask or the HSM-H model to the DSC model

are listed in Appendix 4.16.1.

The calculation of the heat generation rates as a function of fuel parameters is shown in Appendix 4.16.2.

Table 4-1
Maximum Component Temperatures during Transfer Operations at 115°F ambient

Component	Maximum Temperature (°F)	Allowable Maximum Temperature (°F)
DSC shell	475	
Cask inner shell	340	
Lead gamma shielding	337	621 [3]
Cask structural shell	280	
Neutron shield panel	263	
Cask lid inner plate *	275	
Cask lid outer plate	217	
Solid neutron shield	265	320 [1]
Cask lid seal †	240	400 [24]
Bottom plate seal ‡	255	400 [24]
Liquid neutron shield (Bulk temperature) §	265	
Liquid neutron shield (Maximum temperature)	275	

	Maximum Temperature (°F)					Allowable Max. Temp. (°F)
Basket Type	Type I				Type II	
Component	Conf. # 1	Conf. # 2	Conf. # 3	Conf. # 4	Conf. # 1	
Fuel cladding	719	705	700	715	723	752 [2]
Fuel compartment	693	667	673	689	697	
Basket Al plates	692	666	672	688	696	
Basket rails	561	559	559	558	561	

* Temperatures of cask lid, solid neutron absorber, and seals are from the transfer cask sub-models.
† Maximum temperature of cask body at seal location
‡ Maximum temperature of ram access ring at seal location
§ Bulk temperature is the volumetric average temperature of the elements in shielding segments 8 and 9, see Figure 4-2.

Table 4-2
Maximum Component Temperatures for Storage Conditions at 115°F ambient

HSM-H with Finned Aluminum Side Heat Shields		
Component	**Maximum Temperature @ 34.8 kW (°F)**	**Allowable Max. Temp. (°F)**
Fuel cladding	684	752 [2] *
Fuel compartment	656	
Basket Al plates	655	
Basket rails	511	
DSC shell	422	
Concrete structure	190	200-300 †
Top heat shield	183	
Side heat shield	173	
DSC supporting structure	261	

	Unfinned Aluminum Side Heat Shields @ 32.0 kW	Unfinned Galvanized Steel Side Heat Shields @ 26.1 kW	
Component	**Maximum Temperature (°F)**	**Maximum Temperature (°F)**	**Allowable Max. Temp. (°F)**
Fuel cladding	‡	‡	752 [2] †
DSC shell	414	384	
Concrete structure	202	201	200-300 ‡
Top heat shield	181	173	
Side heat shield	228	180	
DSC supporting structure	256	237	

* The ambient temperature of 115°F is the maximum off-normal temperature. Based on reference [2], maximum allowable fuel cladding temperature is 1058°F (570°C) for off-normal storage conditions and 752°F (400°C) for normal storage conditions. The maximum fuel cladding temperatures in Table 4-2 are all below 752°F.

† For concrete temperatures below 200°F in normal or off-normal conditions no tests of concrete strength are required. For concrete temperatures above 200°F but lower than 300°F no tests to verify capability for elevated temperatures or reduction of concrete strength are required, if the cement type and concrete aggregates are selected based on the guidelines in NUREG 1536, Section V.2 [22]

‡ Bounded by 34.8 kW case in the upper part of the table

Table 4-3
Maximum Component Temperatures during Transfer Operations
at -20°F ambient

Component	Maximum Temperature (°F)
Fuel cladding	650
Fuel compartment	620
Basket Al plates	619
Basket rails	487
DSC shell	398
Cask inner shell	249
Lead gamma shielding	245
Cask structural shell	178
Neutron shield panel	157
Cask lid inner plate	76
Cask lid outer plate	65
Solid neutron shield	97
Cask lid seal	88
Cask bottom plate seal	70
Liquid neutron shield (Bulk temperature)	162
Liquid neutron shield (Maximum temperature)	172

Table 4-4
Maximum Component Temperatures for Storage Conditions
at -20°F ambient, 34.8 kW

HSM-H with Finned Aluminum Side Heat Shields	
Component	**Maximum Temperature (°F)**
Fuel cladding	596
Fuel compartment	565
Basket Al plates	564
Basket rails	418
DSC shell	319
Concrete structure	44
Top heat shield	38
Side heat shield	30
DSC supporting structure	130

Table 4-5
Maximum Component Temperatures for Fire Accident Case
Transfer Cask, 34.8 kW

Component	Maximum Temperature (°F)	Time (hr)	Allowable Max. Temp. (°F)
Fuel cladding	1036	200	1058 [2]
Basket Al plates	1021	200	
Basket rails	878	200	
DSC shell	790	200	
Gamma shell (lead)	618	200	
Cask structural shell	553	200	
Shielding shell	598	0.25	

Table 4-6
Maximum Component Temperatures for Blocked Vent Accident Case

	Max. Temp (°F) HSM-H with Finned Aluminum Side Heat Shields, 34.8 kW		Allowable Max. Temp. (°F)
Component	34 hours after complete blockage	48 hours after complete blockage	
Fuel Cladding	773	796	1058 [2]
Fuel Compartment	749	774	
Basket Al Plates	749	773	
Basket Rails	605	631	
DSC Shell	511	537	
Concrete Structure	347	392	350 [21]*
Top Heat Shield	285	317	
Side Heat Shield	385	424	
DSC support Str.	461	487	

* Capability of concrete will be verified at elevated temperatures above 350°F via test, if applicable.

Table 4-7
Average Heat up Rates

Average Heat up Rate of Transfer Cask and DSC with Water in DSC

Component	Volume (in^3)	Mass (lbm)	C_p (Btu/lbm-°F)	C_p x M (Btu/°F)
Fuel Assemblies	148488	50720	0.06 *	3043
DSC w/o cover pl.	89838	26053	0.114 †	2970
Basket,ss	75928	22019	0.114	2510
Basket,Al	79952	7835	0.216 ‡	1692
TC,ss	149276	43290	0.114	4935
TC,resin	8927	579	0.256 §	148
TC,lead	152121	62369	0.030 **	1871
Tc,water	234294	8458	1.0 ††	8458
Water in DSC	308146	11124	1.0	11124
Water in annulus	15350	554	1.0	554
Total	1262320	233002		37306

$$\overline{C}_p = \frac{37306}{233002} = 0.160 \text{ Btu/lbm-°F,} \quad \text{heat up rate} = \frac{118748}{(233002 \times 0.16)} = 3.2 \text{ °F/hr}$$

Average Heat up Rate of Transfer Cask and DSC without Water in DSC

Component	Volume (in^3)	Mass (lbm)	C_p (Btu/lbm-°F)	C_p x M (Btu/°F)
Fuel Assemblies	148488	50720	0.06	3043
DSC w/o cover pl.	89837	26053	0.114	2970
Basket,ss	75928	22019	0.114	2510
Basket,Al	79952	7835	0.216	1692
TC,ss	149276	43290	0.114	4935
TC,resin	8927	579	0.256	148
TC,lead	152121	62369	0.030	1871
Tc,water	234294	8458	1.0	8458
Water in DSC	0	0	1.0	0
Water in annulus	14358	518	1.0	518
Total	953181	221841		26146

$$\overline{C}_p = \frac{26146}{221841} = 0.118 \text{ Btu/lbm-°F,} \quad \text{heat up rate} = \frac{118748}{(221841 \times 0.118)} = 4.5 \text{ °F/hr}$$

* Effective Cp of fuel assembly at 400°F from Section 4.8
† Cp of SA240, type 304 at 100°F from [6]
‡ Cp of Aluminum at 100°F from [6]
§ Cp of solid neutron absorber at 104°F from [1]
** Cp of lead from [3]
†† Cp of water from Section 3

Table 4-8
Maximum Temperatures During Vacuum Drying Process

Component	Procedure A* T_{max} (°F)	Procedure B† T_{max} (°F)	Procedure B‡ T_{max} (°F)	Procedure C§ T_{max} (°F)	Allowable Limit (°F)
Fuel assembly	732	686	744	735	752 [2]
Basket Al plates	695	640	724	713	---
Basket rails	529	530	597	587	---
DSC shell	218	364	518	511	---
TC inner shell	215	199	272	275	---
Lead gamma shield	214	197	269	271	---
TC Structural shell	186	168	212	217	---
Liquid neutron shield - T_{max}	183	166	207	212	---
Liquid neutron shield – T_{bulk}	180	162	200	206	---
Neutron shield panel	177	160	197	202	---

Table 4-9
Maximum Decay Heat Load Without Time Limitation for Vacuum Drying

	Max. Decay Heat Load (kW)	Max. Fuel Assembly Temperature (°F)	Allowable Limit (°F)
Procedure A	23.2	736	752 [2]
Procedure B	16.0	745	752 [2]
Procedure C	22.4	742	752 [2]

* 36 hours after complete drainage of water from the DSC
† 28 hours after complete drainage of the DSC water or 14 hours after drainage of the annulus water, whichever is the limiting time
‡ 12 after completion of the vacuum drying
§ 42 hours after complete DSC drainage or 28 hours after drainage of the annulus water, whichever is the limiting time

Table 4-10
32PTH DSC Internal Pressure

Operating Condition Without BPRA		n_{back}	f_B	n_{free}	n_{total}	$\overline{T}_{DSC}$	P_{DSC}		Design Pressure
		(lbmoles)	(—)	(lbmoles)	(lbmoles)	(°F)	(psia)	(psig)	(psig)
Storage	Normal	0.326	0.01	0.721	0.333	515	19.5	4.8	15
	Off-Normal	0.326	0.1	0.721	0.398	515	23.3	8.6	20
	Accident	0.326	0.1	0.721	0.398	631	26.1	11.4	70
Transfer	Normal	0.326	0.01	0.721	0.333	537	20.0	5.3	15
	Off-Normal	0.326	0.1	0.721	0.398	537	23.9	9.2	20
	Accident	0.326	1.0	0.721	1.047	961	89.5	74.8	120

Operating Condition With BPRA		n_{back}	f_B	n_{free}	n_{total}	$\overline{T}_{DSC}$	P_{DSC}		Design Pressure
		(lbmoles)	(—)	(lbmoles)	(lbmoles)	(°F)	(psia)	(psig)	(psig)
Storage	Normal	0.326	0.01	0.849	0.334	515	20.6	5.9	15
	Off-Normal	0.326	0.1	0.849	0.411	515	25.4	10.7	20
	Accident	0.326	0.1	0.849	0.411	631	28.4	13.7	70
Transfer	Normal	0.326	0.01	0.849	0.334	537	21.1	6.4	15
	Off-Normal	0.326	0.1	0.849	0.411	537	25.9	11.2	20
	Accident	0.326	1.0	0.849	1.175	961	105.7	91.0	120

Table 4-11
Average Peaking Factors

	Height from Bottom of Active Fuel (in)	P_i [4]	P_i (interpolated)	A_i	$P_{avg,i}$
1	0	0.000			
	1.32		0.215	0.142	0.107
2	4.00	0.652			
	7.0675		0.773	3.346	0.582
3	12.00	0.967			
	14.5		1.000	6.751	0.908
4	20.00	1.074			
	22.0675		1.081	7.933	1.048
5	27.99	1.103			
6	36.00	1.108			
	37.0675		1.108	16.506	1.100
7	44.01	1.106			
8	52.00	1.102			
	57.69		1.098	22.766	1.104
9	60.00	1.097			
	66.9425		1.094	10.143	1.096
10	68.00	1.094			
11	76.00	1.094			
	82.0675		1.095	16.549	1.094
12	84.00	1.095			
13	92.00	1.096			
	97.0675		1.095	16.432	1.095
14	99.99	1.095			
15	108.00	1.086			
	111.943		1.073	16.191	1.088
16	116.01	1.059			
	121.26		1.001	9.743	1.046
17	124.00	0.971			
	127.068		0.882	5.543	0.955
18	132.00	0.738			
	136.26		0.591	6.826	0.743
19	140.00	0.462			
	144		0.000	2.892	0.374
20	144.00	0.000			

Table 4-12
Characteristics of Fuel Assemblies

Fuel Type	WE 15x15	WE 17x17 Standard/ Vantage 5H	Framatome 17x17 MK BW	WE 17x17 OFA
Active fuel length	142-144	144	144	144
Pellet OD	0.3649-0.3669	0.3225	0.3195	0.3088
Rod OD	0.422	0.374	0.374	0.360
Clad wall thickness	0.0243	0.0225	0.0240	0.0225
Rod pitch	0.563	0.496	0.496	0.496
No. of fuel rods	204	264	264	264
No. of Guide/Instrument tubes	21	25	25	25
Guide tube OD	0.484-0.545	0.429-0.482	0.482	0.429-0.482
Guide tube wall thickness	0.015	0.016	0.016	0.016
Instrument tube OD	0.545	0.474-0.545	0.482	0.474-0.545
Instrument tube wall thickness	0.015	0.015-.016	0.016	0.015-.016

All Dimensions are in inches

Table 4-13
Effective Fuel Properties

Transverse Effective Fuel Conductivity in Helium

Fuel Type	WE 15x15			WE 17x17 Std		
T_o (°F)	T_c (°F)	T_{avg} (°F)	k (Btu/hr-in-°F)	T_c (°F)	T_{avg} (°F)	k (Btu/hr-in-°F)
100	172	136	0.0194	171	136	0.0194
200	261	231	0.0230	261	231	0.0226
300	352	326	0.0269	352	326	0.0266
400	445	423	0.0311	445	423	0.0307
500	538	519	0.0368	539	520	0.0354
600	633	617	0.0424	633	617	0.0418
700	729	714	0.0490	729	715	0.0476
800	825	813	0.0560	825	813	0.0552
1000	1019	1010	0.0737	1019	1010	0.0727
Q_{react} (Btu/hr-in)	4.751			4.685		
Q (Btu/hr) / kW	2699 / 0.8			2699 / 0.8		

Fuel Type	17x17MK BW			WE 17x17 OFA		
T_o (°F)	T_c (°F)	T_{avg} (°F)	k (Btu/hr-in-°F)	T_c (°F)	T_{avg} (°F)	k (Btu/hr-in-°F)
100	170	135	0.0197	173	137	0.0189
200	260	230	0.0230	262	231	0.0223
300	352	326	0.0266	353	327	0.0260
400	445	423	0.0307	445	423	0.0307
500	539	520	0.0354	539	520	0.0354
600	633	617	0.0418	633	617	0.0418
700	729	715	0.0476	729	715	0.0476
800	825	813	0.0552	825	813	0.0552
1000	1020	1010	0.0690	1019	1010	0.0727
Q_{react} (Btu/hr-in)	4.685			4.685		
Q (Btu/hr) / kW	2699 / 0.8			2699 / 0.8		

Transverse Effective Fuel Conductivity for Vacuum Conditions

Fuel Type	WE15x15			WE 17x17 Std		
T_o (°F)	T_c (°F)	T_{avg} (°F)	k (Btu/hr-in-°F)	T_c (°F)	T_{avg} (°F)	k (Btu/hr-in-°F)
100	272	186	0.0081	275	188	0.0079
200	336	268	0.0103	340	270	0.0099
300	408	354	0.0130	411	356	0.0124
400	486	443	0.0163	489	445	0.0155
500	569	535	0.0203	572	536	0.0192
600	656	628	0.0250	658	629	0.0238
700	746	723	0.0304	748	724	0.0288
800	838	819	0.0368	839	820	0.0354
Q_{react} (Btu/hr-in)	4.685			4.685		
Q (Btu/hr) / kW	2699 / 0.8			2699 / 0.8		

Fuel Type	17x17MK BW			WE 17x17 OFA		
T_o (°F)	T_c (°F)	T_{avg} (°F)	k (Btu/hr-in-°F)	T_c (°F)	T_{avg} (°F)	k (Btu/hr-in-°F)
100	276	188	0.0078	275	188	0.0079
200	340	270	0.0099	339	270	0.0099
300	412	356	0.0123	410	355	0.0126
400	490	445	0.0153	488	444	0.0157
500	572	536	0.0192	570	535	0.0197
600	659	630	0.0234	657	629	0.0242
700	748	724	0.0288	746	723	0.0300
800	840	820	0.0345	838	819	0.0363
Q_{react} (Btu/hr-in)	4.685			4.685		
Q (Btu/hr) / kW	2699 / 0.8			2699 / 0.8		

Table 4-13 – Continued
Effective Fuel Properties

Axial Effective Fuel Conductivity in Helium or Vacuum

Fuel type	WE 15x15	WE 17x17 Standard/ Vantage 5H	Framatome 17x17 MK BW	WE 17x17 OFA
No of fuel rods	204	264	264	264
OD fuel rod (in)	0.422	0.374	0.374	0.360
Clad thickness (in)	0.0243	0.0225	0.0240	0.0225
No of guides tubes	20	24	24	24
OD guide tubes (in)	0.484	0.429	0.482	0.429
Wall thickness (in)	0.015	0.016	0.016	0.016
No of Instrument tubes	1	1	1	1
OD Instrument tube (in)	0.545	0.474	0.482	0.474
Wall thickness (in)	0.015	0.015	0.016	0.015

Fuel type	WE 15x15	WE 17x17 Standard/ Vantage 5H	Framatome 17x17 MK BW	WE 17x17 OFA
Cladding area (in^2)	6.66	7.08	7.55	6.82
Compartment area (in^2)	75.69	75.69	75.69	75.69
Temperature	k-axial	k-axial	k-axial	k-axial
(°F)	(Btu/hr-in-°F)	(Btu/hr-in-°F)	(Btu/hr-in-°F)	(Btu/hr-in-°F)
212	0.0576	0.0612	0.0653	0.0590
392	0.0606	0.0644	0.0687	0.0620
572	0.0644	0.0685	0.0730	0.0659
752	0.0695	0.0739	0.0788	0.0711
932	0.0763	0.0811	0.0865	0.0781
1112	0.0852	0.0905	0.0966	0.0872

Table 4-13 – Continued
Effective Fuel Properties

Effective Fuel Density

Fuel Type	WE 15x15	WE 17x17 Std	17x17 MK BW	WE 17x17 OFA
No of fuel rods	204	264	264	264
OD fuel rod (in)	0.422	0.374	0.374	0.360
Clad thickness (in)	0.0243	0.0225	0.0240	0.0225
No of guides tubes	20	24	24	24
OD guide tubes (in)	0.484	0.429	0.482	0.429
Wall thickness (in)	0.015	0.016	0.016	0.016
No of Instrument tubes	1	1	1	1
OD Instrument tube (in)	0.545	0.474	0.482	0.474
Wall thickness (in)	0.015	0.015	0.016	0.015
Active fuel length (in)	142	144	144	144
Pellet OD (in)	0.3649	0.3225	0.3195	0.3088
Fuel Type	**WE 15x15**	**WE 17x17 Std**	**17x17 MK BW**	**WE 17x1 7OFA**
Cladding area (in^2)	6.66	7.08	7.55	6.82
Cladding volume (in^3)	946	1019	1088	982
Pellet area (in^2)	21.33	21.57	21.17	19.77
UO_2 volume (in^3)	3029	3105	3048	2847
ρ eff (lbm/in^3)	0.1325	0.1350	0.1344	0.1248

Effective Specific Heat of Fuel

Fuel Type	WE 15x15	WE 17x17 Std	17x17 MK BW	WE 17x17 OFA
No of fuel rods	204	264	264	264
OD fuel rod (in)	0.422	0.374	0.374	0.360
Clad thickness (in)	0.0243	0.0225	0.0240	0.0225
No of guides tubes	20	24	24	24
OD guide tubes (in)	0.484	0.429	0.482	0.429
Wall thickness (in)	0.015	0.016	0.016	0.016
No of Instrument tubes	1	1	1	1
OD Instrument tube (in)	0.545	0.474	0.482	0.474
Wall thickness (in)	0.015	0.015	0.016	0.015
Active fuel length (in)	142	144	144	144
Pellet OD (in)	0.3649	0.3225	0.3195	0.3088
	WE 15x15	**WE 17x17 Std**	**17x17 MK BW**	**WE 17x17 OFA**
Cladding area (in^2)	6.66	7.08	7.55	6.82
Cladding volume (in^3)	946	1019	1088	982
Pellet area (in^2)	21.33	21.57	21.17	19.77
UO_2 volume (in^3)	3029	3105	3048	2847
Temperature	Cp eff	Cp eff	Cp eff	Cp eff
(°F)	(Btu/lbm-°F)	(Btu/lbm-°F)	(Btu/lbm-°F)	(Btu/lbm-°F)
80	0.0593	0.0594	0.0595	0.0594
260	0.0654	0.0655	0.0656	0.0656
692	0.0726	0.0727	0.0728	0.0727
1502	0.0779	0.0780	0.0782	0.0781

Table 4-14
Effective Conductivity of Liquid Neutron Shielding – Sections 1 and 16

Ti	To	Tavg	Tavg	k	β	ν	Pr	C 1	Ra	Nu COND	Nu l	Nu	k eff
(°F)	(°F)	(°F)	(K)	(W/m-K)	(1/K)	(m^2/s)	(---)	(---)	(---)	(---)	(---)	(---)	(Btu/hr-in-°F)
134	126	130	328	0.648	4.159E-04	5.171E-07	3.29	0.5883	4.751E+08	1.00	21.62	21.62	0.674
144	136	140	333	0.653	4.501E-04	4.815E-07	3.04	0.5852	5.477E+08	1.00	22.29	22.29	0.701
154	146	150	339	0.658	4.844E-04	4.460E-07	2.79	0.5819	6.304E+08	1.00	22.96	22.96	0.727
164	156	160	344	0.663	5.186E-04	4.104E-07	2.54	0.5780	7.253E+08	1.00	23.62	23.62	0.754
174	166	170	350	0.668	5.528E-04	3.749E-07	2.29	0.5737	8.352E+08	1.00	24.28	24.28	0.781
184	176	180	356	0.671	5.858E-04	3.552E-07	2.16	0.5712	9.292E+08	1.00	24.83	24.83	0.802
194	186	190	361	0.674	6.187E-04	3.355E-07	2.03	0.5684	1.033E+09	1.00	25.37	25.37	0.823
204	196	200	367	0.677	6.517E-04	3.158E-07	1.90	0.5654	1.149E+09	1.00	25.92	25.92	0.844
214	206	210	372	0.680	6.846E-04	2.962E-07	1.77	0.5622	1.277E+09	1.00	26.46	26.46	0.866
224	216	220	378	0.682	7.167E-04	2.802E-07	1.66	0.5593	1.404E+09	1.00	26.96	26.96	0.885
234	226	230	383	0.683	7.481E-04	2.681E-07	1.58	0.5570	1.525E+09	1.00	27.40	27.40	0.902
244	236	240	389	0.685	7.794E-04	2.559E-07	1.50	0.5545	1.655E+09	1.00	27.85	27.85	0.918
254	246	250	394	0.686	8.108E-04	2.437E-07	1.42	0.5518	1.797E+09	1.00	28.29	28.29	0.935
264	256	260	400	0.688	8.421E-04	2.315E-07	1.34	0.5490	1.951E+09	1.00	28.73	28.73	0.952
274	266	270	406	0.688	8.815E-04	2.231E-07	1.29	0.5471	2.117E+09	1.00	29.22	29.22	0.968
284	276	280	411	0.688	9.210E-04	2.147E-07	1.24	0.5451	2.296E+09	1.00	29.71	29.71	0.984
294	286	290	417	0.688	9.604E-04	2.063E-07	1.19	0.5430	2.489E+09	1.00	30.20	30.20	1.000
304	296	300	422	0.687	9.906E-04	1.990E-07	1.15	0.5411	2.660E+09	1.00	30.60	30.60	1.012

Table 4-14 – Continued
Effective Conductivity of Liquid Neutron Shielding – Sections 2 and 12

Ti	To	Tavg	Tavg	k	β	ν	Pr	C_l	Ra	Nu_COND	Nu_l	Nu	k_eff
(°F)	(°F)	(°F)	(K)	(W/m-K)	(1/K)	(m^2/s)	(---)	(---)	(---)	(---)	(---)	(---)	(Btu/hr-in-°F)
156.5	143.5	150	339	0.658	4.844E-04	4.460E-07	2.79	0.5819	1.024E+09	1.00	25.92	25.92	0.821
166.5	153.5	160	344	0.663	5.186E-04	4.104E-07	2.54	0.5780	1.179E+09	1.00	26.67	26.67	0.851
176.5	163.5	170	350	0.668	5.528E-04	3.749E-07	2.29	0.5737	1.357E+09	1.00	27.42	27.42	0.882
186.5	173.5	180	356	0.671	5.858E-04	3.552E-07	2.16	0.5712	1.510E+09	1.00	28.03	28.03	0.906
196.5	183.5	190	361	0.674	6.187E-04	3.355E-07	2.03	0.5684	1.679E+09	1.00	28.65	28.65	0.929
206.5	193.5	200	367	0.677	6.517E-04	3.158E-07	1.90	0.5654	1.866E+09	1.00	29.26	29.26	0.953
216.5	203.5	210	372	0.680	6.846E-04	2.962E-07	1.77	0.5622	2.076E+09	1.00	29.88	29.88	0.978
226.5	213.5	220	378	0.682	7.167E-04	2.802E-07	1.66	0.5593	2.282E+09	1.00	30.44	30.44	0.999
236.5	223.5	230	383	0.683	7.481E-04	2.681E-07	1.58	0.5570	2.478E+09	1.00	30.94	30.94	1.018
246.5	233.5	240	389	0.685	7.794E-04	2.559E-07	1.50	0.5545	2.690E+09	1.00	31.44	31.44	1.037
256.5	243.5	250	394	0.686	8.108E-04	2.437E-07	1.42	0.5518	2.920E+09	1.00	31.94	31.94	1.056
266.5	253.5	260	400	0.688	8.421E-04	2.315E-07	1.34	0.5490	3.171E+09	1.00	32.43	32.43	1.074
276.5	263.5	270	406	0.688	8.815E-04	2.231E-07	1.29	0.5471	3.441E+09	1.00	32.99	32.99	1.093
286.5	273.5	280	411	0.688	9.210E-04	2.147E-07	1.24	0.5451	3.731E+09	1.00	33.54	33.54	1.111
296.5	283.5	290	417	0.688	9.604E-04	2.063E-07	1.19	0.5430	4.044E+09	1.00	34.09	34.09	1.129
306.5	293.5	300	422	0.687	9.906E-04	1.990E-07	1.15	0.5411	4.323E+09	1.00	34.54	34.54	1.143
316.5	303.5	310	428	0.685	1.007E-03	1.934E-07	1.12	0.5396	4.528E+09	1.00	34.85	34.85	1.150
326.5	313.5	320	433	0.684	1.023E-03	1.877E-07	1.08	0.5381	4.745E+09	1.00	35.17	35.17	1.157

Table 4-14 – Continued
Effective Conductivity of Liquid Neutron Shielding – Sections 13 to 15

Ti	To	Tavg	Tavg	k	β	ν	Pr	C_l	Ra	Nu_COND	Nu_l	Nu	k_eff
(°F)	(°F)	(°F)	(K)	(W/m-K)	(1/K)	(m^2/s)	(---)	(---)	(---)	(---)	(---)	(---)	(Btu/hr-in-°F)
135	125	130	328	0.648	4.159E-04	5.171E-07	3.29	0.5883	5.938E+08	1.00	22.83	22.83	0.712
145	135	140	333	0.653	4.501E-04	4.815E-07	3.04	0.5852	6.846E+08	1.00	23.54	23.54	0.740
155	145	150	339	0.658	4.844E-04	4.460E-07	2.79	0.5819	7.880E+08	1.00	24.24	24.24	0.768
165	155	160	344	0.663	5.186E-04	4.104E-07	2.54	0.5780	9.066E+08	1.00	24.94	24.94	0.796
175	165	170	350	0.668	5.528E-04	3.749E-07	2.29	0.5737	1.044E+09	1.00	25.64	25.64	0.825
185	175	180	356	0.671	5.858E-04	3.552E-07	2.16	0.5712	1.162E+09	1.00	26.22	26.22	0.847
195	185	190	361	0.674	6.187E-04	3.355E-07	2.03	0.5684	1.291E+09	1.00	26.79	26.79	0.869
205	195	200	367	0.677	6.517E-04	3.158E-07	1.90	0.5654	1.436E+09	1.00	27.37	27.37	0.892
215	205	210	372	0.680	6.846E-04	2.962E-07	1.77	0.5622	1.597E+09	1.00	27.94	27.94	0.914
225	215	220	378	0.682	7.167E-04	2.802E-07	1.66	0.5593	1.755E+09	1.00	28.46	28.46	0.934
235	225	230	383	0.683	7.481E-04	2.681E-07	1.58	0.5570	1.906E+09	1.00	28.94	28.94	0.952
245	235	240	389	0.685	7.794E-04	2.559E-07	1.50	0.5545	2.069E+09	1.00	29.40	29.40	0.970
255	245	250	394	0.686	8.108E-04	2.437E-07	1.42	0.5518	2.246E+09	1.00	29.87	29.87	0.987
265	255	260	400	0.688	8.421E-04	2.315E-07	1.34	0.5490	2.439E+09	1.00	30.33	30.33	1.005
275	265	270	406	0.688	8.815E-04	2.231E-07	1.29	0.5471	2.647E+09	1.00	30.85	30.85	1.022
285	275	280	411	0.688	9.210E-04	2.147E-07	1.24	0.5451	2.870E+09	1.00	31.37	31.37	1.039
295	285	290	417	0.688	9.604E-04	2.063E-07	1.19	0.5430	3.111E+09	1.00	31.88	31.88	1.056
305	295	300	422	0.687	9.906E-04	1.990E-07	1.15	0.5411	3.325E+09	1.00	32.31	32.31	1.069

Table 4-15
Verification of the Calculated Effective Conductivities for Liquid Neutron Shielding

At 115°F Ambient Temperature

Sec. #	Ti *	To †	$\overline{T}$ ‡	$\overline{T}$ §	k	β	ν	Pr	C_1	Ra	Nu	Calculated. k_eff**	k_eff in Model ††	Diff. %
(---)	(°F)	(°F)	(°F)	(K)	(W/m-K)	(1/K)	(m^2/s)	(---)	(---)	(---)	(---)	(Btu/hr-in-°F)	(Btu/hr-in-°F)	(---)
1	*213*	*205*	*209*	372	0.679	6.83E-04	2.974E-07	1.77	0.5624	1.245E+09	26.30	0.860	0.865	0.5%
2	231	220	225	381	0.683	7.35E-04	2.731E-07	1.61	0.5580	2.047E+09	29.55	0.971	1.008	3.7%
3	245	234	239	389	0.685	7.78E-04	2.565E-07	1.50	0.5546	2.325E+09	30.32	1.000	1.035	3.5%
4	256	244	249	395	0.686	8.11E-04	2.436E-07	1.42	0.5518	2.780E+09	31.55	1.043	1.055	1.1%
5	264	251	256	398	0.688	8.33E-04	2.350E-07	1.36	0.5498	3.091E+09	32.28	1.069	1.068	0.1%
6	268	255	261	401	0.688	8.48E-04	2.302E-07	1.33	0.5487	3.294E+09	32.73	1.084	1.076	0.7%
7	271	257	263	402	0.688	8.58E-04	2.281E-07	1.32	0.5482	3.412E+09	32.99	1.093	1.081	1.1%
8	272	258	265	403	0.688	8.63E-04	2.271E-07	1.31	0.5480	3.469E+09	33.11	1.097	1.083	1.3%
9	272	259	265	403	0.688	8.64E-04	2.270E-07	1.31	0.5479	3.475E+09	33.12	1.097	1.083	1.3%
10	271	258	264	403	0.688	8.60E-04	2.277E-07	1.32	0.5481	3.433E+09	33.03	1.094	1.081	1.2%
11	269	256	262	401	0.688	8.52E-04	2.295E-07	1.33	0.5485	3.328E+09	32.80	1.087	1.078	0.8%
12	265	252	258	399	0.688	8.37E-04	2.336E-07	1.35	0.5495	3.016E+09	32.06	1.062	1.070	0.8%
13	257	245	251	395	0.687	8.14E-04	2.424E-07	1.41	0.5515	2.600E+09	30.97	1.024	0.988	3.5%
14	246	236	241	389	0.685	7.83E-04	2.546E-07	1.49	0.5542	2.235E+09	29.96	0.988	0.971	1.8%
15	232	223	227	382	0.683	7.39E-04	2.716E-07	1.60	0.5577	1.689E+09	28.11	0.924	0.946	2.4%
16	215	207	211	373	0.680	6.87E-04	2.947E-07	1.76	0.5619	1.225E+09	26.17	0.857	0.865	0.9%

* This value is the average temperature of the structural shell retrieved from the solid elements in the model
† This value is the average temperature of the shielding shell retrieved from the solid elements in the model
‡ This value is the average temperature of the water within the shielding shell retrieved from the model
§ This value is the calculated average temperature (Ti+To)/2 converted to Kelvin
** This value is calculated using the correlations discussed in Section 4.9.1
†† This value is resulted from interpolation between the values used in the ANSYS model

Table 4-15 – Continued
Verification of the Calculated Effective Conductivities for Liquid Neutron Shielding

At -20°F Ambient Temperature

Sec. #	Ti	To	$\overline{T}$	$\overline{T}$	k	β	ν	Pr	C_l	Ra	Nu	Calculated k_eff	k_eff in Model	Diff. %
(---)	(°F)	(°F)	(°F)	(K)	(W/m-K)	(1/K)	(m^2/s)	(---)	(---)	(---)	(---)	(Btu/hr-in-°F)	(Btu/hr-in-°F)	(---)
1	100	90	95	308	0.623	2.11E-04	7.519E-07	5.04	0.6030	2.232E+08	18.35	0.551	0.674	22.4%
2	121	107	113	319	0.637	3.33E-04	6.117E-07	3.99	0.5952	5.807E+08	23.01	0.706	0.761	7.8%
3	138	124	130	328	0.648	4.19E-04	5.141E-07	3.27	0.5880	8.705E+08	25.15	0.785	0.762	2.9%
4	152	136	143	336	0.655	4.64E-04	4.672E-07	2.94	0.5839	1.134E+09	26.68	0.841	0.801	4.8%
5	161	145	152	340	0.659	4.94E-04	4.359E-07	2.72	0.5808	1.325E+09	27.59	0.876	0.827	5.5%
6	167	150	158	344	0.662	5.13E-04	4.162E-07	2.58	0.5787	1.457E+09	28.15	0.897	0.844	6.0%
7	170	153	161	345	0.664	5.24E-04	4.047E-07	2.50	0.5774	1.539E+09	28.48	0.910	0.854	6.2%
8	171	155	162	346	0.664	5.29E-04	3.992E-07	2.46	0.5767	1.580E+09	28.63	0.916	0.858	6.3%
9	172	155	163	346	0.665	5.30E-04	3.986E-07	2.46	0.5767	1.585E+09	28.65	0.917	0.859	6.3%
10	170	154	161	346	0.664	5.26E-04	4.028E-07	2.49	0.5772	1.554E+09	28.53	0.912	0.855	6.2%
11	168	151	159	344	0.663	5.17E-04	4.126E-07	2.56	0.5783	1.479E+09	28.24	0.901	0.847	6.0%
12	162	146	154	341	0.660	4.99E-04	4.311E-07	2.69	0.5803	1.293E+09	27.40	0.871	0.832	4.5%
13	153	138	145	336	0.655	4.68E-04	4.627E-07	2.91	0.5835	1.073E+09	26.26	0.829	0.753	9.1%
14	140	126	133	329	0.649	4.26E-04	5.065E-07	3.22	0.5874	8.544E+08	24.97	0.780	0.719	7.9%
15	122	110	116	320	0.639	3.44E-04	5.985E-07	3.90	0.5944	5.077E+08	22.18	0.682	0.712	4.4%
16	102	92	97	309	0.625	2.25E-04	7.357E-07	4.92	0.6023	2.361E+08	18.59	0.559	0.674	20.5%

Note: The applied k_{eff} values in the model for sections 1 and 16 at -20°F ambient are accepted, because these values are higher than the calculated values, which cause higher temperature gradient in the model for minimum ambient conditions.

Table 4-16
Effective Conductivity of Liquid Neutron Shield during Burning Period

Ti	To	Tavg	Tavg	k	β	ν	Pr	C_l	Ra	Nu_COND	Nu_l	Nu	k_eff
(°F)	(°F)	(°F)	(K)	(W/m-K)	(1/K)	(m^2/s)	(---)	(---)	(---)	(---)	(---)	(---)	(Btu/hr-in-°F)
680	700	212	373	0.680	6.91E-04	2.92E-07	1.74	0.561	3.26E+09	1.00	33.4	33.4	1.09
650	700	212	373	0.680	6.91E-04	2.92E-07	1.74	0.561	8.16E+09	1.00	42.0	42.0	1.37
620	700	212	373	0.680	6.91E-04	2.92E-07	1.74	0.561	1.30E+10	1.00	47.2	47.2	1.55
580	600	212	373	0.680	6.91E-04	2.92E-07	1.74	0.561	3.26E+09	1.00	33.4	33.4	1.09
550	600	212	373	0.680	6.91E-04	2.92E-07	1.74	0.561	8.16E+09	1.00	42.0	42.0	1.37
500	600	212	373	0.680	6.91E-04	2.92E-07	1.74	0.561	1.63E+10	1.00	49.9	49.9	1.63
480	500	212	373	0.680	6.91E-04	2.92E-07	1.74	0.561	3.26E+09	1.00	33.4	33.4	1.09
450	500	212	373	0.680	6.91E-04	2.92E-07	1.74	0.561	8.16E+09	1.00	42.0	42.0	1.37
420	500	212	373	0.680	6.91E-04	2.92E-07	1.74	0.561	1.30E+10	1.00	47.2	47.2	1.55
380	400	390	472	0.665	1.25E-03	1.56E-07	0.92	0.529	1.09E+10	1.00	42.5	42.5	1.36
350	400	375	464	0.670	1.18E-03	1.61E-07	0.94	0.531	2.48E+10	1.00	52.4	52.4	1.69
320	400	360	456	0.675	1.12E-03	1.67E-07	0.97	0.532	3.60E+10	1.00	57.7	57.7	1.87
280	300	290	417	0.688	9.60E-04	2.06E-07	1.19	0.543	6.22E+09	1.00	37.9	37.9	1.26
250	300	275	408	0.688	9.01E-04	2.19E-07	1.27	0.546	1.38E+10	1.00	46.5	46.5	1.54
220	300	260	400	0.688	8.42E-04	2.32E-07	1.34	0.549	1.95E+10	1.00	51.0	51.0	1.69

Table 4-17
Effective Conductivity of Air within Shielding Panel during Cool Down Period

T_i	T_o	T_{avg}	k	β	ν	Pr	C_l	Ra	Nu_{COND}	Nu_l	Nu	k_{conv}	k_r	k_eff*
(°F)	(°F)	(K)	(W/m-K)	(1/K)	(m2/s)	(---)	(---)	(---)	(---)	(---)	(---)	(Btu/hr-in-°F)	(Btu/hr-in-°F)	(Btu/hr-in-°F)
540	1200	870	0.054	1.38E-03	7.52E-05	0.70	0.514	1.31E+06	1.00	4.3	4.3	0.01	0.18	0.19
480	1200	840	0.053	1.41E-03	7.25E-05	0.70	0.514	1.57E+06	1.00	4.5	4.5	0.01	0.17	0.18
500	1000	750	0.051	1.52E-03	6.44E-05	0.70	0.514	1.47E+06	1.00	4.5	4.5	0.01	0.13	0.14
400	1000	700	0.049	1.57E-03	5.99E-05	0.69	0.513	2.11E+06	1.00	4.9	4.9	0.01	0.12	0.13
460	800	630	0.047	1.66E-03	5.36E-05	0.69	0.513	1.57E+06	1.00	4.5	4.5	0.01	0.09	0.11
410	800	605	0.046	1.69E-03	5.16E-05	0.69	0.513	1.99E+06	1.00	4.8	4.8	0.01	0.09	0.10
310	800	555	0.044	1.79E-03	4.77E-05	0.69	0.513	3.08E+06	1.00	5.3	5.3	0.01	0.08	0.09
420	600	510	0.043	1.87E-03	4.42E-05	0.69	0.513	1.38E+06	1.00	4.4	4.4	0.01	0.06	0.08
370	600	485	0.042	1.92E-03	4.23E-05	0.69	0.513	1.97E+06	1.00	4.8	4.8	0.01	0.06	0.07
270	600	435	0.040	2.01E-03	3.84E-05	0.69	0.513	3.59E+06	1.00	5.6	5.6	0.01	0.05	0.06
330	450	390	0.039	2.14E-03	3.53E-05	0.69	0.513	1.64E+06	1.00	4.6	4.6	0.01	0.04	0.05
340	300	320	0.036	2.33E-03	3.05E-05	0.69	0.513	8.03E+05	1.00	3.8	3.8	0.01	0.03	0.04
190	300	245	0.033	2.57E-03	2.55E-05	0.70	0.514	3.49E+06	1.00	5.5	5.5	0.01	0.02	0.03
160	150	155	0.029	2.99E-03	2.03E-05	0.70	0.514	5.90E+05	1.00	3.5	3.5	0.01	0.02	0.02

* The calculated k_{eff} values are smoothed to use in the ANSYS model

Table 4-17 - Continued
Effective Conductivity of Air within Shielding Panel during Cool Down Period – Verification

time	Ti *	To †	T_{avg} ‡	T_{avg}	k	β	ν	Pr	C_l	Ra	Nu	Calculated k_{eff} §	k_eff in Model **	Diff. %
(hr)	(°F)	(°F)	(°F)	(K)	(W/m-K)	(1/K)	(m^2/s)	(---)	(---)	(---)	(---)	(Btu/hr-in-°F)	(Btu/hr-in-°F)	(---)
0.26	370	559	456	509	0.041	120E-03	4.00E-05	0.69	0.513	1.86E+06	4.7	0.066	0.064	2.3%
1	356	255	308	427	0.035	2.4E-03	2.97E-05	0.69	0.513	2.18E+06	4.9	0.040	0.038	4.4%
2	352	227	292	418	0.035	2.4E-03	2.86E-05	0.69	0.513	2.97E+06	5.3	0.039	0.036	6.7%
5	357	219	290	417	0.035	2.4E-03	2.85E-05	0.69	0.513	3.30E+06	5.4	0.039	0.036	7.4%
10	378	227	305	425	0.035	2.4E-03	2.95E-05	0.69	0.513	3.29E+06	5.4	0.041	0.038	6.9%
15	399	235	320	433	0.036	2.3E-03	3.05E-05	0.69	0.513	3.27E+06	5.4	0.043	0.040	6.6%
20	415	243	333	440	0.036	2.3E-03	3.14E-05	0.69	0.513	3.22E+06	5.4	0.045	0.042	6.2%
50	491	277	391	473	0.039	2.1E-03	3.54E-05	0.69	0.513	2.92E+06	5.3	0.053	0.050	5.3%
80	521	292	415	486	0.039	2.1E-03	3.70E-05	0.69	0.513	2.76E+06	5.2	0.057	0.055	2.0%
120	535	299	426	492	0.040	2.0E-03	3.78E-05	0.69	0.513	2.68E+06	5.2	0.058	0.058	0.6%
175	540	302	430	494	0.040	2.0E-03	3.81E-05	0.69	0.513	2.65E+06	5.2	0.059	0.059	0.3%
200	540	302	430	495	0.040	2.0E-03	3.81E-05	0.69	0.513	2.65E+06	5.2	0.059	0.059	0.2%

* This value is the average temperature of the structural shell retrieved from the solid elements in the model
† This value is the average temperature of the shielding shell retrieved from the solid elements in the model
‡ This value is the average temperature of the air within the shielding shell retrieved from the model
§ This value is calculated using the correlations discussed in Section 4.9.
** This value is resulted from interpolation between the values used in the ANSYS model

Table 4-18
Verification of the selected k_{eff} value for Water in the Annulus

time	T_h *	T_c **	T_{avg} †	T_{avg}	k	β	ν	Pr	Ra
(hr)	(°F)	(°F)	(°F)	(K)	(W/m-K)	(1/K)	(m^2/s)	(---)	(---)
1	159.9	159.6	160	344	0.663	5.18E-04	4.11E-07	1.83	7.93E+03
5	164.0	161.0	163	346	0.664	5.27E-04	4.02E-07	1.80	8.30E+04
8	169.4	164.1	167	348	0.666	5.42E-04	3.86E-07	1.74	1.58E+05
10	175.1	168.7	172	351	0.669	5.59E-04	3.71E-07	1.68	2.06E+05
14	186.4	177.5	182	357	0.671	5.92E-04	3.51E-07	1.60	3.22E+05

$Ra(H/L)^3$	Nu_ct	Nu_l	Nu_t	Nu_0.7	Nu_c	Nu_l	Nu_t	Nu_4.0	Nu ‡	k_eff
(---)	(---)	(---)	(---)	(---)	(---)	(---)	(---)	(---)	(---)	(Btu/hr-in-°F)
8.34E+11	1.2	0.5	1.2	1.2	1.0	0.4	0.7	1.0	1.1	0.03
8.73E+12	2.8	1.0	2.6	2.8	1.0	0.7	1.4	1.7	2.1	0.07
1.66E+13	3.5	1.2	3.3	3.5	1.0	0.8	1.7	2.1	2.5	0.08
2.17E+13	3.7	1.3	3.6	3.7	1.0	0.8	1.8	2.3	2.7	0.09
3.39E+13	4.3	1.4	4.1	4.3	1.0	0.9	2.1	2.7	3.1	0.10

time	Tavg	Calculated k_eff	k_eff in Model
(hr)	(°F)	(Btu/hr-in-°F)	(Btu/hr-in-°F)
1	159.8	0.03	0.055
5	162.5	0.07	0.055
8	166.9	0.08	0.055
10	171.9	0.09	0.055
14	181.9	0.10	0.055

* Average temperature of the DSC shell retrieved from the model
** Average temperature of the cask inner shell retrieved from the model
† Average temperature of water in the annulus retrieved from the model
‡ Linear interpolation between Nu-0.7 and Nu_4.0 based on the Pr number

Table 4-19
Total Heat Transfer Coefficient during Fire

T_{amb} = 1475 °F
L = 92.2 in
F_{12} = 1.0
ε = 0.9

T_s (°F)	T_f (°F)	h_c (Btu/hr-in^2-°F)	h_r (Btu/hr-in^2-°F)	H_t (Btu/hr-in^2-°F)
226	1475	4.5	0.095	0.126
251	1475	4.5	0.096	0.127
276	1475	4.5	0.098	0.129
301	1475	4.5	0.100	0.131
326	1475	4.5	0.101	0.133
351	1475	4.5	0.103	0.134
376	1475	4.5	0.105	0.136
401	1475	4.5	0.107	0.138
426	1475	4.5	0.109	0.140
451	1475	4.5	0.111	0.142
476	1475	4.5	0.113	0.144
501	1475	4.5	0.115	0.146
526	1475	4.5	0.117	0.148
551	1475	4.5	0.119	0.151
576	1475	4.5	0.121	0.153
601	1475	4.5	0.124	0.155
626	1475	4.5	0.126	0.157
651	1475	4.5	0.128	0.159
676	1475	4.5	0.131	0.162
701	1475	4.5	0.133	0.164
726	1475	4.5	0.135	0.167
751	1475	4.5	0.138	0.169
776	1475	4.5	0.140	0.171
801	1475	4.5	0.143	0.174
826	1475	4.5	0.145	0.176
851	1475	4.5	0.147	0.179
876	1475	4.5	0.150	0.181
901	1475	4.5	0.152	0.184
926	1475	4.5	0.155	0.186
951	1475	4.5	0.155	0.186

Table 4-20
Effective Conductivity of Air in the Closed HSM-H Cavity

Di = 67.19 (in) = 1.707 (m)
Do = 115 (in) = 2.920 (m)
E = 13 (in) = 0.330 (m)
L = 23.9 (in) = 0.607 (m)

Ti	To	T_{avg}	T_{avg}	k	β	ν	Pr	C_l	Ra	Nu_{COND}	Nu_l	Nu	k_eff
(°F)	(°F)	(°F)	(K)	(W/m-K)	(1/K)	(m^2/s)	(—)	(—)	(—)	(—)	(—)	(—)	(Btu/hr-in-°F)
825	350	588	582	0.045	1.73E-03	5.02E-05	0.69	0.513	2.73E+08	1.00	23.5	23.5	0.05
775	350	563	568	0.045	1.77E-03	4.83E-05	0.69	0.513	2.71E+08	1.00	23.4	23.4	0.05
725	350	538	554	0.044	1.82E-03	4.63E-05	0.69	0.513	2.67E+08	1.00	23.3	23.3	0.05
675	350	513	540	0.043	1.87E-03	4.44E-05	0.69	0.513	2.58E+08	1.00	23.1	23.1	0.05
625	350	488	526	0.042	1.91E-03	4.25E-05	0.69	0.513	2.44E+08	1.00	22.8	22.8	0.05
775	300	538	554	0.044	1.82E-03	4.63E-05	0.69	0.513	3.38E+08	1.00	24.8	24.8	0.05
725	300	513	540	0.043	1.87E-03	4.44E-05	0.69	0.513	3.37E+08	1.00	24.7	24.7	0.05
675	300	488	526	0.042	1.91E-03	4.25E-05	0.69	0.513	3.33E+08	1.00	24.7	24.7	0.05
625	300	463	513	0.041	1.96E-03	4.05E-05	0.69	0.513	3.25E+08	1.00	24.5	24.5	0.05
575	300	438	499	0.040	2.01E-03	3.86E-05	0.69	0.513	3.10E+08	1.00	24.2	24.2	0.05
725	250	488	526	0.042	1.91E-03	4.25E-05	0.69	0.513	4.22E+08	1.00	26.2	26.2	0.05
675	250	463	513	0.041	1.96E-03	4.05E-05	0.69	0.513	4.25E+08	1.00	26.2	26.2	0.05
625	250	438	499	0.040	2.01E-03	3.86E-05	0.69	0.513	4.23E+08	1.00	26.2	26.2	0.05
575	250	413	485	0.039	2.08E-03	3.69E-05	0.69	0.513	4.16E+08	1.00	26.1	26.1	0.05
525	250	388	471	0.038	2.15E-03	3.52E-05	0.69	0.513	4.01E+08	1.00	25.8	25.8	0.05
675	200	438	499	0.040	2.01E-03	3.86E-05	0.69	0.513	5.36E+08	1.00	27.8	27.8	0.05
625	200	413	485	0.039	2.08E-03	3.69E-05	0.69	0.513	5.44E+08	1.00	27.9	27.9	0.05
575	200	388	471	0.038	2.15E-03	3.52E-05	0.69	0.513	5.46E+08	1.00	27.9	27.9	0.05
525	200	363	457	0.037	2.22E-03	3.34E-05	0.69	0.513	5.41E+08	1.00	27.9	27.9	0.05
475	200	338	443	0.037	2.28E-03	3.17E-05	0.69	0.513	5.25E+08	1.00	27.7	27.7	0.05
625	150	388	471	0.038	2.15E-03	3.52E-05	0.69	0.513	6.92E+08	1.00	29.6	29.6	0.05
575	150	363	457	0.037	2.22E-03	3.34E-05	0.69	0.513	7.07E+08	1.00	29.8	29.8	0.05
525	150	338	443	0.037	2.28E-03	3.17E-05	0.69	0.513	7.16E+08	1.00	29.9	29.9	0.05
475	150	313	429	0.036	2.35E-03	3.00E-05	0.69	0.513	7.16E+08	1.00	29.9	29.9	0.05
425	150	288	415	0.035	2.42E-03	2.83E-05	0.69	0.513	7.02E+08	1.00	29.7	29.7	0.05
625	200	413	485	0.039	2.08E-03	3.69E-05	0.69	0.513	5.44E+08	1.00	27.9	27.9	0.05
575	200	388	471	0.038	2.15E-03	3.52E-05	0.69	0.513	5.46E+08	1.00	27.9	27.9	0.05
525	200	363	457	0.037	2.22E-03	3.34E-05	0.69	0.513	5.41E+08	1.00	27.9	27.9	0.05
475	200	338	443	0.037	2.28E-03	3.17E-05	0.69	0.513	5.25E+08	1.00	27.7	27.7	0.05

Table 4-21
Summary of the Energy-Hydraulic Calculation Results for 34.8 kW

Section	No. of Flow Paths	Subsection	Type of Flow Resistance	Ref.	K_{EI} at 115°F	K_{EI} at -20°F	$\Sigma(K_{EI}/A_{EI}^2)$ at 115°F (in^{-4})	$\Sigma(K_{EI}/A_{EI}^2)$ at -20°F (in^{-4})
1	Two parallel flows *	Entrance $A_0 = 30 \times 36 = 1080\ in^2$	Entrance effect	[35]	0.5	0.5	9.26×10^{-7}	9.26×10^{-7}
			Screen	[35]	0.58	0.58		
		Contraction & Tee $A_0 = 12 \times 30 = 360\ in^2$	Contraction	[36]	0.033	0.033	5.23×10^{-6}	5.23×10^{-6}
			Friction in entrance channel **	[35]	0.014	0.014		
			Splitting	[36]	0.63	0.63		
		Inlet opening $A_0 = 8 \times 148 = 1184\ in^2$	Friction thru Sidewall	[35]	0.0387	0.0413		
			Discharge	[35]	1	1	7.41×10^{-6}	7.43×10^{-6}
			Equivalent Losses in Section 1 for two Parallel Flows				*1.72×10^{-6}*	*1.73×10^{-6}*
2	One flow	Lower part of HSM-H cavity $A_0 = 68 \times 185.25 = 12597\ in^2$	Friction through lower part	[35]	0.009	0.010	5.5×10^{-11}	6.1×10^{-11}
	One flow	HSM-H cavity below DSC $A_0 = 82.4 \times 185.25 = 15260\ in^2$	Expansion	[36]	0.0305	0.0305	1.5×10^{-10}	1.6×10^{-10}
			Friction after expansion	[35]	0.005	0.006		
	3 parallel flow couples	Flow thru holes of the beam $A_0 = 12.7 \times 185.25 = 2355\ in^2$	Orifice or perforated plates	[36]	18.19	18.19	2.1×10^{-9}	2.1×10^{-9}
		Flow through slotted bar $A_0 = 1 \times 185.25 = 185.25\ in^2$	Orifice or perforated plates	[36]	112.5	112.5		
		Flow bypassing Support rails $A_0 = 12 \times 185.25 = 2223\ in^2$	Contraction with $\alpha = 30°$	[36]	0.403	0.403		
	One flow	Middle part of HSM-H cavity $A_0 =$ in^2	DSC as solid object in flow	[36]	4.69	4.33	2.02×10^{-8}	1.87×10^{-8}
			Friction on side heat shields	[35]	0.025	0.028		
	One flow	Upper part of HSM-H cavity $A_0 =$ in^2	Top heat shields as louver	[36]	5.44	5.44	2.6×10^{-8}	2.6×10^{-8}
			Splitting to outlets	[36]	0.63	0.63		
			Equivalent Losses in Section 2 for one Flow Path				*4.9×10^{-8}*	*4.7×10^{-8}*

Table 4-21 – Continued
Summary of the Energy-Hydraulic Calculation Results for 34.8 kW

Section	No. of Flow Paths	Subsection	Type of Flow Resistance	Ref.	K_{EI} at 115°F	K_{EI} at -20°F	$\Sigma(K_{EI}/A_{EI}^2)$ at 115°F (in^{-4})	$\Sigma(K_{EI}/A_{EI}^2)$ at -20°F (in^{-4})
3	Two parallel flows	Outlet opening $A_0 = 8 \times 148 = 1184\ in^2$	Entrance	[35]	0.5	0.5	1.76×10^{-6}	1.84×10^{-6}
			Friction thru sidewall	[35]	0.026	0.028		
			First bend (friction included)	[36]	1.94	2.05		
		Exhaust channel $A_0 = 4 \times 148 = 592\ in^2$	Friction	[35]	0.23	0.24		
			Second bend (friction included)	[36]	0.79	0.84	2.92×10^{-6}	3.08×10^{-6}
		Exhaust to Ambient $A_0 = 6 \times 148 = 888\ in^2$	Screen	[35]	0.58	0.58		
			Discharge	[35]	1	1	2.00×10^{-6}	2.00×10^{-6}
Equivalent Losses in Section 3 for two Parallel Flows							*1.67×10^{-6}*	*1.73×10^{-6}*
Total Equivalent Losses (in^{-4})							**3.44×10^{-6}**	**3.51×10^{-6}**
Total Equivalent Losses (ft^{-4})							**0.0714**	**0.0726**

Ambient (°F)	$\Sigma(K_{EI}/A_{EI}^2)$ (ft^{-4})	T_{exit} (°F)	T_s (°F)	T_0 (°F)	T_1 (°F)	T_2 (°F)	T_3 (°F)	T_4 (°F)	T_5 (°F)	T_6 (°F)	T_7 (°F)	T_8 (°F)
115	0.0714	178	135	110	114	123	132	142	151	160	169	178
-20	0.0726	36	3	-17	-13	-6	1	8	15	22	29	36

* The equivalent loss coefficient for parallel flow paths can be expressed as follows:

$$\frac{K_E}{A_E^2} = \frac{1}{\left(\sum \frac{A_j}{\sqrt{K_j}}\right)^2}$$ using continuity and pressure loss equations. $\Delta p_E = \Delta p_j = K_j \frac{\rho V_j^2}{2}$; $\dot{m}_j = \rho\, A_j\, V_j$

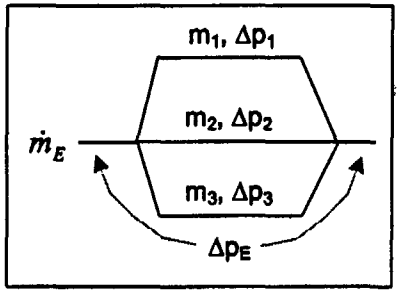

** Friction loss coefficient is $K_f = f\frac{L}{D_h}$ with L=channel length, Dh = hydraulic diameter,

$$f = \begin{cases} f' & if\ f' \geq 0.018 \\ 0.85f' + 0.0028 & if\ f' < 0.018 \end{cases}, \text{ and } f' = 0.11\left[\frac{\varepsilon}{D_h} + \frac{64}{\mathrm{Re}}\right]^{0.25}$$ [35]

Table 4-22
Summary of the Energy-Hydraulic Calculation Results for 32.0 kW

Section	No. of Flow Paths	Subsection	Type of Flow Resistance	Ref.	K_{EI} at 115°F	$\Sigma(K_{EI}/A_{EI}^2)$ at 115°F (in^{-4})
1	Two parallel flows	Entrance $A_0 = 30 \times 36 = 1080\ in^2$	Entrance effect	[35]	0.5	9.26E-07
			Screen	[35]	0.58	
		Contraction & Tee $A_0 = 12 \times 30 = 360\ in^2$	Contraction	[36]	0.033	5.23E-06
			Friction in entrance channel	[35]	0.014	
			Splitting	[36]	0.63	
		Inlet opening $A_0 = 8 \times 148 = 1184\ in^2$	Friction thru Sidewall	[35]	0.041	7.43E-07
			Discharge	[35]	1.0	
Equivalent Losses in Section 1 for two Parallel Flows						*1.725E-06*
2	One flow	Lower part of HSM-H cavity $A_0 = 68 \times 185.25 = 12597\ in^2$	Friction through lower part	[35]	0.010	6.11E-11
	One flow	HSM-H cavity below DSC $A_0 = 82.4 \times 185.25 = 15260\ in^2$	Expansion	[36]	0.031	1.56E-10
			Friction after expansion	[35]	0.006	
	3 parallel flow couples	Flow thru holes of the beam $A_0 = 12.7 \times 185.25 = 2355\ in^2$	Orifice or perforated plates	[36]	112.5	2.07E-09
		Flow through slotted bar $A_0 = 1 \times 185.25 = 185.25\ in^2$	Orifice or perforated plates	[36]	18.19	
		Flow bypassing Support rails $A_0 = 12 \times 185.25 = 2223\ in^2$	Contraction with $\alpha = 30°$	[36]	0.043	
	One flow	Middle part of HSM-H cavity $A_0 = in^2$	DSC as solid object in flow	[36]	4.31	1.86E-08
			Friction on side heat shields	[35]	0.028	
	One flow	Upper part of HSM-H cavity $A_0 = in^2$	Top heat shields as louver	[36]	5.44	2.61E-08
			Splitting to outlets	[36]	0.63	
Equivalent Losses in Section 2 for one Flow Path						*4.70E-08*
3	Two parallel flows	Outlet opening $A_0 = 8 \times 148 = 1184\ in^2$	Entrance	[35]	0.5	1.84E-06
			Friction thru sidewall	[35]	0.028	
			First bend (friction included)	[36]	2.05	
		Exhaust channel $A_0 = 4 \times 148 = 592\ in^2$	Friction	[35]	0.24	3.09E-06
			Second bend (friction included)	[36]	0.84	
		Exhaust to Ambient $A_0 = 6 \times 148 = 888\ in^2$	Screen	[35]	0.58	2.00E-06
			Discharge	[35]	1.0	
Equivalent Losses in Section 3 for two Parallel Flows						*1.734E-06*
Total Equivalent Losses (in^{-4})						**3.51E-06**
Total Equivalent Losses (ft^{-4})						**0.0727**

Ambient (°F)	Decayeat (kW)	$\Sigma(K_{EI}/A_{EI}^2)$ (ft^{-4})	T_{exit} (°F)	T_8 (°F)	T_8 (°F)	T_1 (°F)	T_2 (°F)	T_3 (°F)	T_4 (°F)	T_5 (°F)	T_6 (°F)	T_7 (°F)	T_8 (°F)
115	32.0	0.0727	174	134	109	114	122	131	139	148	157	165	174

Table 4-23
Summary of the Energy-Hydraulic Calculation Results for 26.1 kW

Section	No. of Flow Paths	Subsection	Type of Flow Resistance	Ref.	K_{Ei} at 115°F	$\Sigma(K_{Ei}/A_{Ei}^2)$ at 115°F (in^{-4})
1	Two parallel flows	Entrance $A_0 = 30 \times 36 = 1080\ in^2$	Entrance effect	[35]	0.5	9.26E-07
			Screen	[35]	0.58	
		Contraction & Tee $A_0 = 12 \times 30 = 360\ in^2$	Contraction	[36]	0.033	5.23E-06
			Friction in entrance channel	[35]	0.015	
			Splitting	[36]	0.63	
		Inlet opening $A_0 = 8 \times 148 = 1184\ in^2$	Friction thru Sidewall	[35]	0.042	7.43E-07
			Discharge	[35]	1.0	
Equivalent Losses in Section 1 for two Parallel Flows						*1.752E-06*
2	One flow	Lower part of HSM-H cavity $A_0 = 68 \times 185.25 = 12597\ in^2$	Friction through lower part	[35]	0.010	6.20E-11
	One flow	HSM-H cavity below DSC $A_0 = 82.4 \times 185.25 = 15260\ in^2$	Expansion	[36]	0.031	1.56E-10
			Friction after expansion	[35]	0.006	
	3 parallel flow couples	Flow thru holes of the beam $A_0 = 12.7 \times 185.25 = 2355\ in^2$	Orifice or perforated plates	[36]	112.5	2.07E-09
		Flow through slotted bar $A_0 = 1 \times 185.25 = 185.25\ in^2$	Orifice or perforated plates	[36]	18.19	
		Flow bypassing Support rails $A_0 = 12 \times 185.25 = 2223\ in^2$	Contraction with $\alpha = 30°$	[36]	0.043	
	One flow	Middle part of HSM-H cavity $A_0 = in^2$	DSC as solid object in flow	[36]	4.25	1.84E-08
			Friction on side heat shields	[35]	0.029	
	One flow	Upper part of HSM-H cavity $A_0 = in^2$	Top heat shields as louver	[36]	5.44	2.61E-08
			Splitting to outlets	[36]	0.63	
Equivalent Losses in Section 2 for one Flow Path						*4.67E-08*
3	Two parallel flows	Outlet opening $A_0 = 8 \times 148 = 1184\ in^2$	Entrance	[35]	0.5	1.85E-06
			Friction thru sidewall	[35]	0.028	
			First bend (friction included)	[36]	2.06	
		Exhaust channel $A_0 = 4 \times 148 = 592\ in^2$	Friction	[35]	0.25	3.11E-06
			Second bend (friction included)	[36]	0.84	
		Exhaust to Ambient $A_0 = 6 \times 148 = 888\ in^2$	Screen	[35]	0.58	2.00E-06
			Discharge	[35]	1.0	
Equivalent Losses in Section 3 for two Parallel Flows						*1.741E-06*
Total Equivalent Losses (in^{-4})						**3.51E-06**
Total Equivalent Losses (ft^{-4})						**0.0728**

Ambient (°F)	Decayeat (kW)	$\Sigma(K_{Ei}/A_{Ei}^2)$ (ft^{-4})	T_{exit} (°F)	T_s (°F)	T_0 (°F)	T_1 (°F)	T_2 (°F)	T_3 (°F)	T_4 (°F)	T_5 (°F)	T_6 (°F)	T_7 (°F)	T_8 (°F)
115	26.1	0.0728	165	130	109	112	120	127	135	142	150	157	165

Table 4-24
Minimum Height of the Fuel Rubble

ρ_{UO2}	= 0.396	lb/in3
ρ_{Zr4}	= 0.237	lb/in3
Fuel Comp width	= 8.70	In

Fuel Type	WE 15x15	WE 17x17 Standard/ Vantage 5H	Framatome 17x17 MK BW	WE 17x17 OFA
No of fuel rods	204	264	264	264
OD fuel rod (in)	0.422	0.374	0.374	0.360
Clad thickness (in)	0.0243	0.0225	0.0240	0.0225
No of guides tubes	20	24	24	24
OD guide tubes (in)	0.484	0.429	0.482	0.429
Wall thickness (in)	0.015	0.016	0.016	0.016
No of Instrument tubes	1	1	1	1
OD Instrument tube (in)	0.545	0.474	0.482	0.474
Wall thickness (in)	0.015	0.015	0.016	0.015
Active fuel length (in)	142	144	144	144
Pellet OD (in)	0.3649	0.3225	0.3195	0.3088
Cladding area (in^2)	6.66	7.08	7.55	6.82
Cladding volume (in^3)	946	1019	1088	982
Pellet area (in^2)	21.33	21.57	21.17	19.77
UO_2 volume (in^3)	3029	3105	3048	2847
H_{min} (in)	63	66	66	61

Table 4-25
Transverse Effective Fuel Conductivity at Various Fuel Rod Pitches

	Assembly Type 17x17 MK BW					
Pitch (in)	T_o (°F)	T_c (°F)	T_{avg} (°F)	Q_{react} (Btu/hr-in)	k (Btu/hr-in-°F)	k @ 800°F (Btu/hr-in-°F)
0.384	700	739	719	4.6770	0.0357	0.0396
	800	834	817	4.6770	0.0405	
0.4	700	740	720	4.6770	0.0347	0.0385
	800	835	818	4.6770	0.0393	
0.438	700	738	719	4.6770	0.0362	0.0405
	800	833	817	4.6770	0.0413	
0.446225	700	737	719	4.6770	0.0371	0.0415
	800	833	816	4.6770	0.0424	
0.46445	700	735	717	4.6770	0.0398	0.0446
	800	830	815	4.6770	0.0455	
0.482675	700	732	716	4.6780	0.0434	0.0488
	800	828	814	4.6787	0.0496	
0.5009	700	728	714	4.6783	0.0493	0.0556
	800	824	812	4.6788	0.0565	
0.519125	700	722	711	4.6786	0.0637	0.0728
	800	819	809	4.6791	0.0738	

	Assembly Type WE17x17OFA					
Pitch (in)	T_o (°F)	T_c (°F)	T_{avg} (°F)	Q_{react} (Btu/hr-in)	k (Btu/hr-in-°F)	k @ 300°F (Btu/hr-in-°F)
0.37	200	286	243	4.6761	0.0159	0.0176
	300	374	337	4.6769	0.0187	
0.4	200	287	244	4.6761	0.0158	0.0174
	300	375	337	4.6769	0.0184	
0.427	200	283	242	4.6762	0.0166	0.0182
	300	372	336	4.6768	0.0193	
0.4501	200	278	239	4.6763	0.0177	0.0195
	300	367	334	4.6768	0.0205	
0.4732	200	271	236	4.6764	0.0194	0.0215
	300	361	331	4.6768	0.0226	
0.4963	200	263	231	4.6767	0.0219	0.0246
	300	354	327	4.6769	0.0256	
0.5194	200	252	226	4.6770	0.0266	0.0305
	300	344	322	4.6769	0.0316	

Table 4-26
Transverse Effective Conductivity of Damaged Fuel

	T_o (°F)	T_c (°F)	T_{avg} (°F)	Q_{react} (Btu/hr-in)	k (Btu/hr-in-°F)
WE 17x17 OFA	100	200	150	4.6770	1.38E-02
	200	285	243	4.6769	1.61E-02
	300	374	337	4.6769	1.87E-02
	400	463	432	4.6769	2.17E-02
	500	555	527	4.6769	2.52E-02
	600	648	624	4.6769	2.90E-02
	700	742	721	4.6769	3.31E-02
	800	837	818	4.6769	3.76E-02
	900	932	916	4.6769	4.26E-02
	1000	1029	1014	4.6769	4.81E-02
17x17 MK BW	100	194	147	4.6762	1.47E-02
	200	281	240	4.6762	1.70E-02
	300	370	335	4.6762	1.98E-02
	400	460	430	4.6762	2.28E-02
	500	552	526	4.6769	2.64E-02
	600	645	623	4.6769	3.04E-02
	700	740	720	4.6770	3.46E-02
	800	835	818	4.6770	3.93E-02
	900	931	916	4.6770	4.44E-02
	1000	1028	1014	4.6770	5.01E-02

Table 4-27
Maximum Component Temperatures in DSC containing 16 Damaged Fuel Assemblies

Normal / Off-Normal Transfer Conditions
for Ambient 115°F, Loading Configuration 1, Basket Type I

	Maximum Temperature (°F)		
Component	**32 Intact Fuel (Section 4.3)**	**16 Damaged Fuel**	**Temp. Limit (°F)**
Fuel Cladding	719	738	752 [2]
Fuel Compartment	693	696	
Basket Al Plates	692	695	
Basket Rails	561	561	
DSC Shell	475	475	

Accident Conditions during Transfer Operation
for Ambient 115°F, Loading Configuration 1, Basket Type I

	32 Intact Fuel (Section 4.3)	16 Damaged Fuel (Fuel Rubble)	
Component	**Maximum Temperature (°F)**		**Temp. Limit (°F)**
Intact Fuel cladding	1036	924	1058 [2]
Basket plates	1021	1008	
Basket rails	878	797	
DSC shell	790	737	
Gamma shell (lead)	618	522	621 [3]
Cask structural shell	553	469	
Shielding shell	598	260	

Table 4-28
Internal DSC Pressure during Transferring of Damaged Fuel

Transfer Operation		n_{total} [Section 4.6]	$\overline{T}_{DSC}$ *	P_{DSC} 16 Damaged Fuel		P_{DSC} 32 Intact Fuel [Section 4.6]	Design Pressure
		(lbmoles)	(°F)	(psia)	(psig)	(psig)	(psig)
Without BPRA	Normal	0.333	540	20.0	5.3	5.3	15
	Off-Normal	0.398	540	24.0	9.3	9.2	20
With BPRA	Normal	0.334	540	21.2	6.5	6.4	15
	Off-Normal	0.411	540	26.0	11.3	11.2	20

* The following temperatures are resulted from the DSC model containing 16 damaged fuel assemblies:
$T_{avg,fuel} = 577°F$, $T_{avg,void} = 401°F$

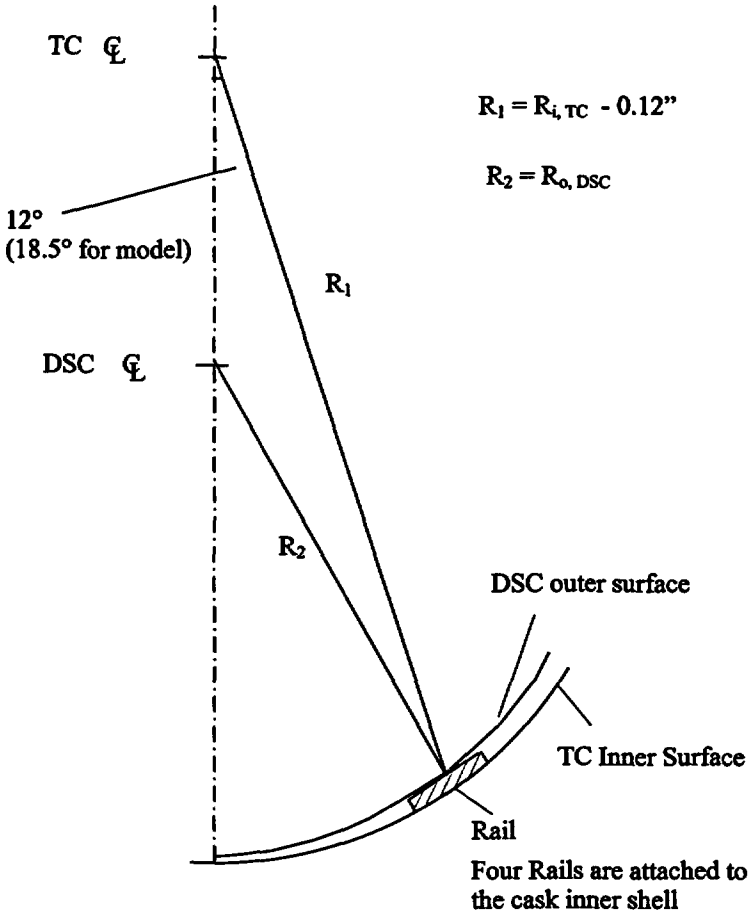

$R_{i,TC}$ = 70.50" ÷2 = 35.250"
$R_{o,DSC}$ = 69.75" ÷2 = 34.875"
x = TC_{CL} - DSC_{CL}
uniform gap = (70.5 -69.75) ÷ 2 = 0.375"
bottom gap = uniform gap – x
top gap = uniform gap + x

$$R_2^2 = R_1^2 + x^2 - 2R_1 x Cos(\alpha)$$

α = 12°

It gives:
x = 0.261"
bottom gap = 0.114"
top gap = 0.636"

Considering the above configuration, the gap between the DSC shell and cask inner shell will be 0.114" at the bottom and 0.636" at the top. The transfer cask model considers a slightly different configuration with an angle of 18.5 degree between the lower rail and the vertical plane. Therefore, the calculated gap between the DSC shell and cask inner shell is 0.106" at the bottom and 0.644" at the top. The nodes of the DSC shell and the cask inner shell are coupled only at the location of the two middle rails to represent the contact area at these locations. The slight difference in temperature profile caused by the smaller gap size in the model will be more than compensated by the fact that the relative thin shell of the DSC will rest on all four rails, which provide more contact area as considered in the model.

Figure 4-1
Position of the DSC in the Transfer Cask

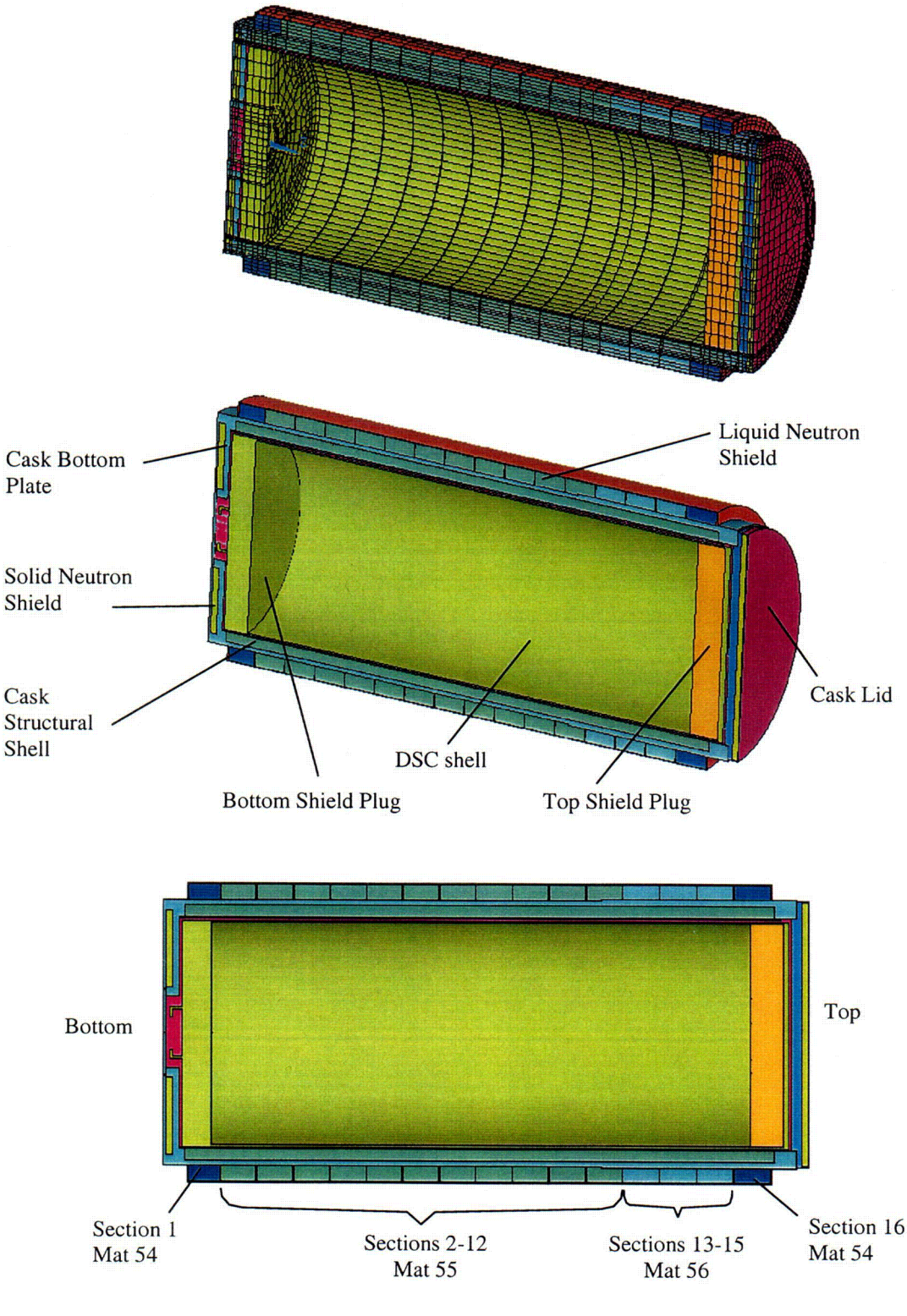

Figure 4-2
Finite element Model of Transfer Cask OS187H

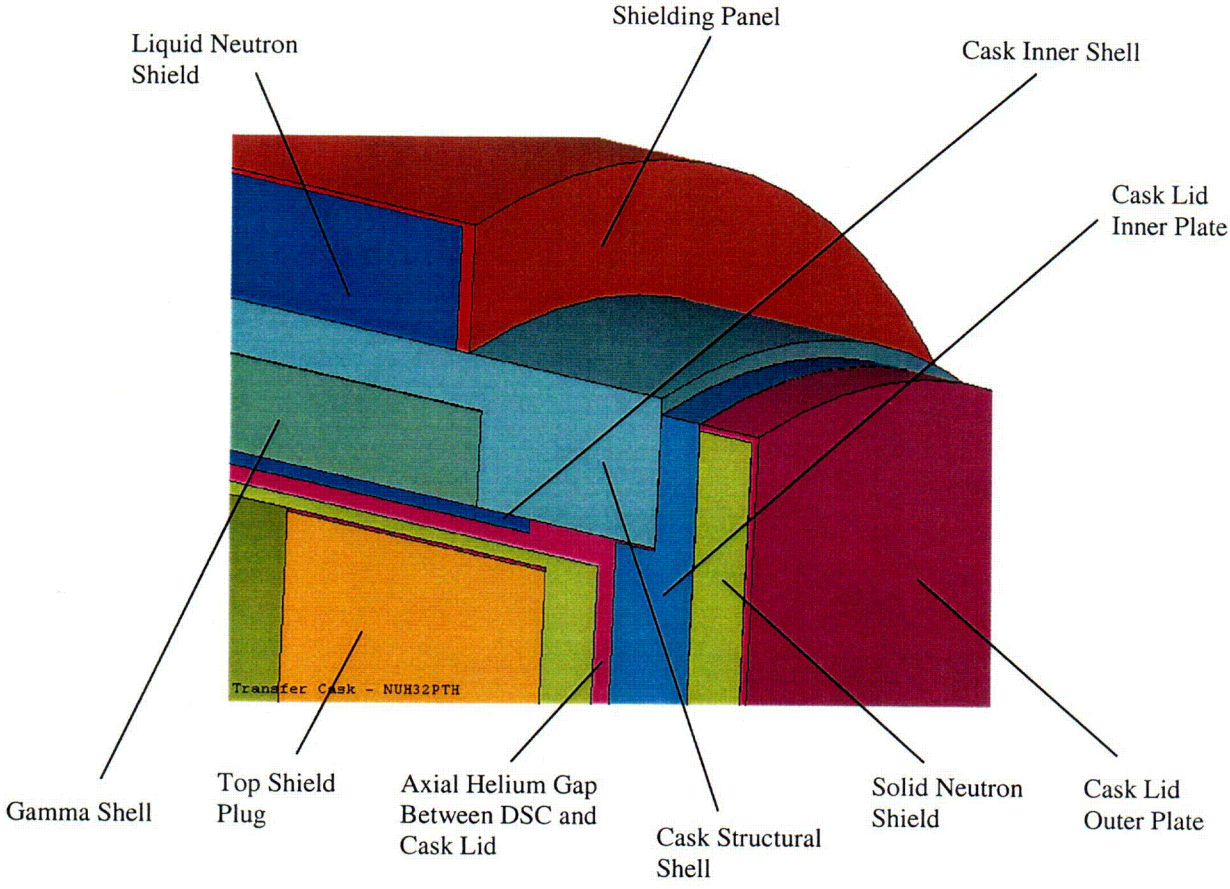

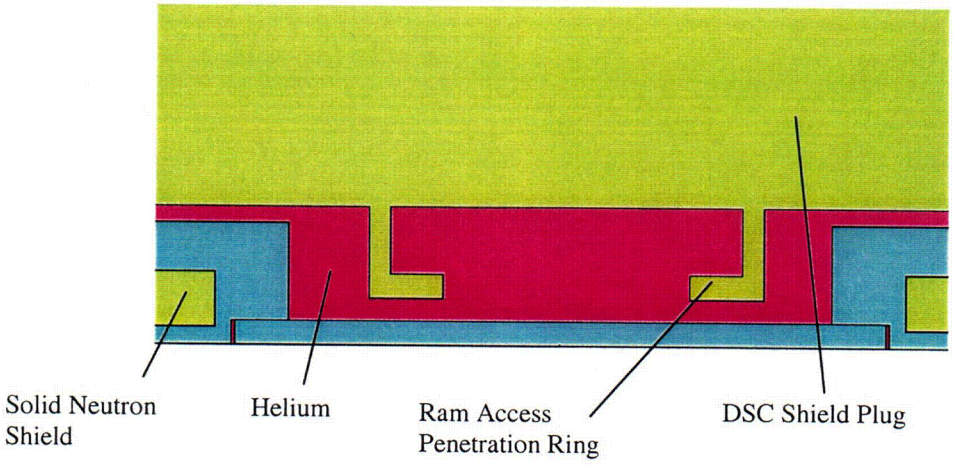

Figure 4-3
FEM of Transfer Cask OS187H, Details

C02

Top of TC Sub-Model

DSC shifted to the cask lid

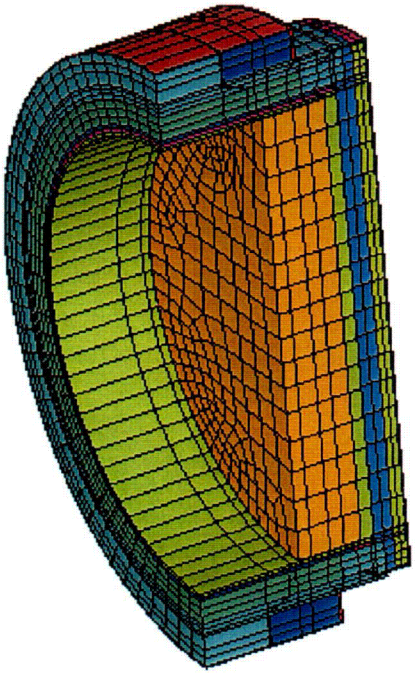

Bottom of TC Sub-Model

DSC shifted to the cask bottom plate

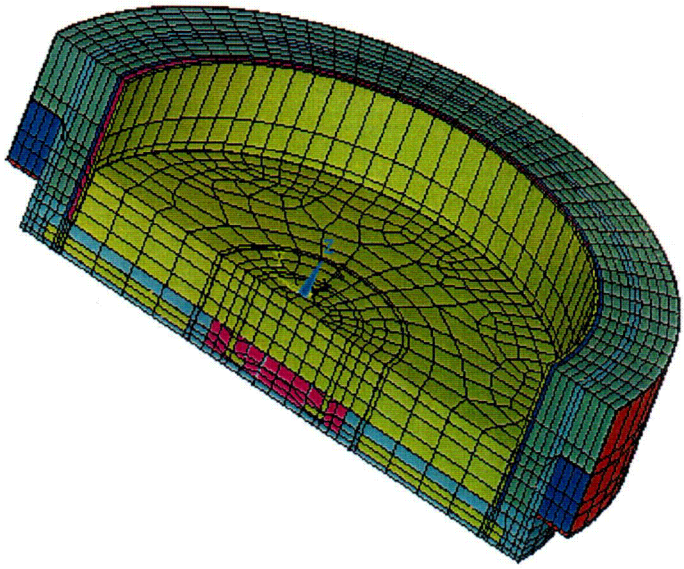

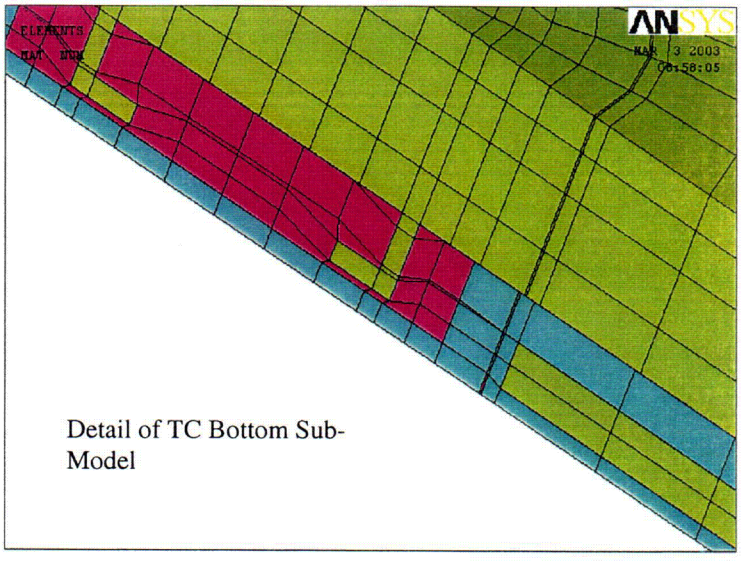

Detail of TC Bottom Sub-Model

Figure 4-4
Top and Bottom Sub-Models of Transfer Cask OS187H

C03

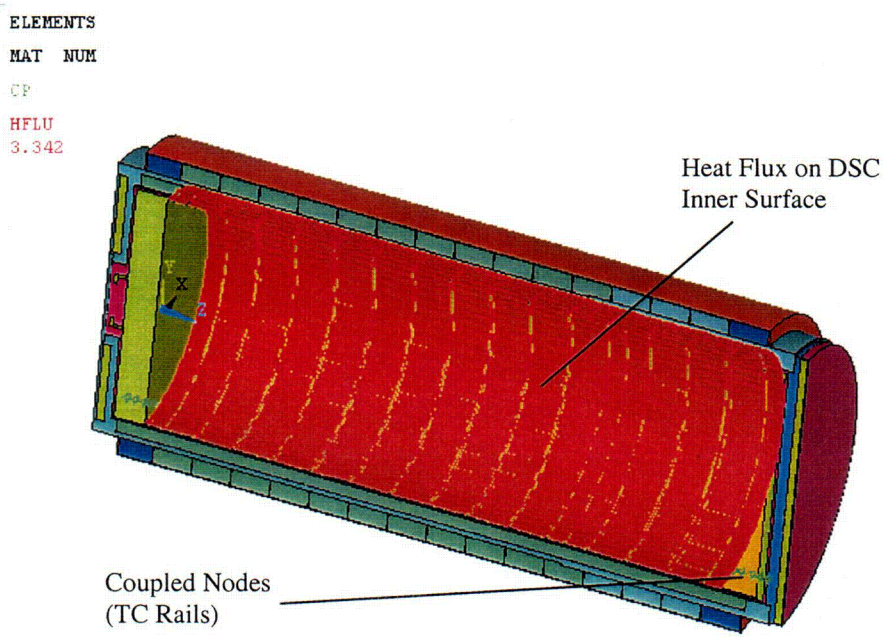

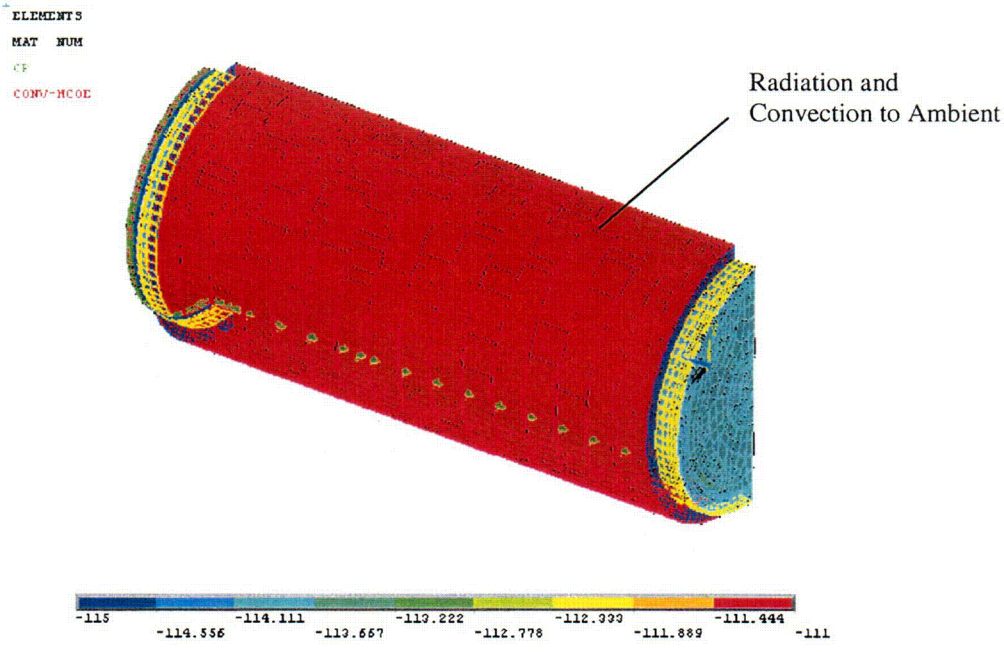

Figure 4-5
Typical Boundary Conditions on the TC Model

C04

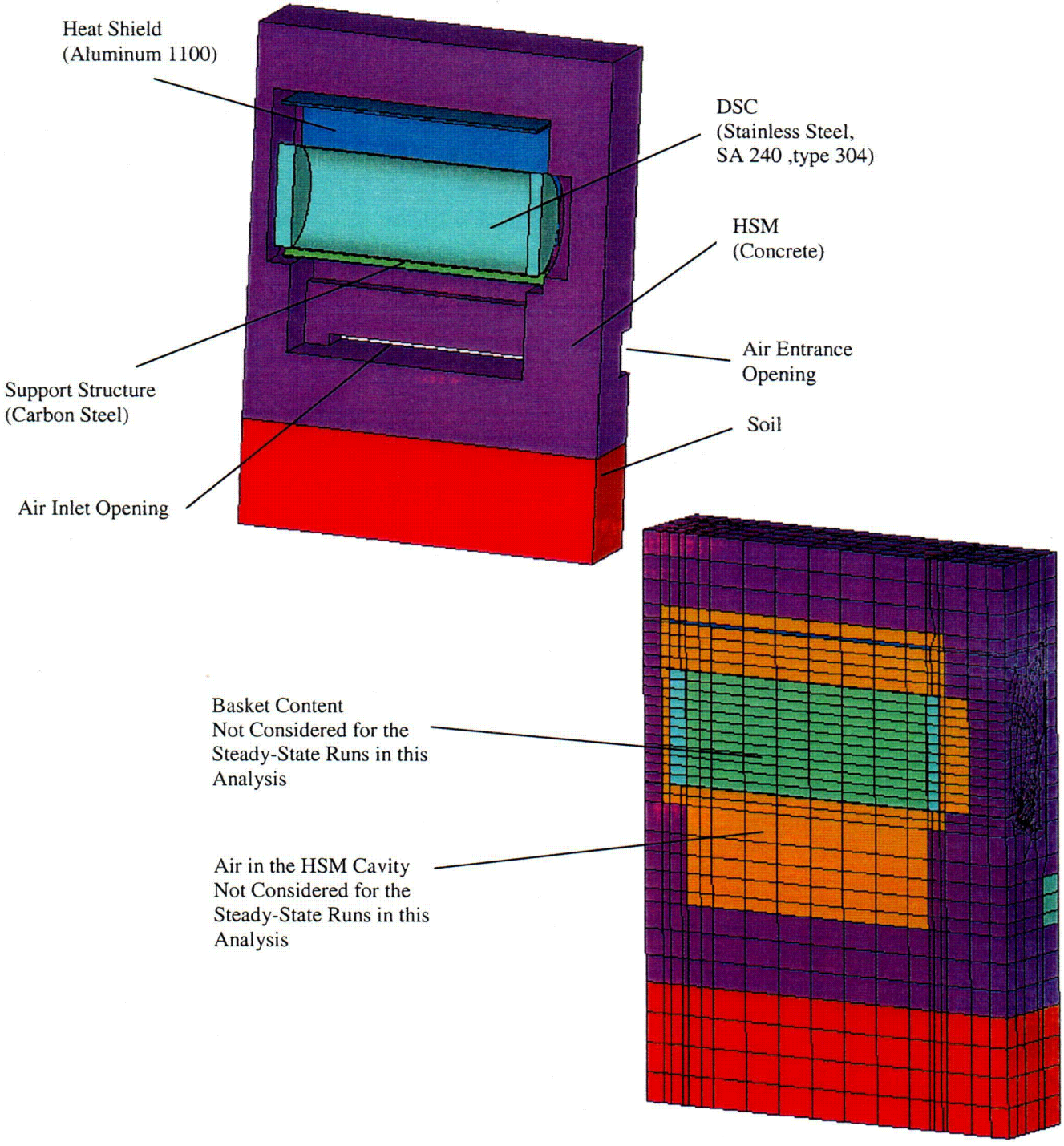

Figure 4-6
Finite Element Model of HSM-H

C 05

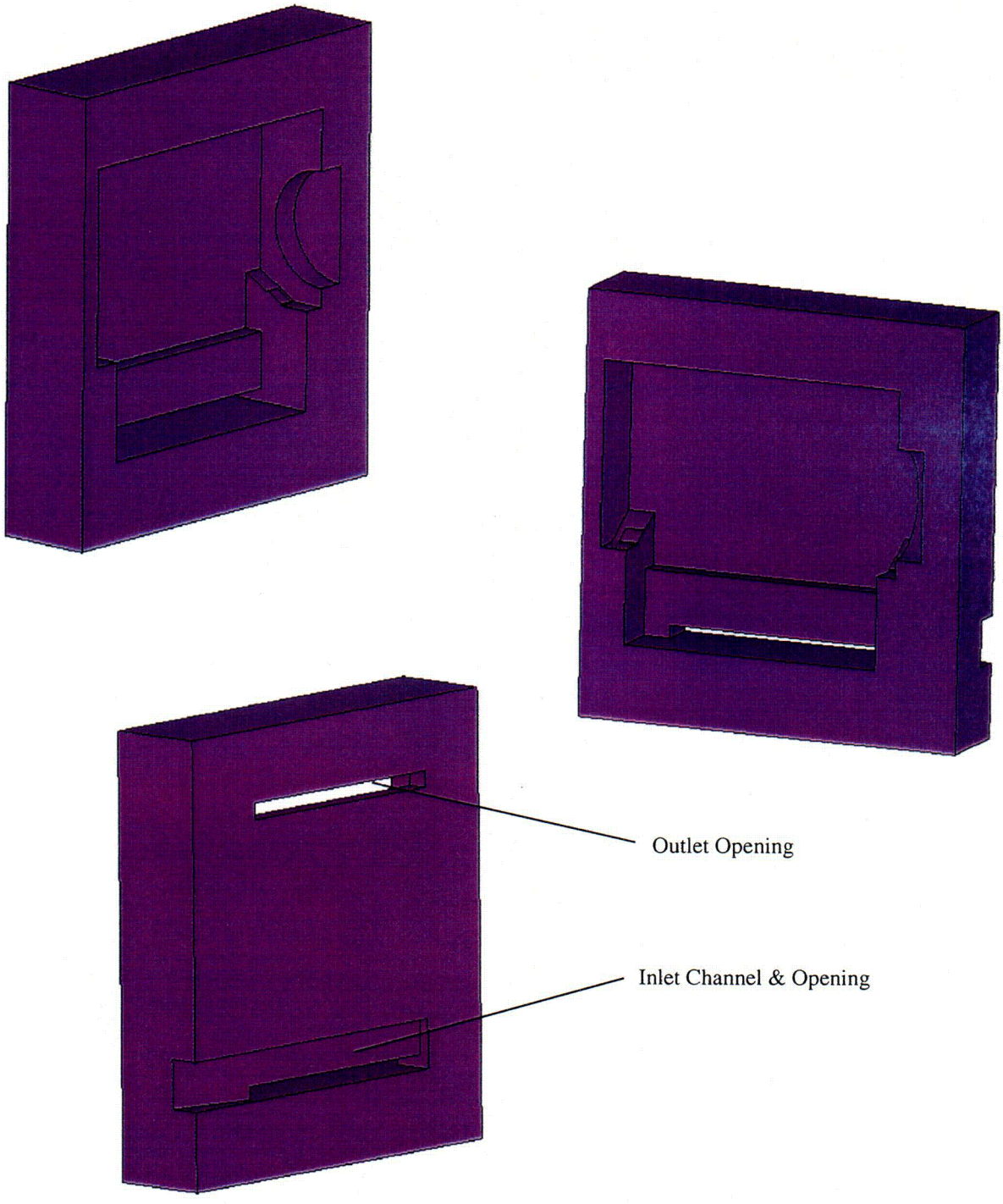

Figure 4-7
FEM of HSM-H, Concrete Structure

C06

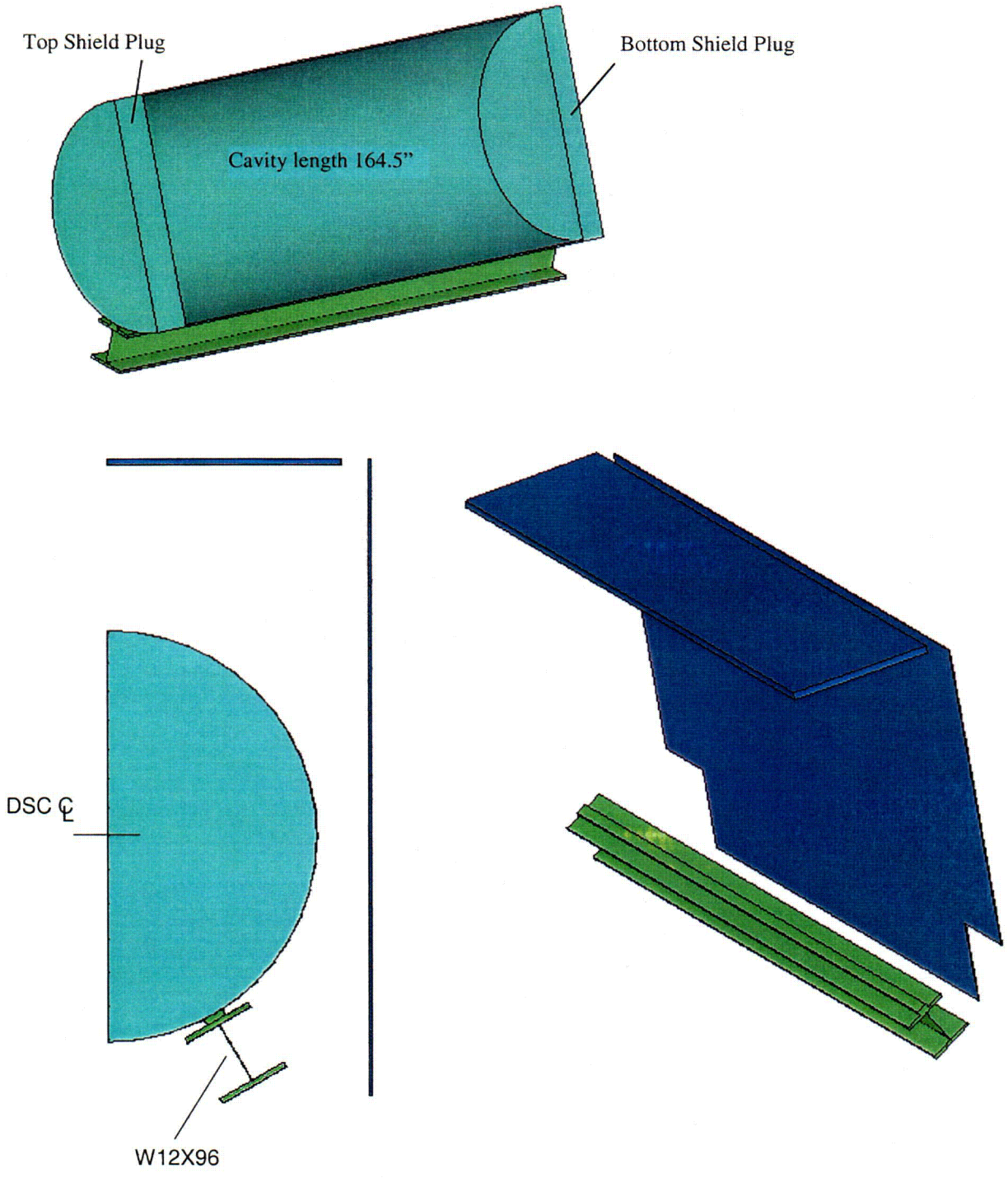

Figure 4-8
FEM of HSM-H, DSC and Support Rails

C07

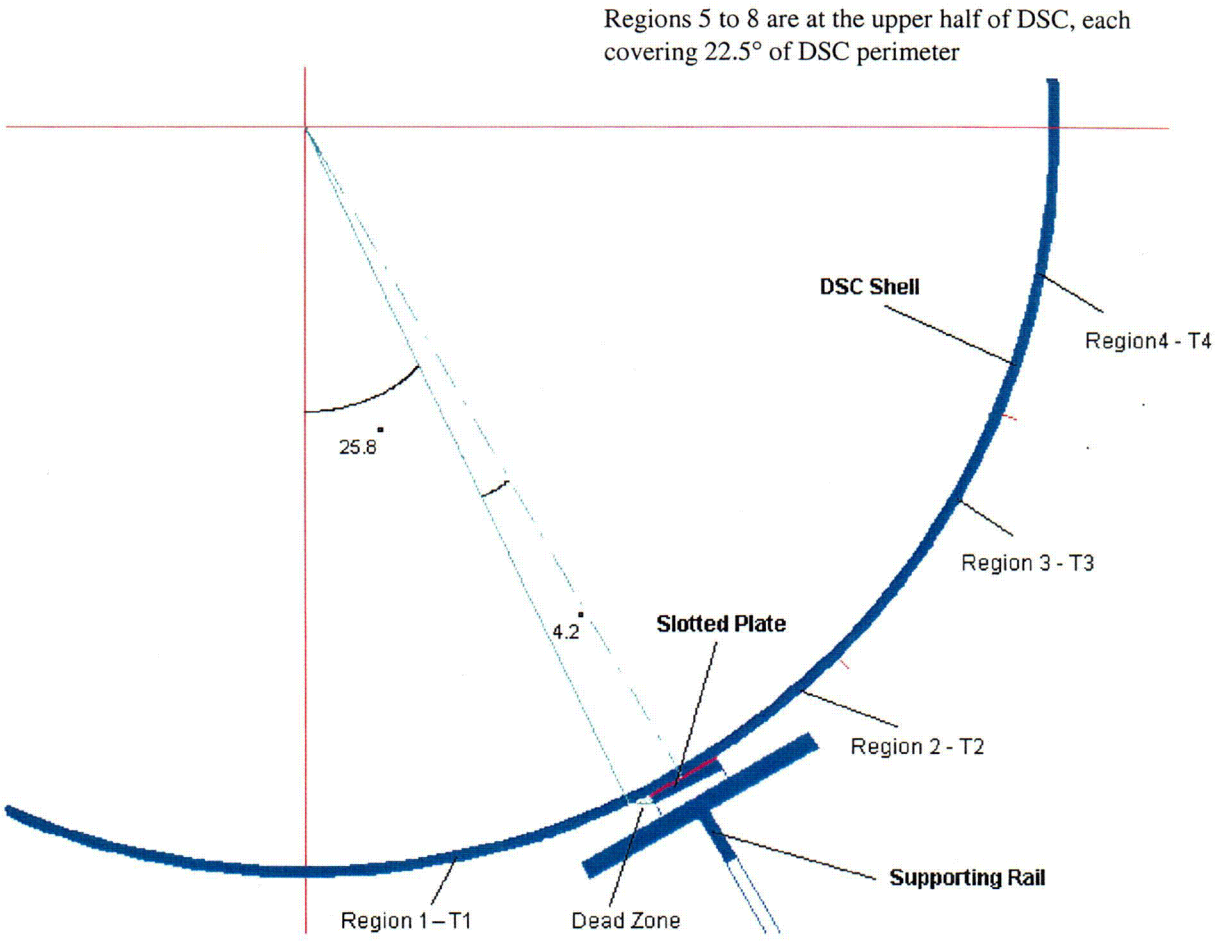

Figure 4-9
DSC Circumferential Convection Regions in the HSM-H Model

C07

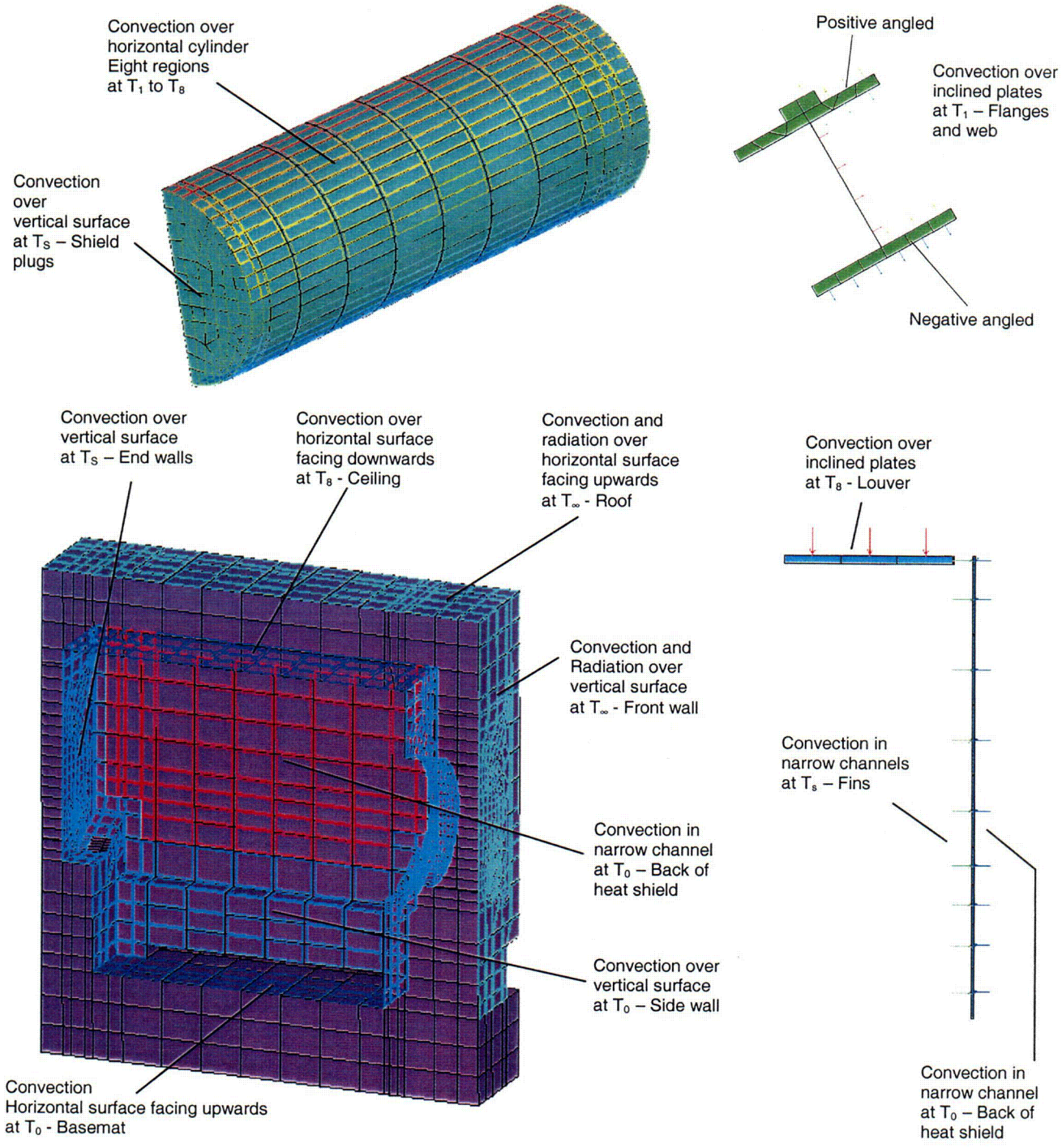

Figure 4-10
Typical Convection Boundary Conditions in the HSM_H Model

C08

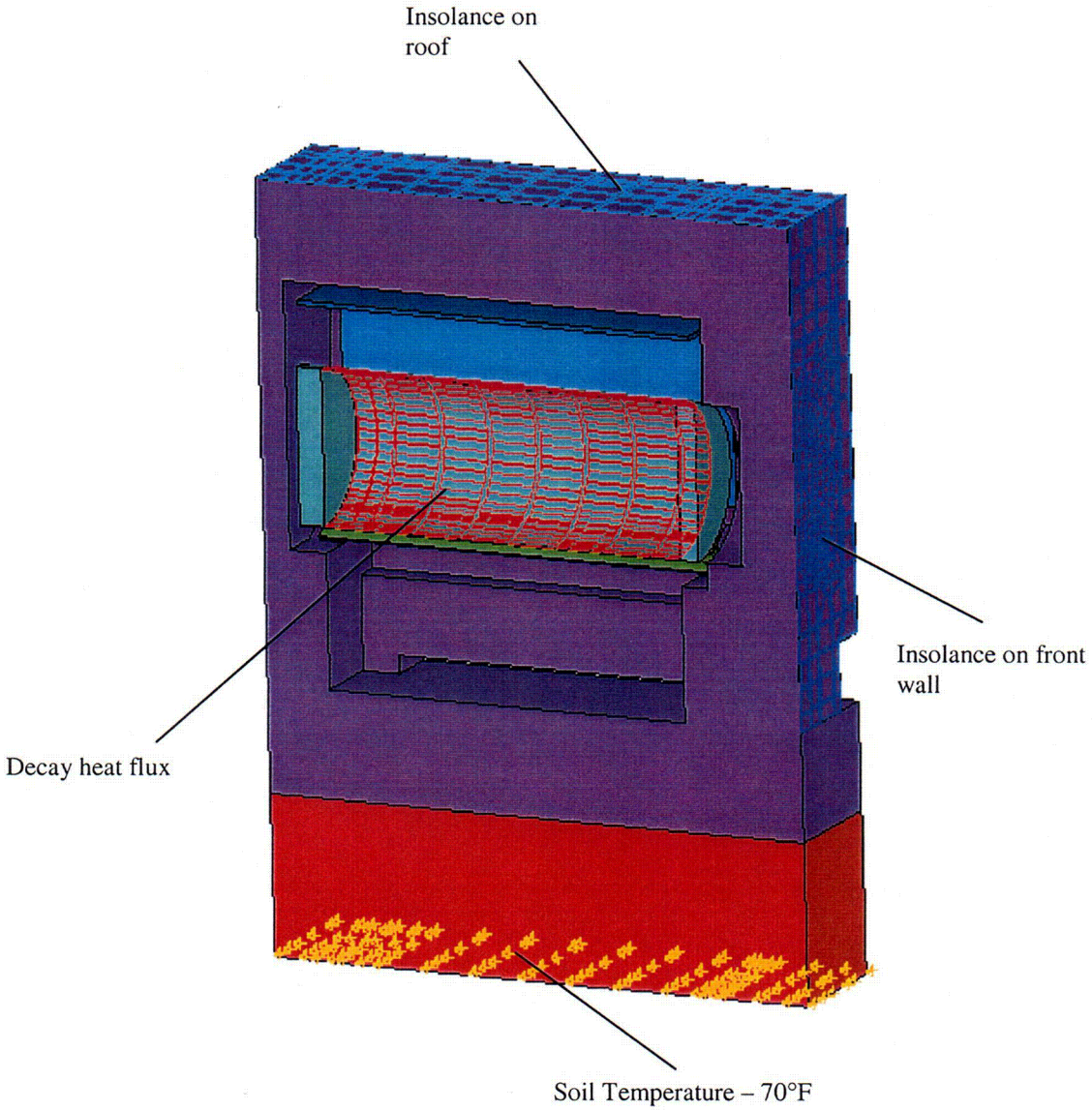

Figure 4-11
Typical Heat Flux and Fixed Temperature Boundary Conditions for HSM-H Model

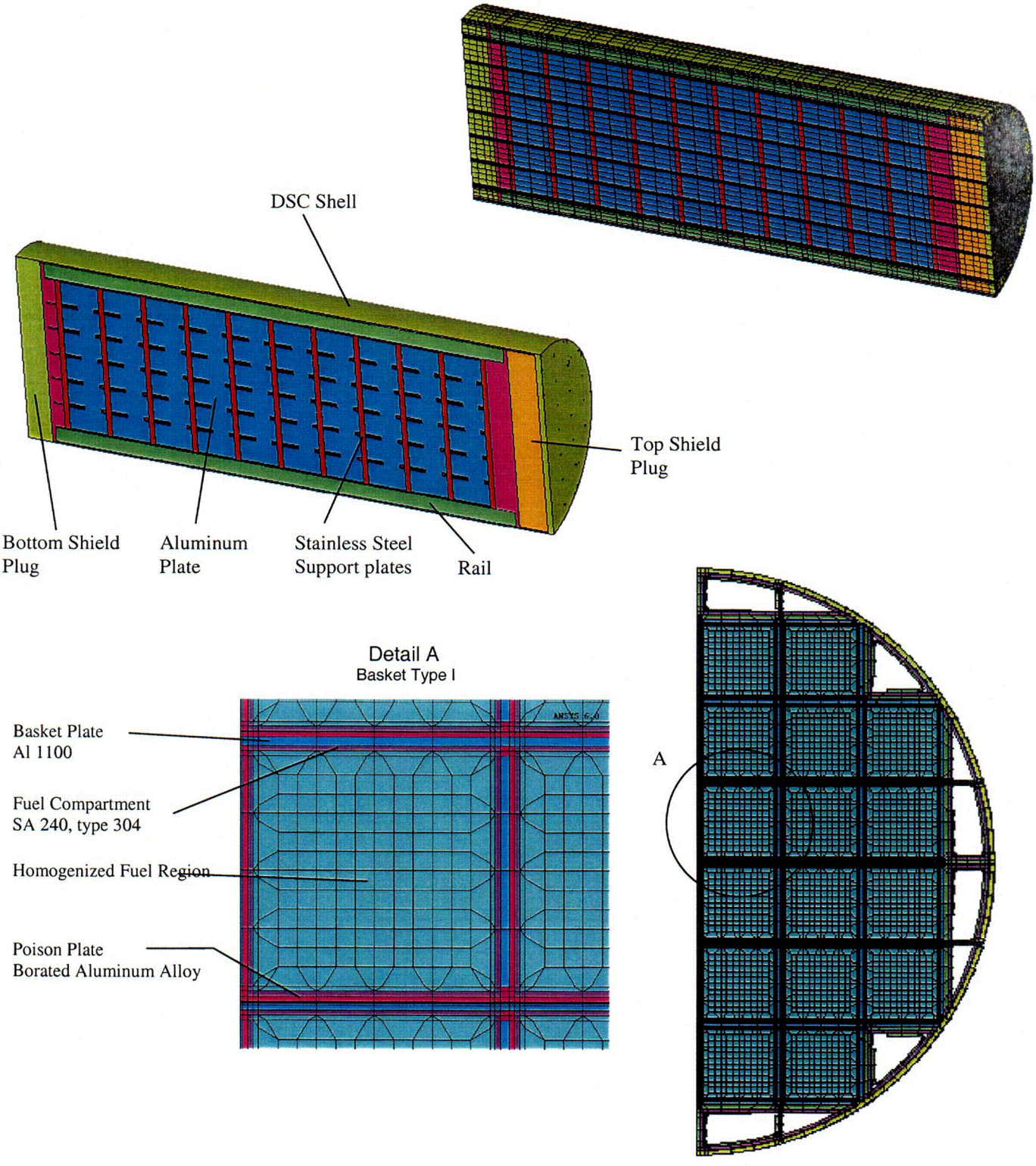

Figure 4-12
Finite Element Model of the DSC

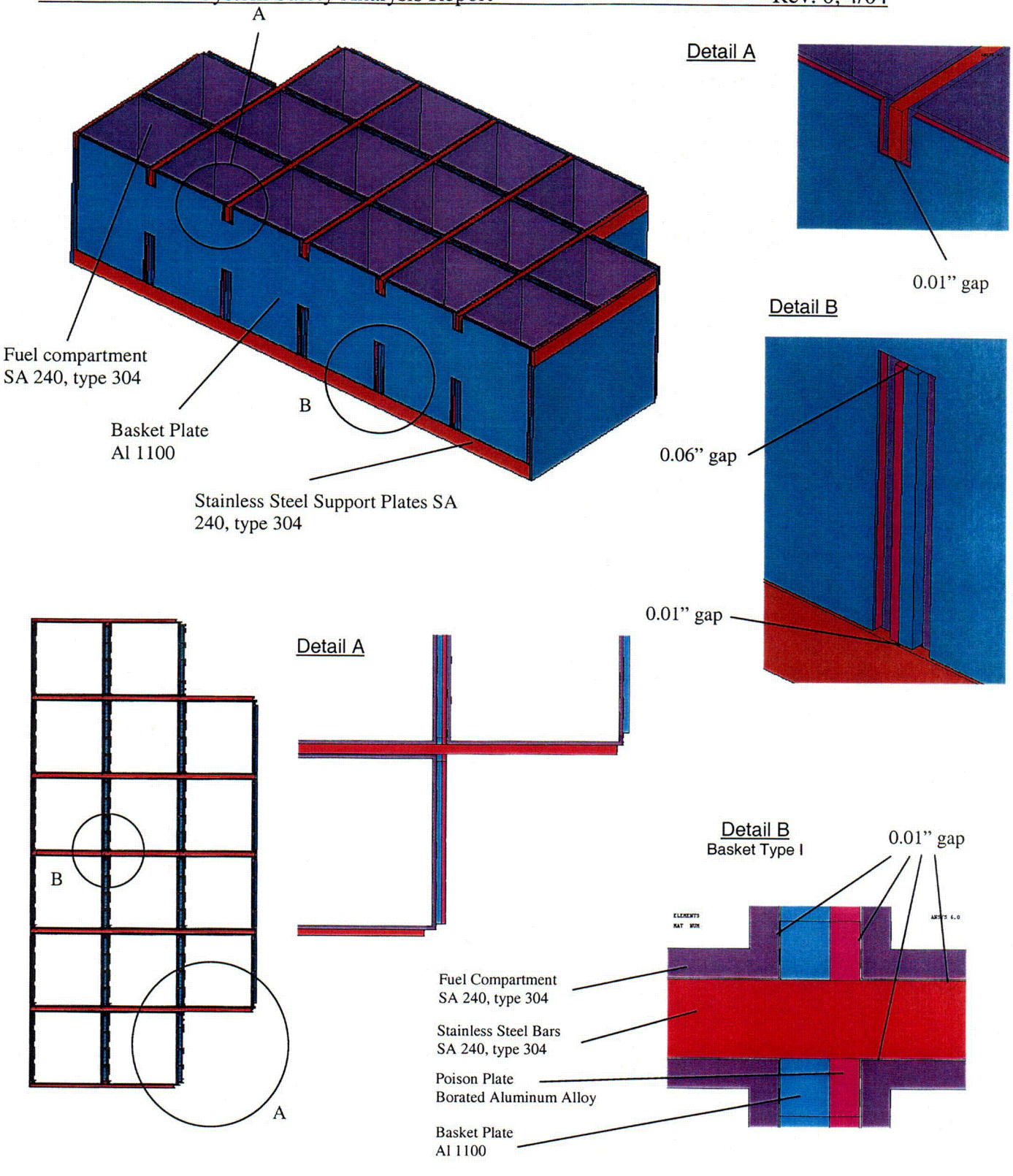

Figure 4-13
FEM of DSC Basket, Details

C 11

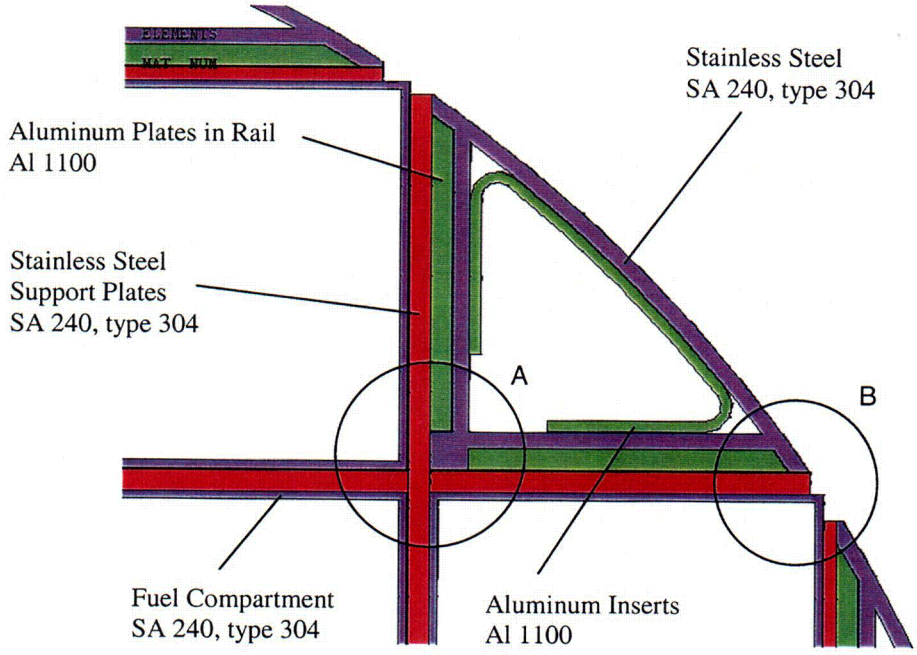

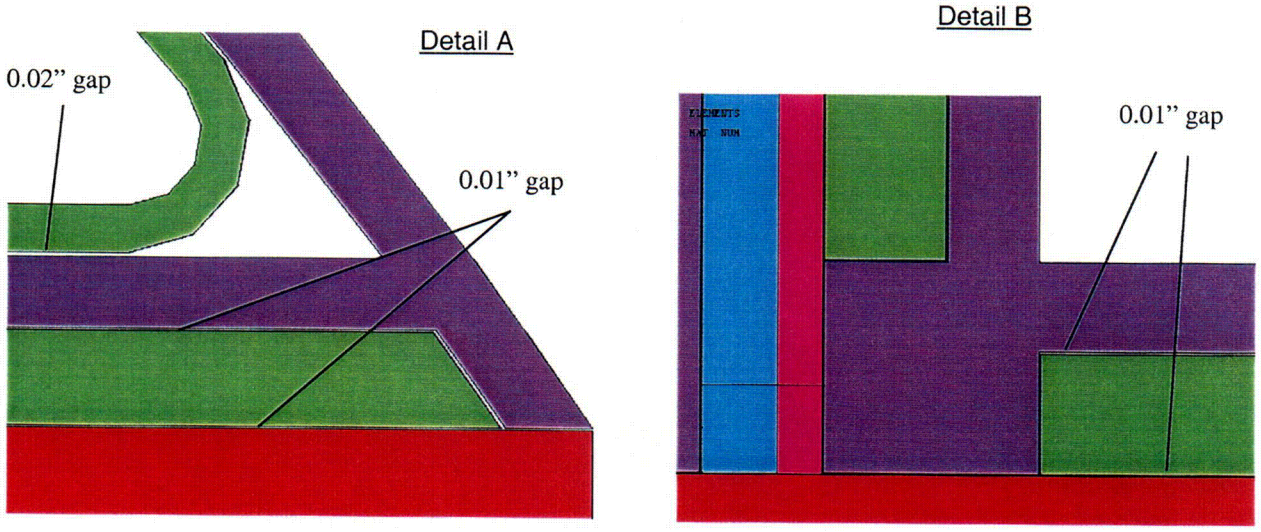

Figure 4-14
FEM of DSC Rails, Details

Configuration 1

	1.1	1.2	1.2	1.1	
1.1	1.1	1.1	1.1	1.1	1.1
1.2	1.1	0.8	0.8	1.1	1.2
1.2	1.1	0.8	0.8	1.1	1.2
1.1	1.1	1.1	1.1	1.1	1.1
	1.1	1.2	1.2	1.1	

Configuration 2

	1.1	1.5	1.5	1.1	
1.1	1.1	1.1	1.1	1.1	1.1
1.5	1.1	0.2	0.2	1.1	1.5
1.5	1.1	0.2	0.2	1.1	1.5
1.1	1.1	1.1	1.1	1.1	1.1
	1.1	1.5	1.5	1.1	

Configuration 3

	1.1	1.5	1.5	1.1	
1.1	1.1	0.925	0.925	1.1	1.1
1.5	0.925	0.55	0.55	0.925	1.5
1.5	0.925	0.55	0.55	0.925	1.5
1.1	1.1	0.925	0.925	1.1	1.1
	1.1	1.5	1.5	1.1	

Configuration 4

	0.98	1.5	1.5	0.98	
0.98	0.98	0.98	0.98	0.98	0.98
1.5	0.98	0.80	0.80	0.98	1.5
1.5	0.98	0.80	0.80	0.98	1.5
0.98	0.98	0.98	0.98	0.98	0.98
	0.98	1.5	1.5	0.98	

Configuration 5

	1.1	1.2	1.2	1.1	
1.1	1.1	1.1	1.1	1.1	1.1
1.2	1.1	0.55	0.55	1.1	1.2
1.2	1.1	1.05	1.05	1.1	1.2
1.1	1.1	1.1	1.1	1.1	1.1
	1.1	1.2	1.2	1.1	

Figure 4-15
Thermally Bounding Loading Configurations Considered in the DSC Model

Temperature Boundary Conditions

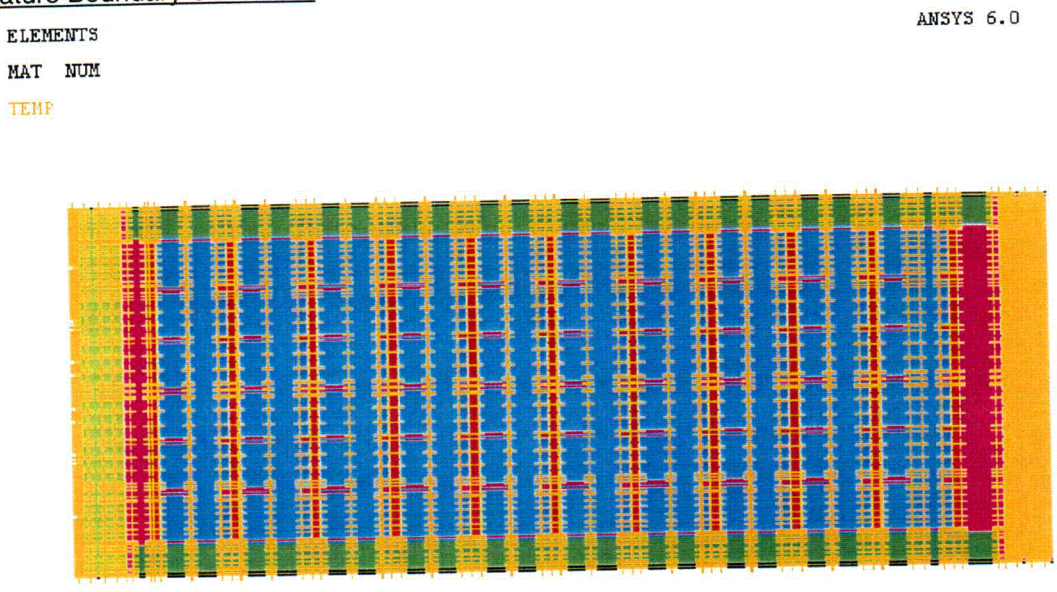

Heat Generating Boundary Conditions

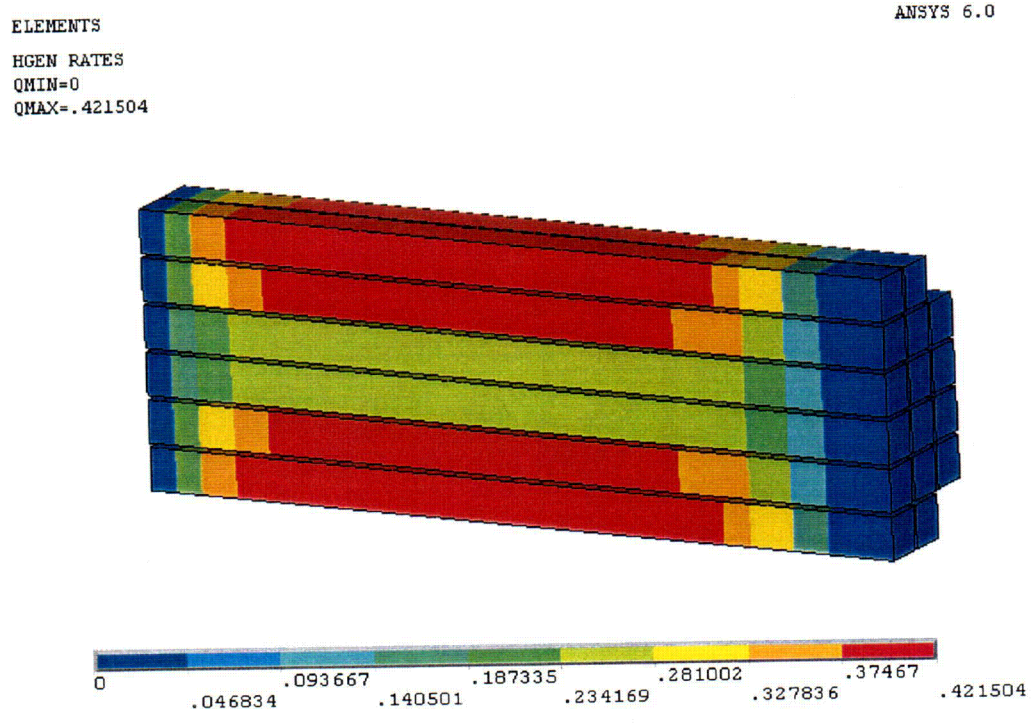

Figure 4-16
Typical Boundary Conditions in the DSC Model

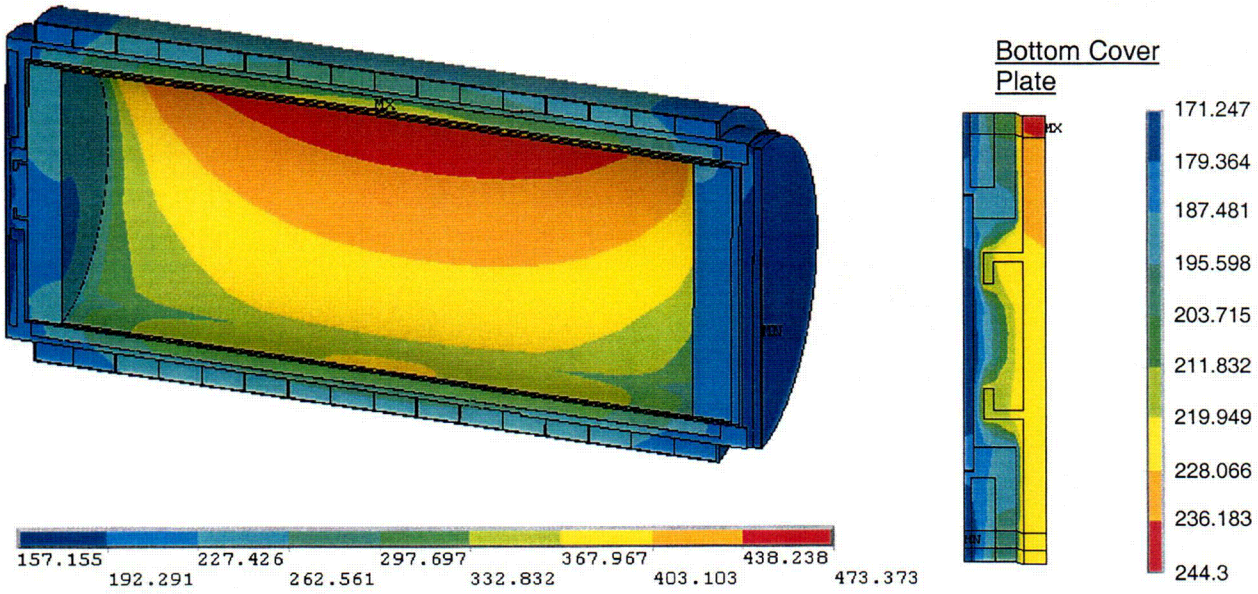

Bottom Cover Plate

Liquid Neutron Shielding

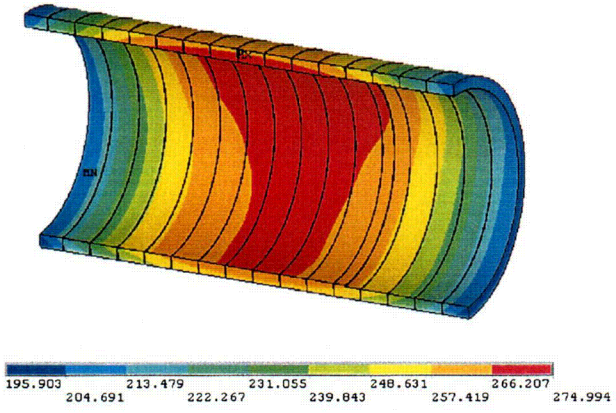

Gamma Shell

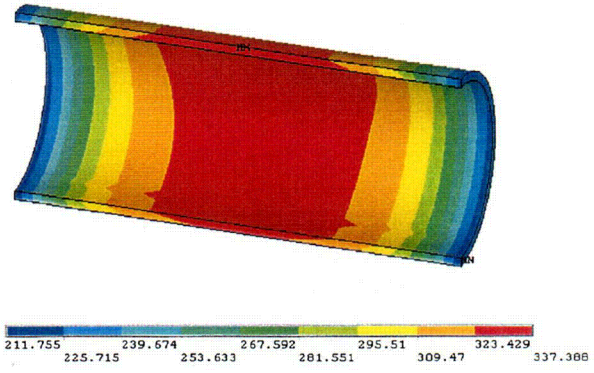

Solid Neutron Absorber

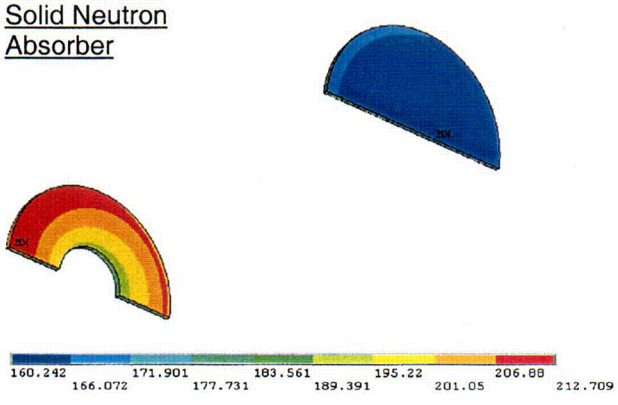

Cask Lid

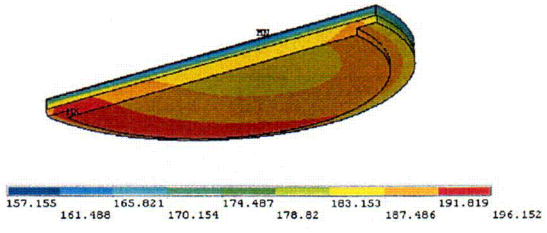

Figure 4-17
Transfer Cask Temperature Distributions, 115°F Ambient

C 14

Cask Bottom, Sub-Model

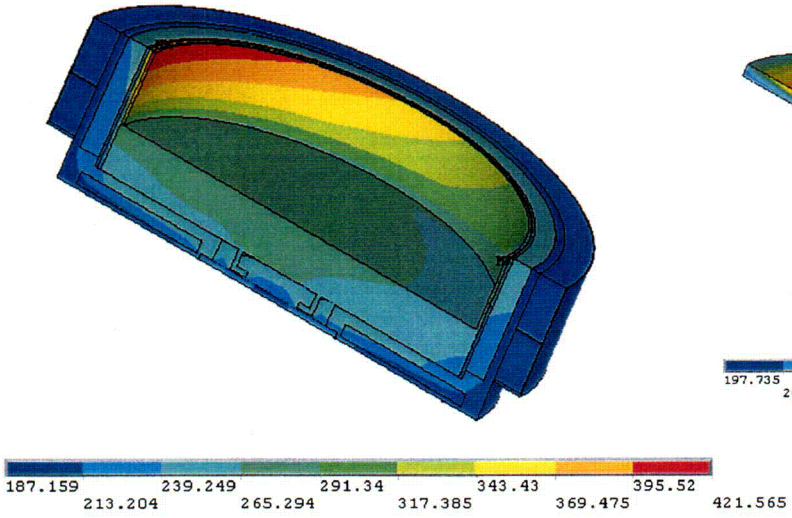

Bottom Solid Neutron Absorber

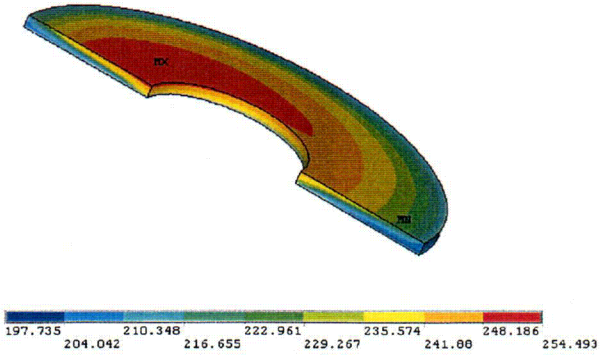

Bottom Cover Plate

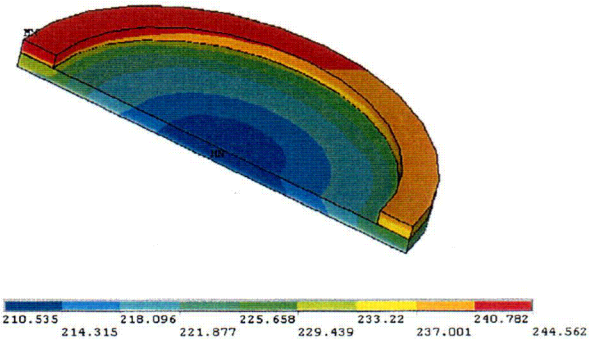

Cask Top, Sub-Model

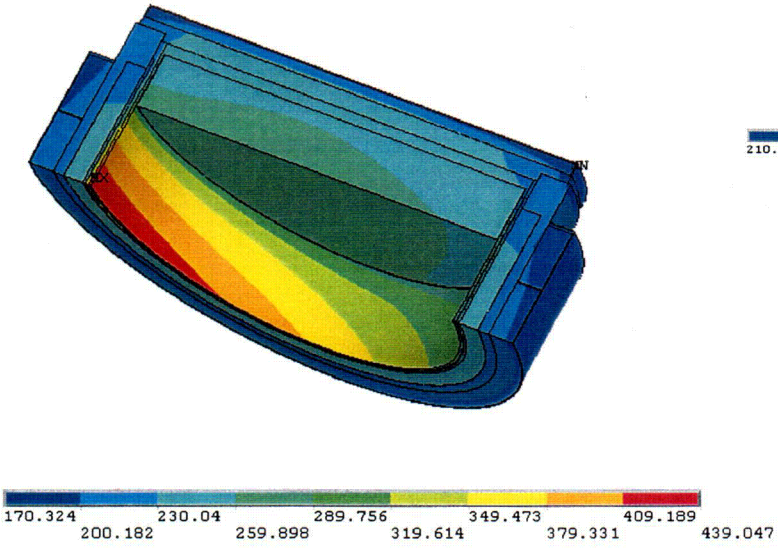

Top Solid Neutron Absorber

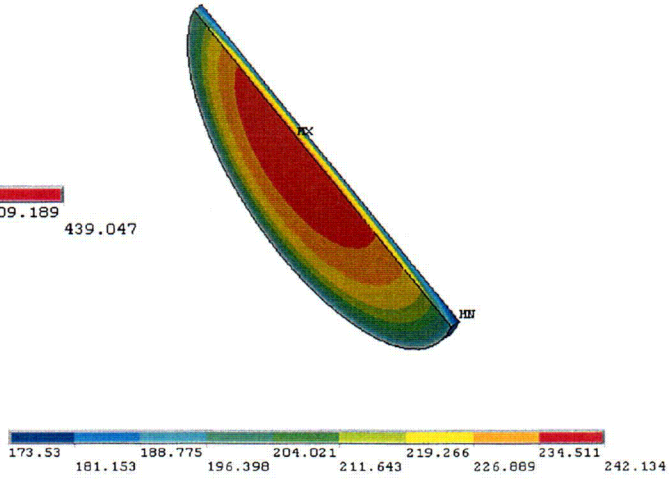

Figure 4-18
Temperature Distributions in Transfer Cask Sub-Models

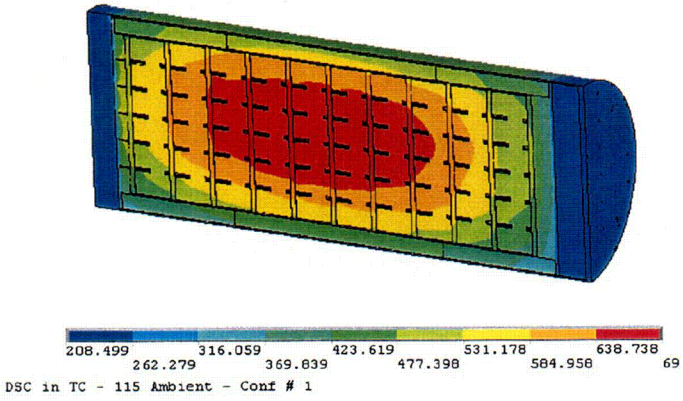

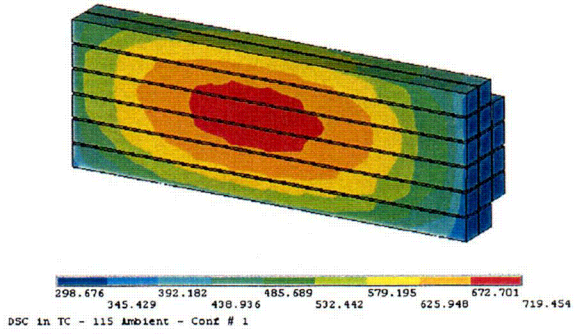

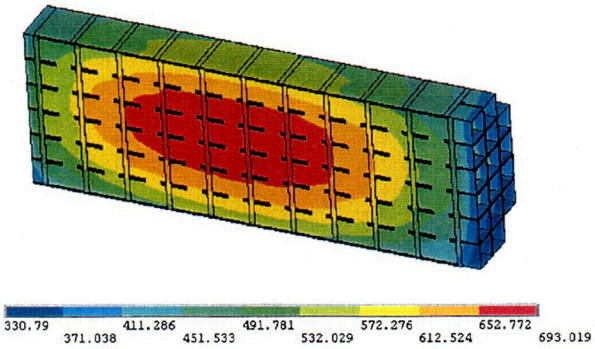

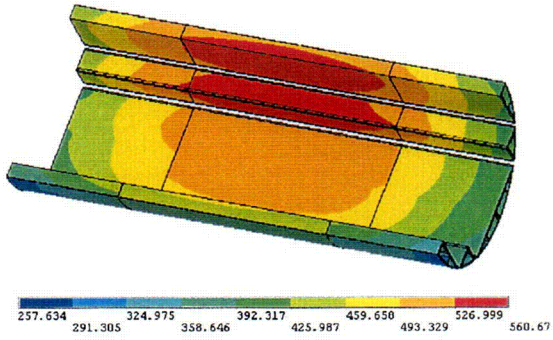

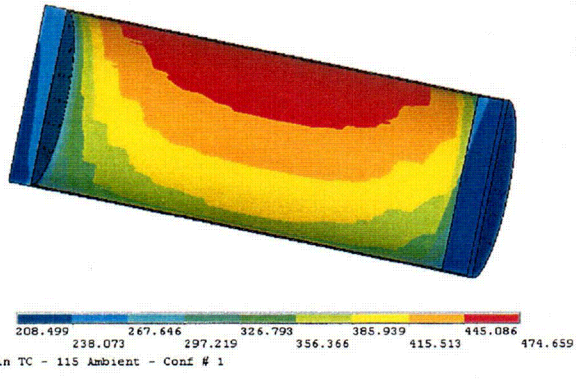

Figure 4-19
DSC Temperature Distribution during Transfer Operation
Basket Type I, Loading Configuration 1, 115°F Ambient

C16

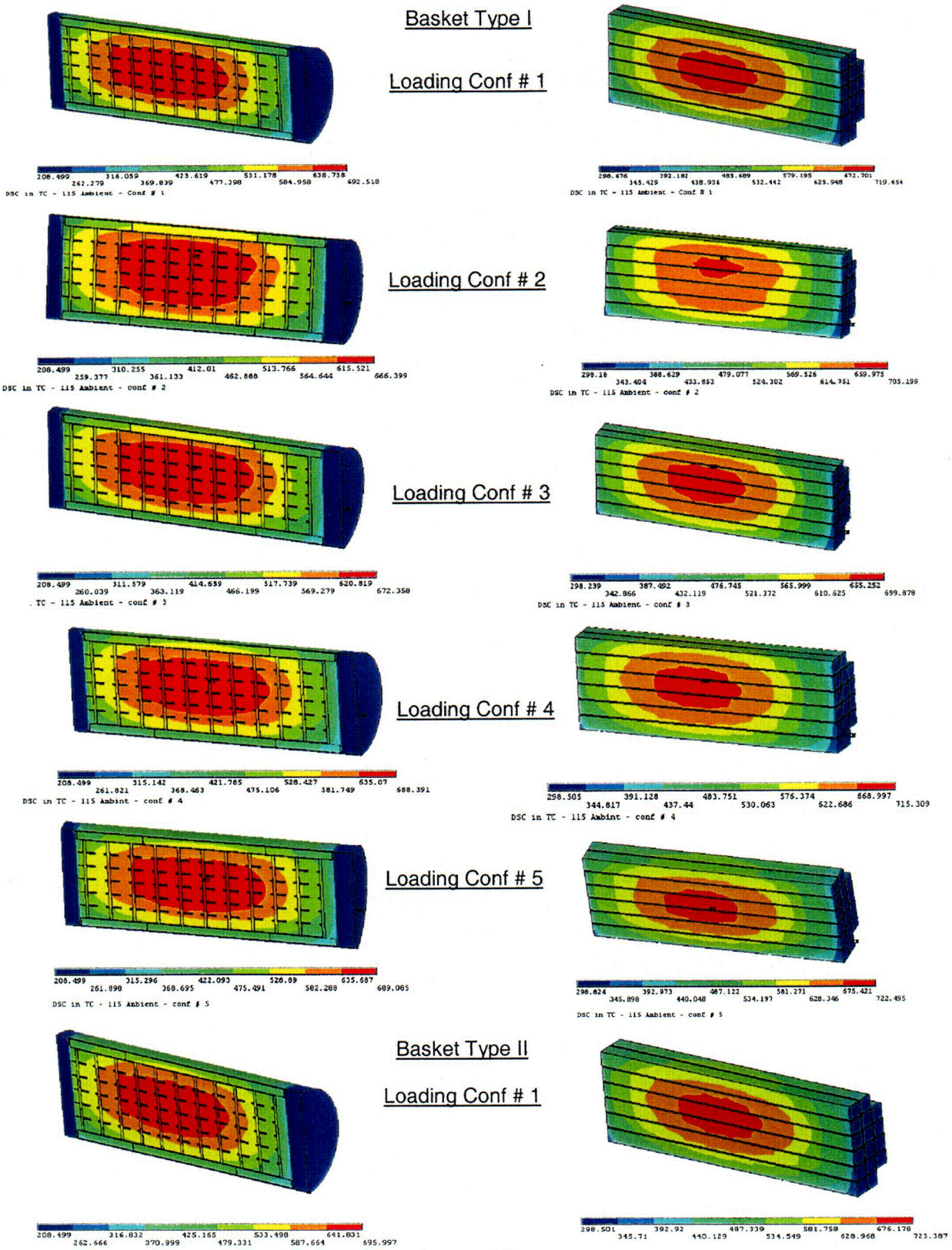

Figure 4-20
Temperature Distribution of DSC and Fuel Assemblies
during Transfer Operations, 115°F Ambien

C17

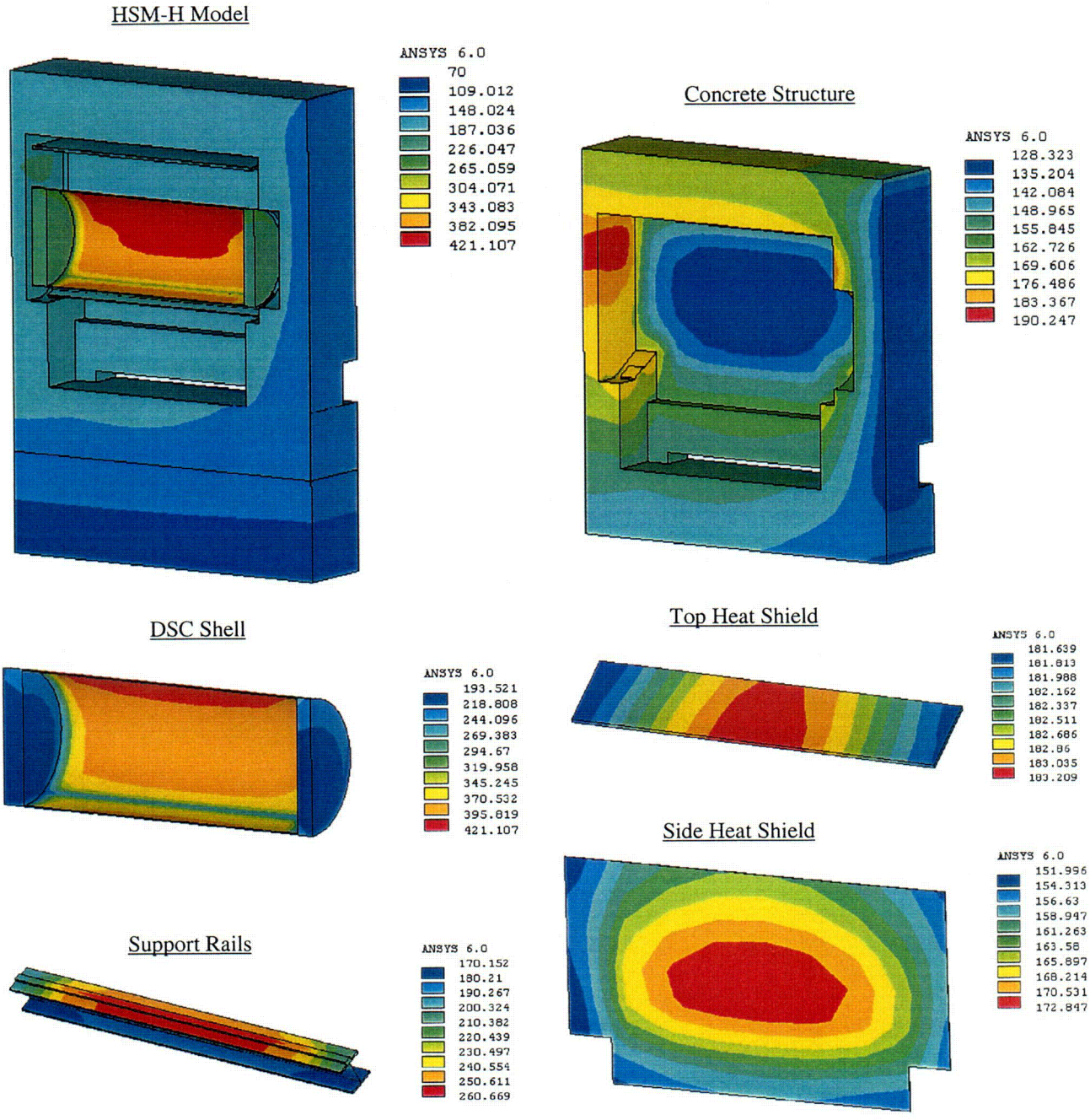

Figure 4-21
HSM-H Temperature Distribution 115°F Ambient
with Finned Aluminum Side Heat Shields, 34.8 kW

C 18

HSM-H with
Unfinned Aluminum Side Heat Shield
32.0 kW

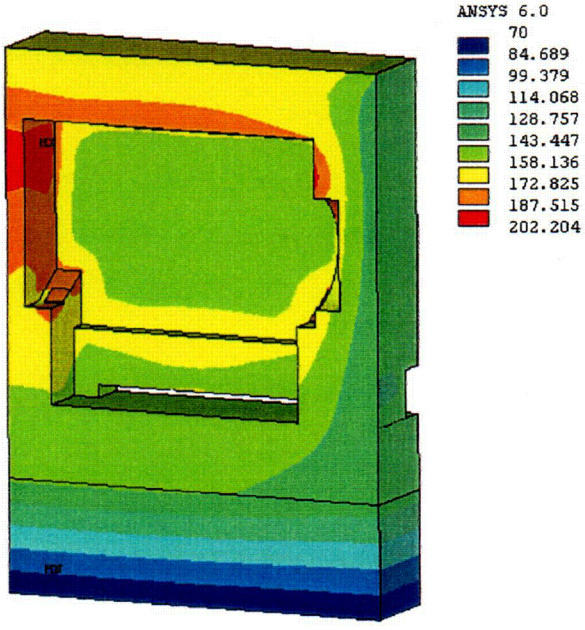

HSM-H with
Galvanized Steel Side Heat Shield
26.1 KW

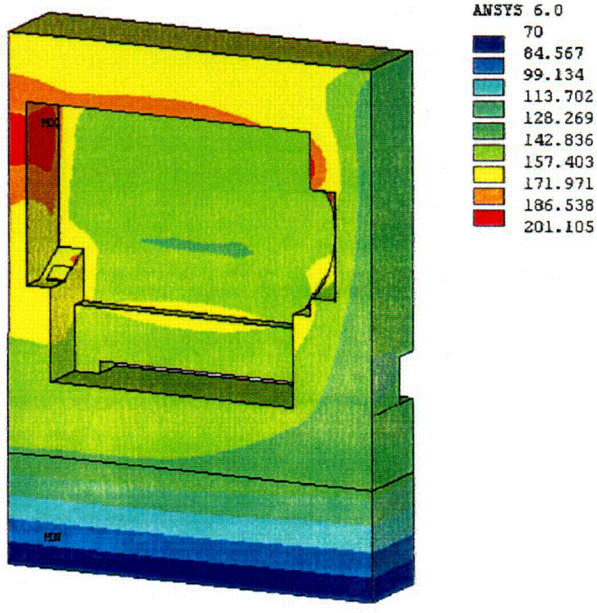

DSC Shell

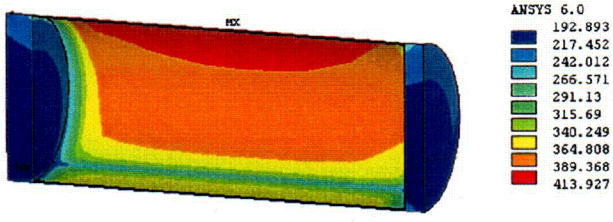

DSC Shell

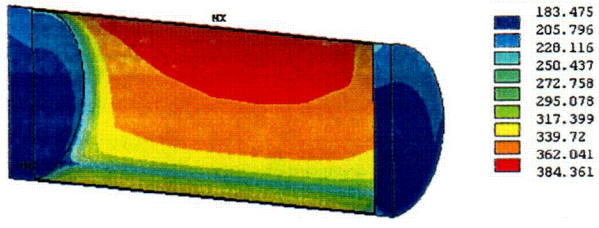

Side Heat Shield

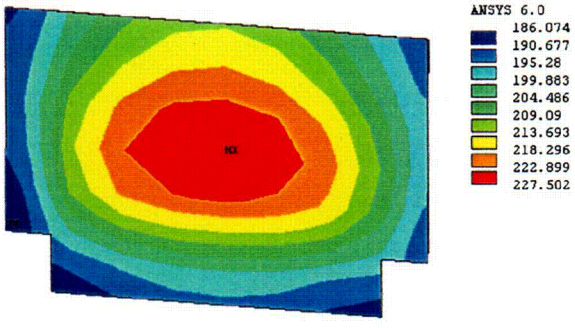

Side Heat Shield

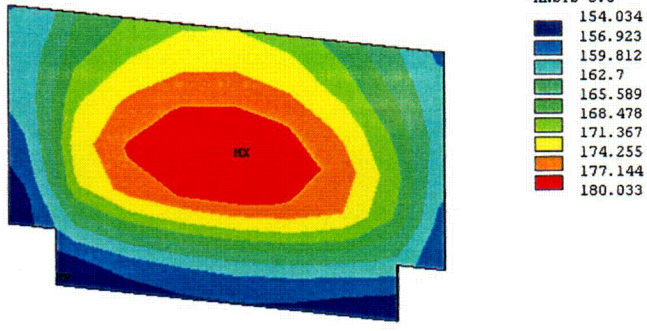

Figure 4-22
HSM-H Temperature Distribution 115°F Ambient
With Unfinned Side Heat Shields

C19

DSC Model

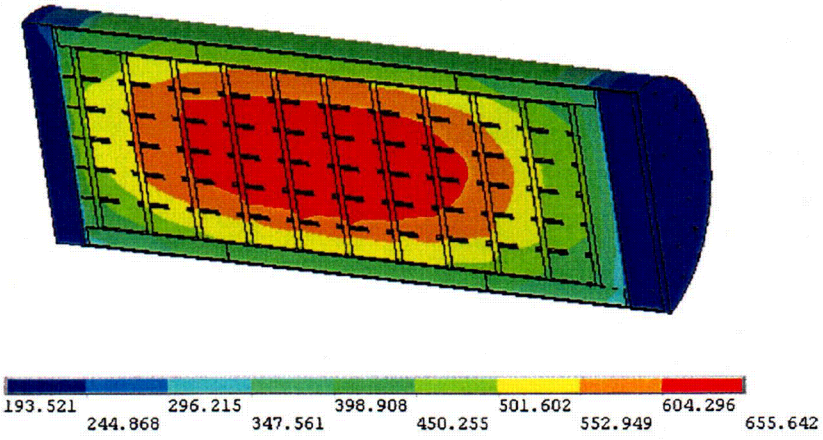

Fuel Assemblies

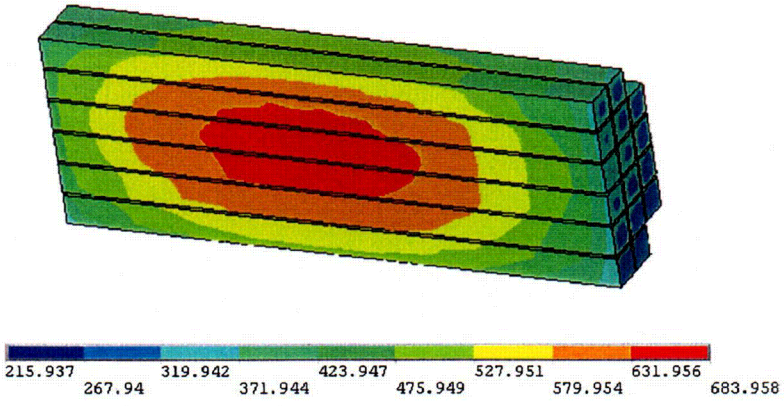

Figure 4-23
DSC Temperature Distribution during Storage – 115°F Ambient, 34.8 kW
In HSM-H with Finned Aluminum Side Heat Shields

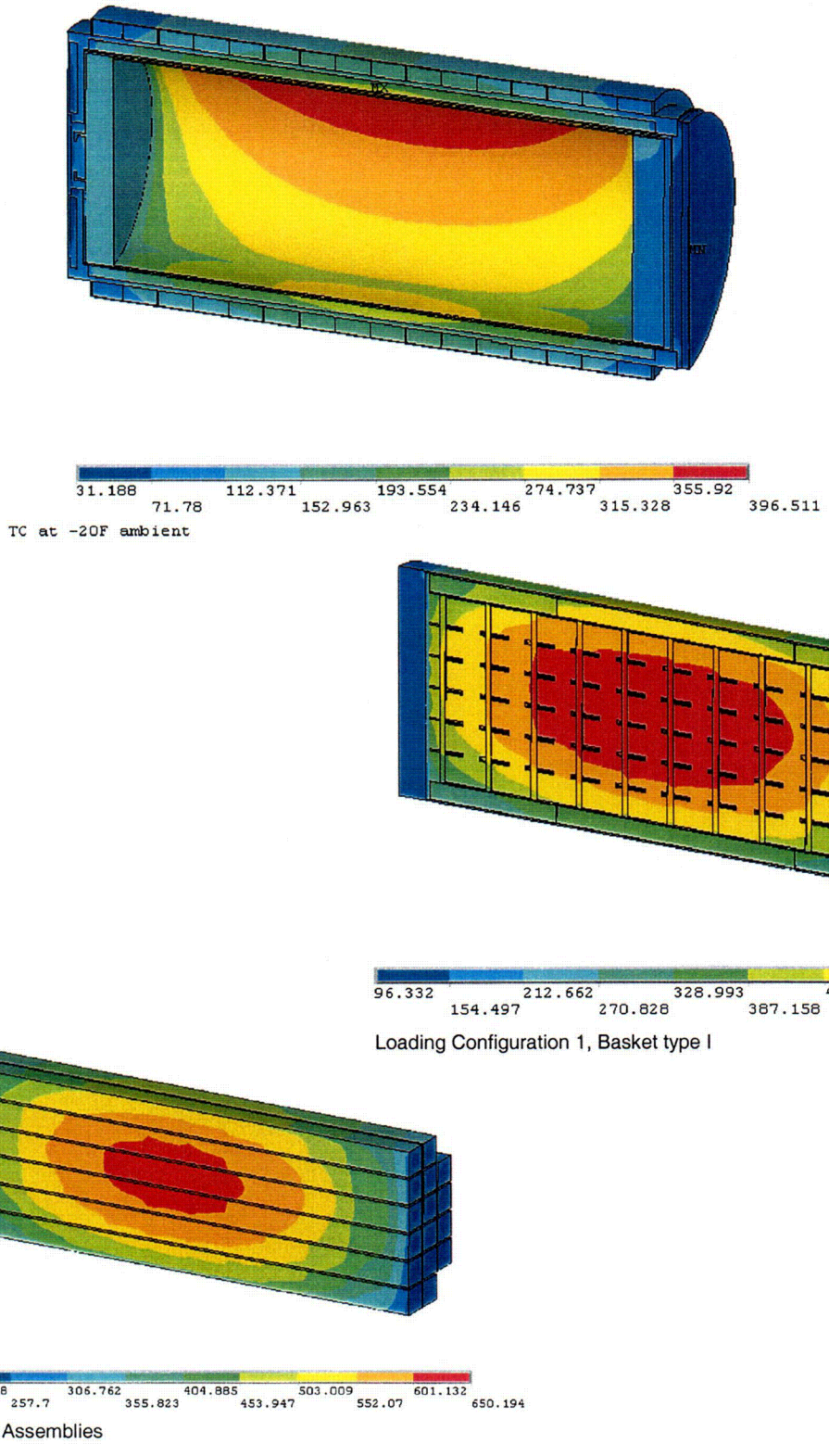

Figure 4-24
Temperature Distributions during Transfer Operations, Ambient -20°F

C 21

HSM-H with Finned Aluminum Side Heat Shields

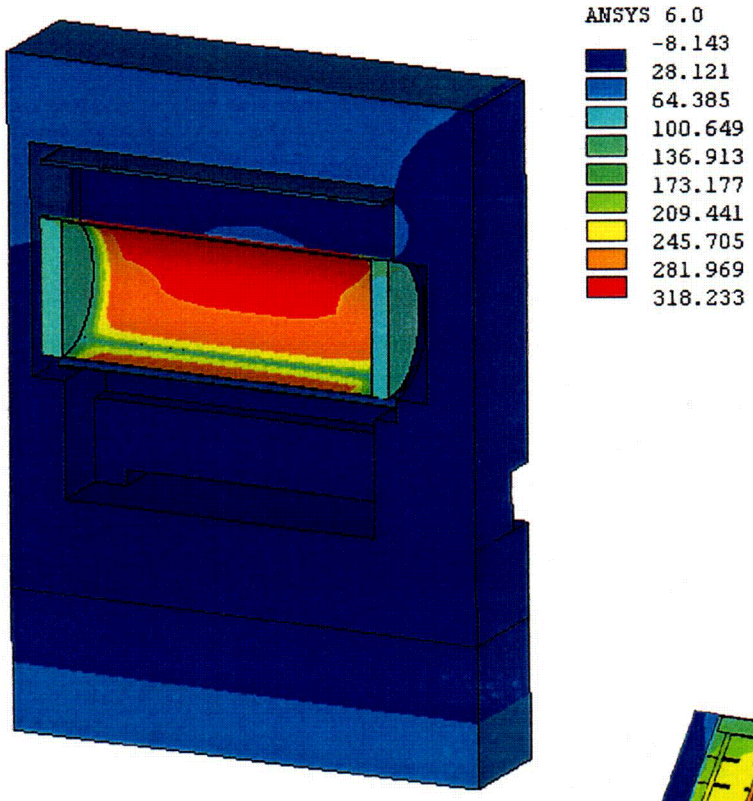

Basket type I, Loading Configuration 1

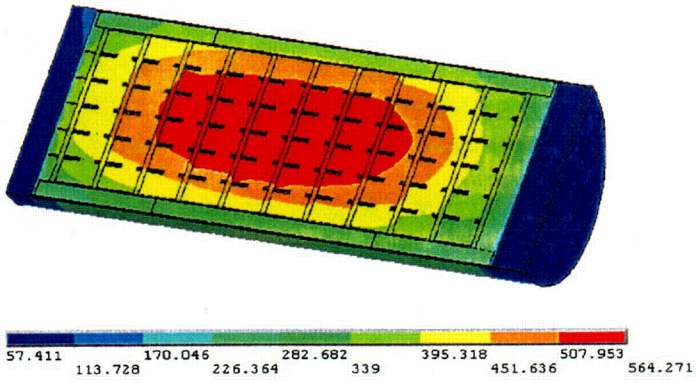

Figure 4-25
Temperature Distributions during Storage, Ambient -20°F, 34.8 kW

C 22

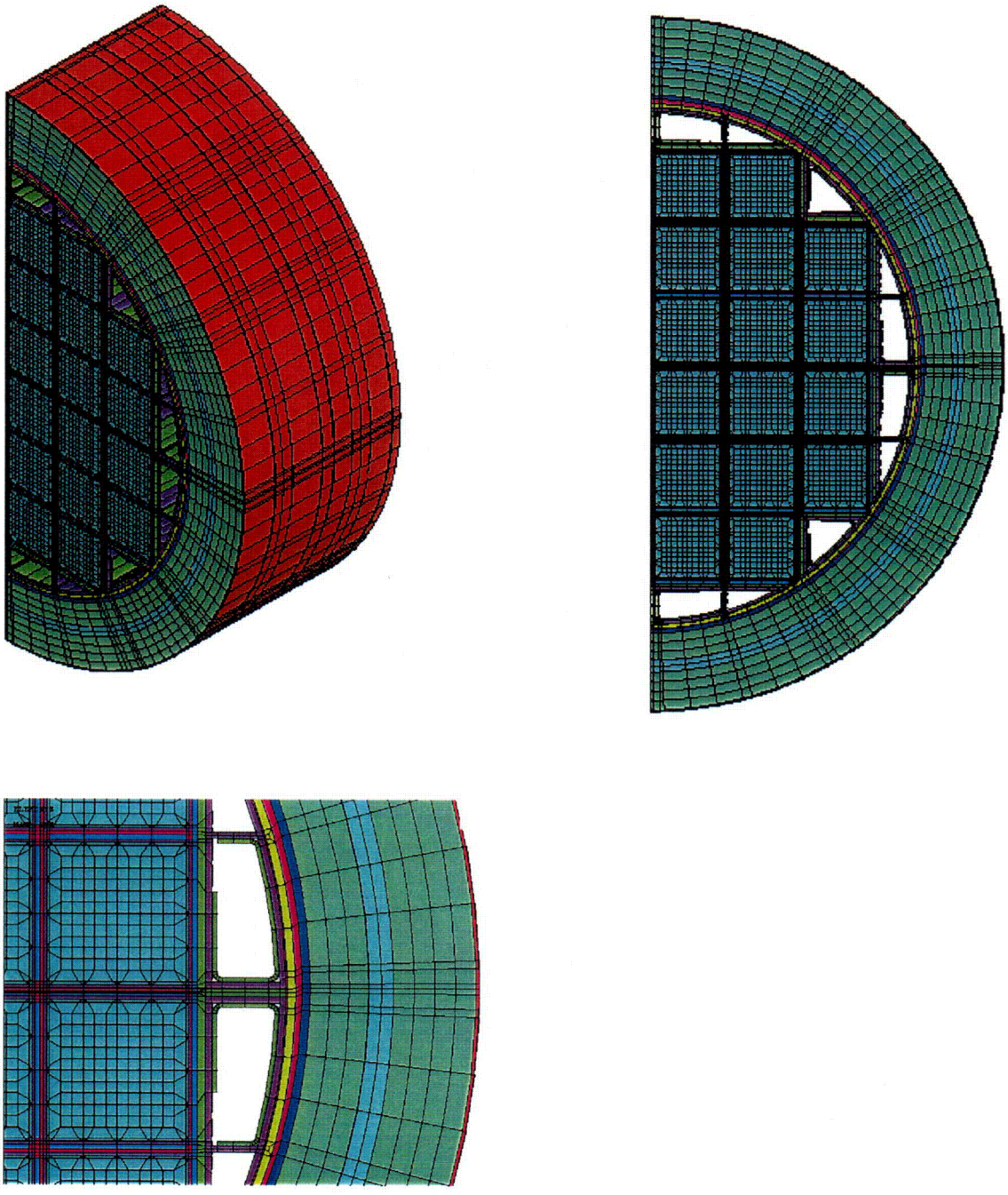

Figure 4-26
FEM of Transfer Cask for Fire Accident Case

Basket Slice Model

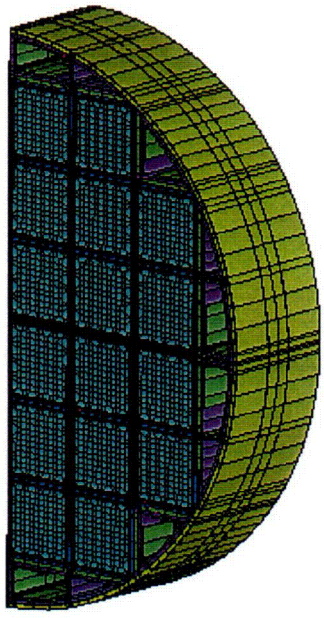

Applied Boundary Conditions
For Axial Effective Basket Conductivity

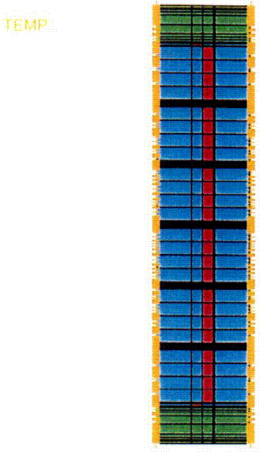

Applied Boundary Conditions
For Radial Effective Basket Conductivity

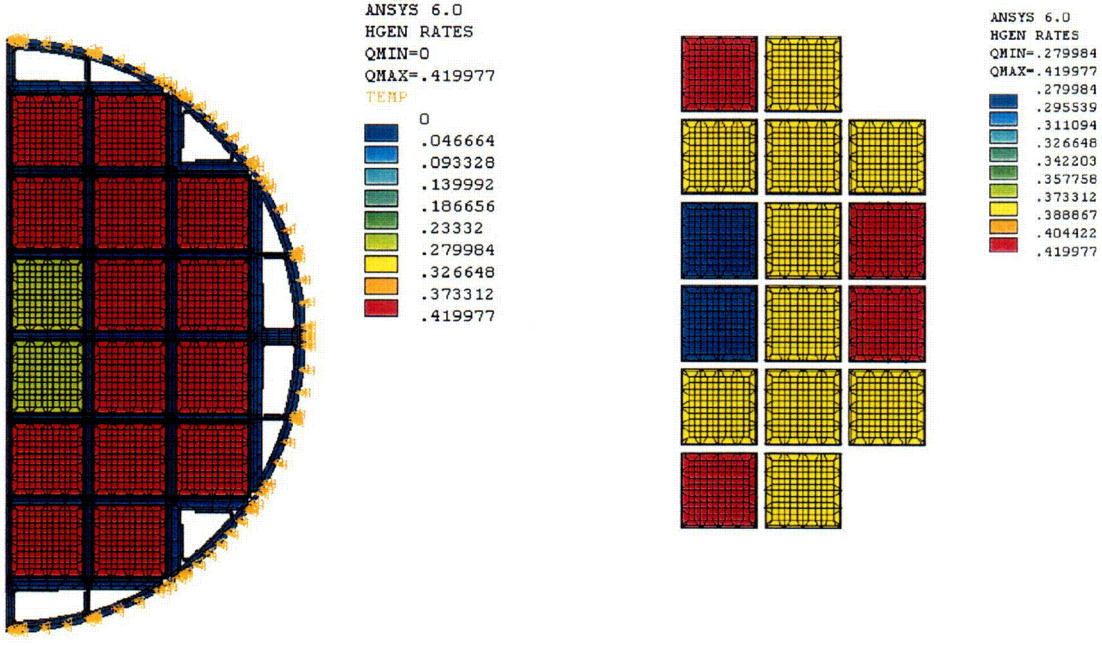

Figure 4-27
Basket Model for Calculation of Effective Conductivities
(HSM-H Model Blocked Vent Accident Case)

C 24

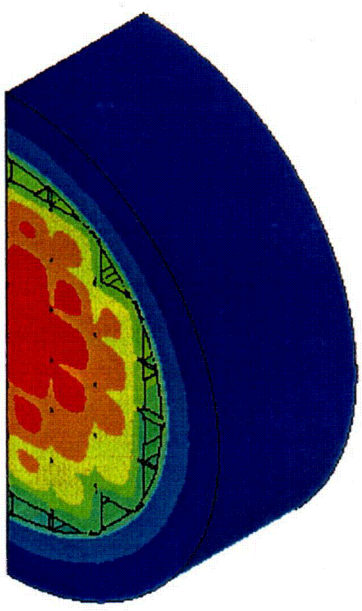

Initial Conditions

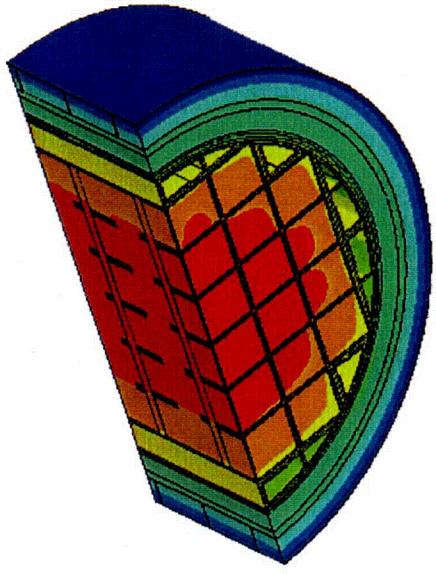

At the End of Fire

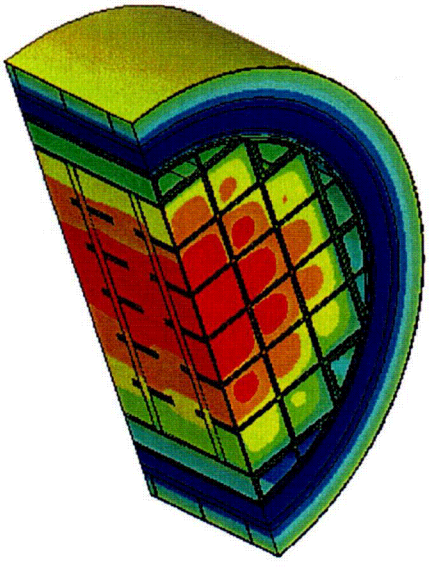

Cooldown Period, 200 hr

Figure 4-28
Temperature Distribution on TC Slice Model for Fire Accident Case

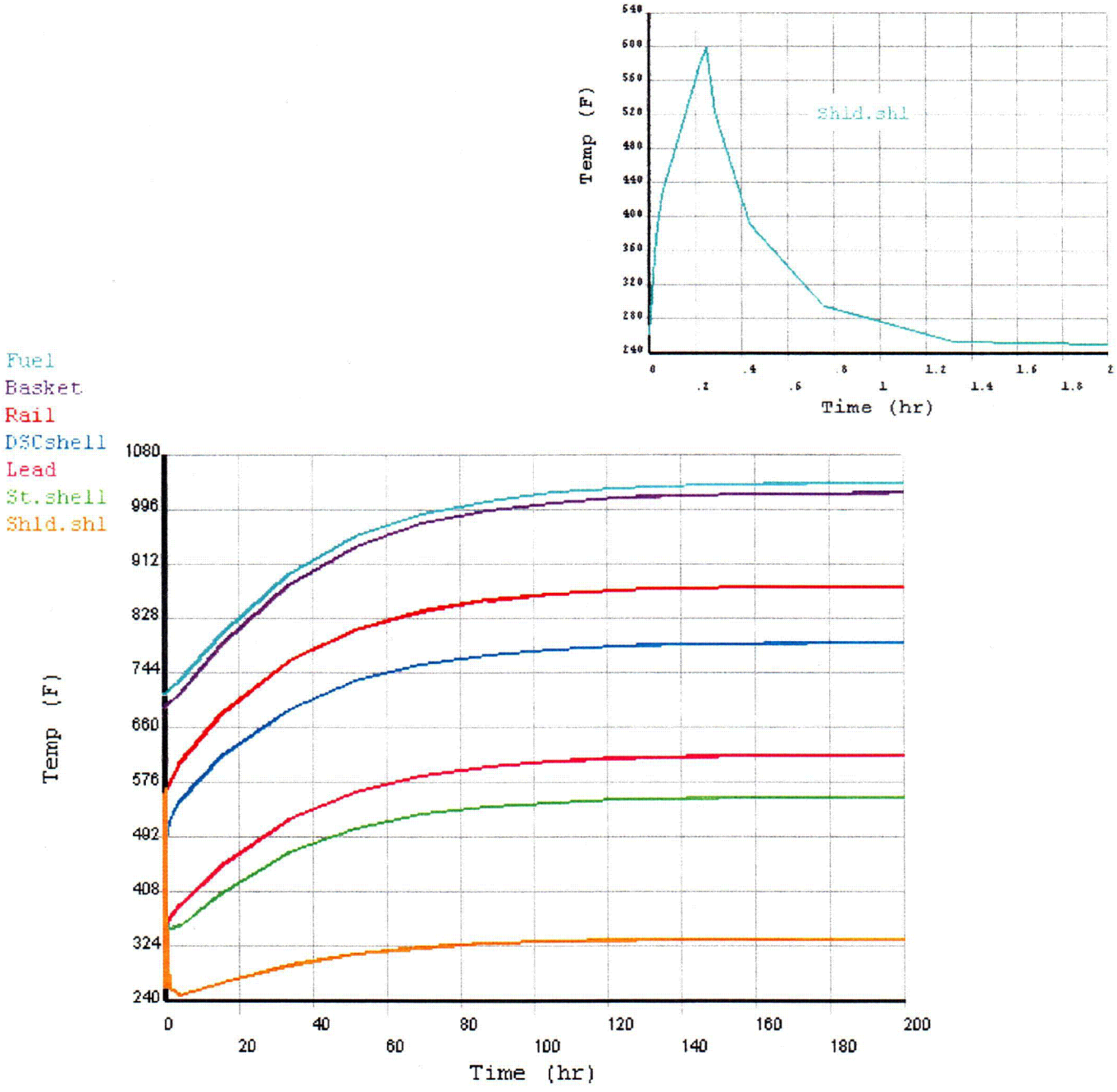

Figure 4-29
Time-History of TC Component Temperatures for the Fire Accident Case

C 26

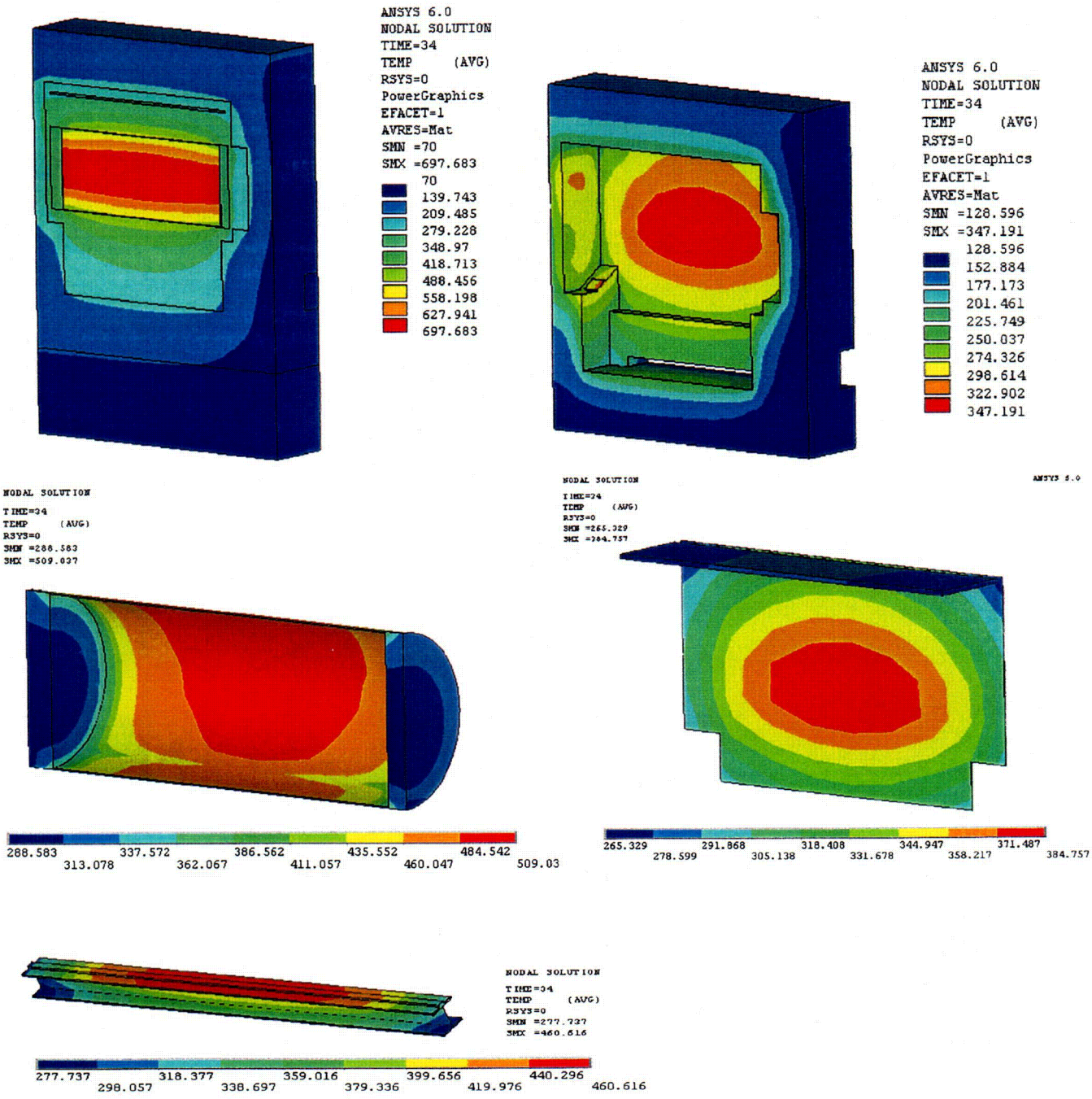

Figure 4-30
Temperature Distribution for HSM-H with Finned Aluminum Side Heat Shields - 34 hours after Blockage of the Vents, 34.8 kW

C27

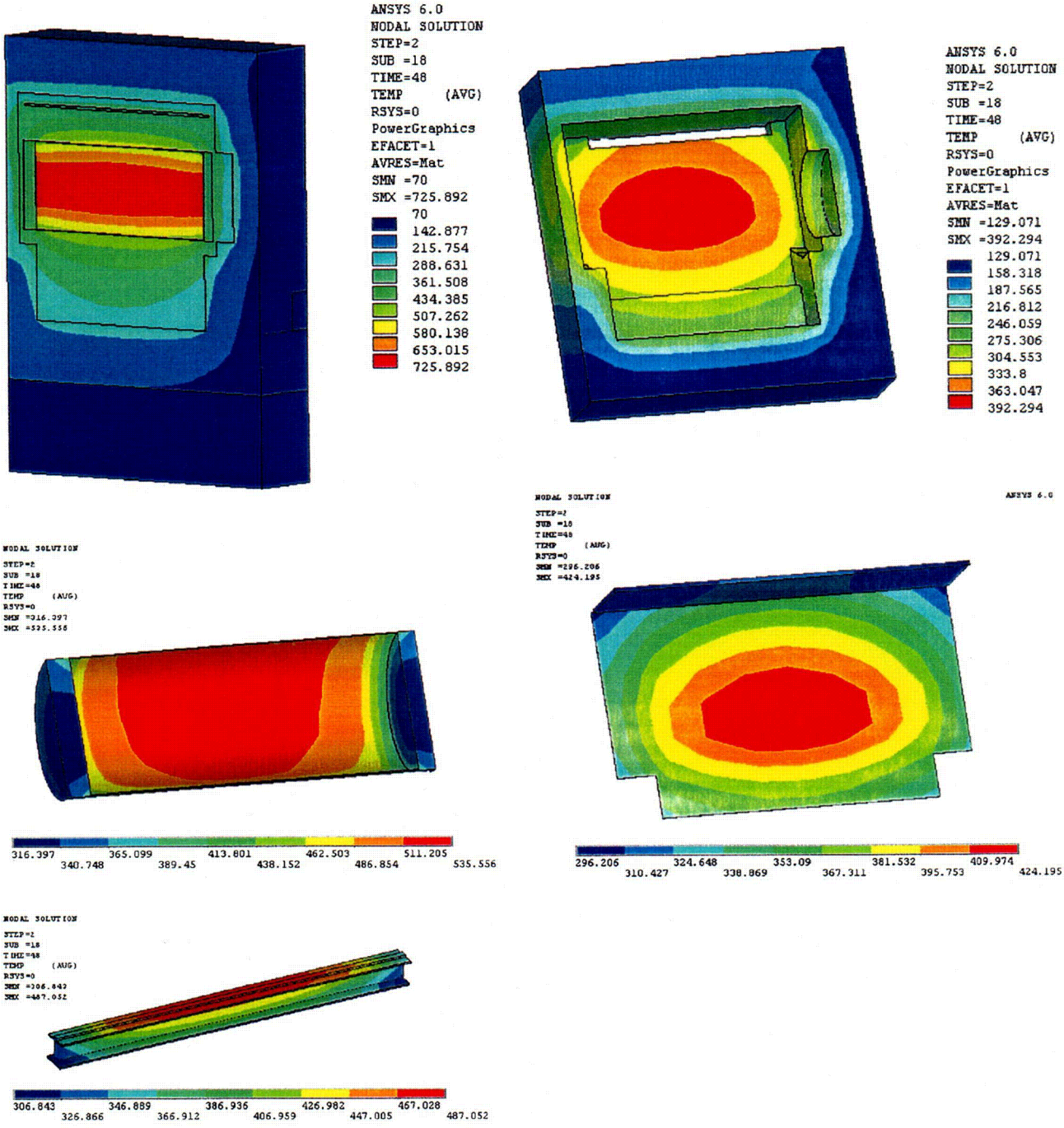

Figure 4-31
Temperature Distribution for HSM-H with Finned Aluminum Side Heat Shields - 48 hours after Blockage of the Vents, 34.8 kW

C 28

In HSM-H with Finned Aluminum Side Heat Shields
34 hours after Vent Blockage, 34.8 kW

DSC Model

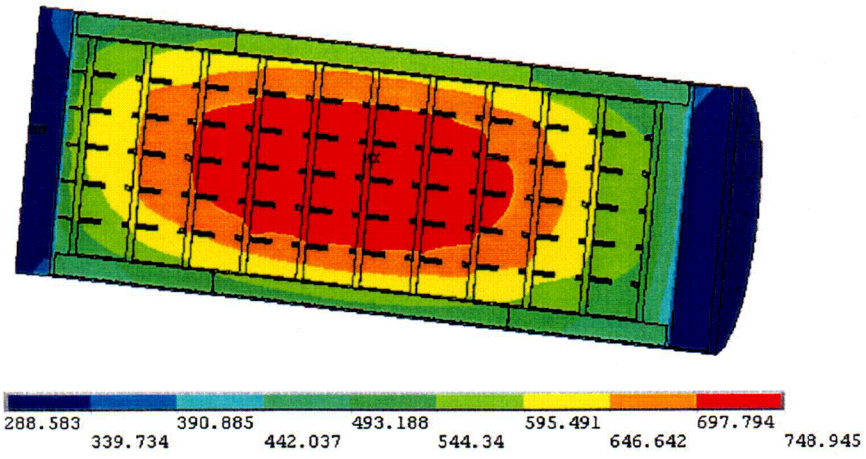

Fuel Assemblies

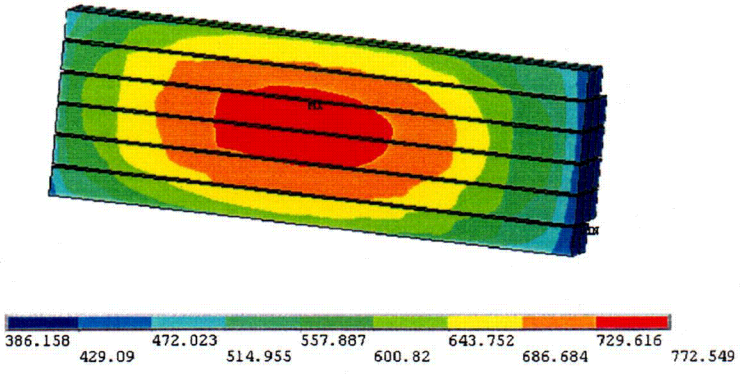

Figure 4-32
Temperature Distribution of DSC Model for Blocked Vents Accident Case

C 29

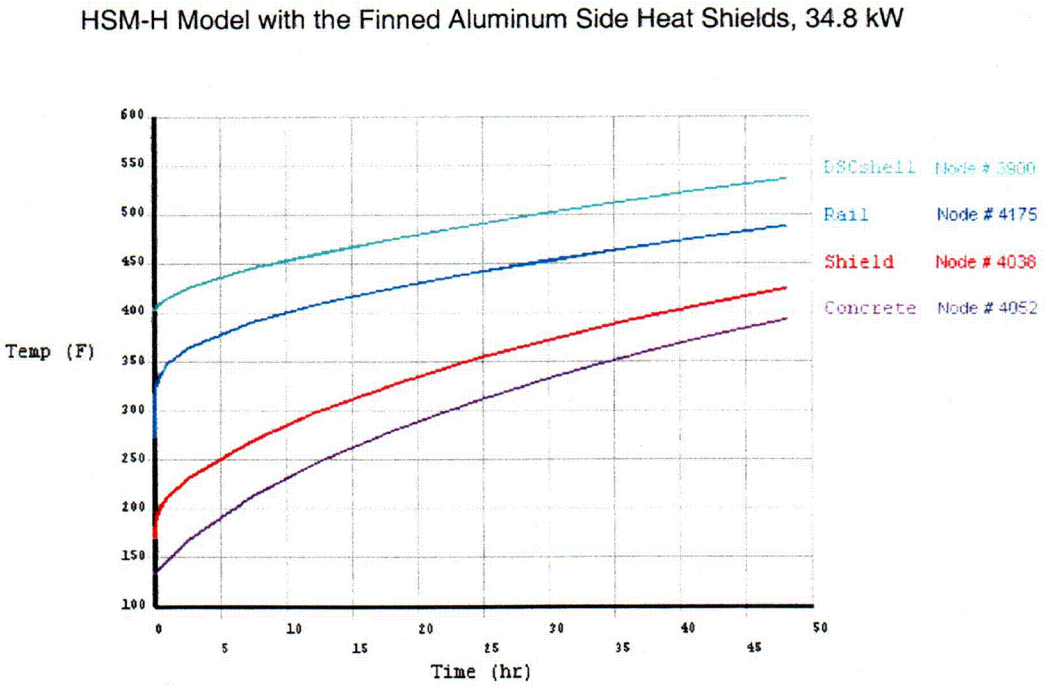

Figure 4-33
Temperature-Time History of HSM-H Components for Blocked Vents Accident Case

Entire Model DSC Transfer Cask

Procedure A

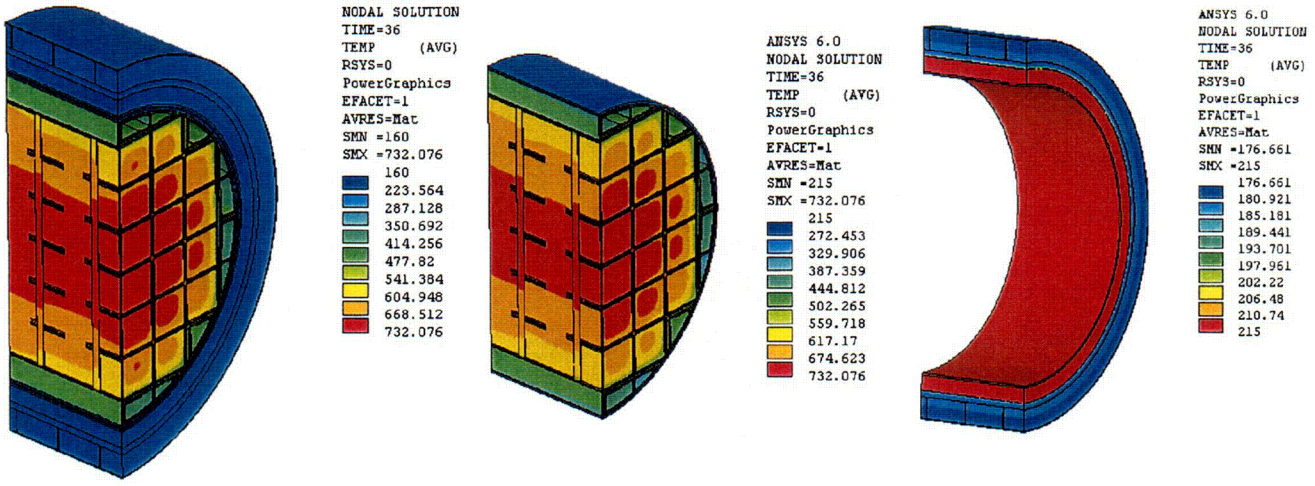

Procedure B

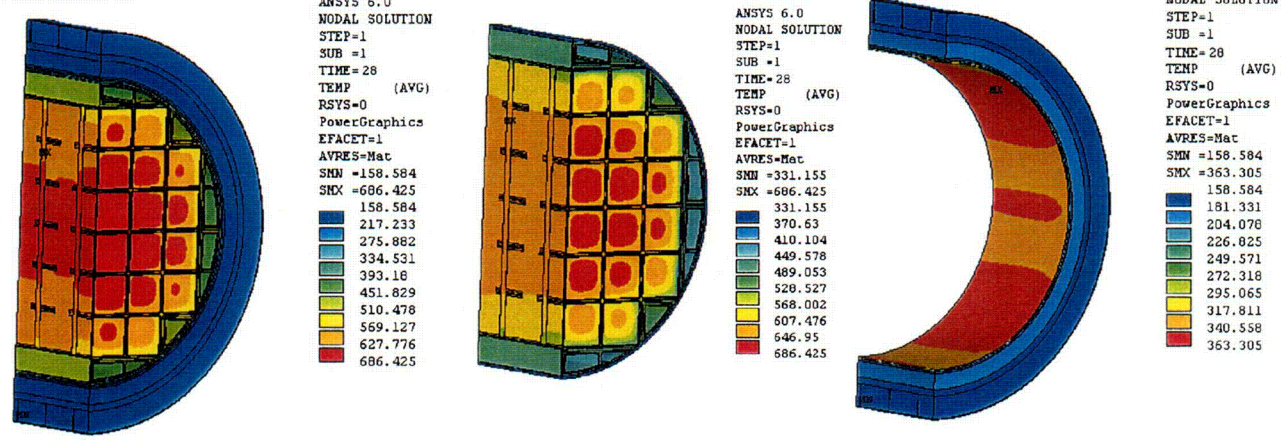

Procedure C

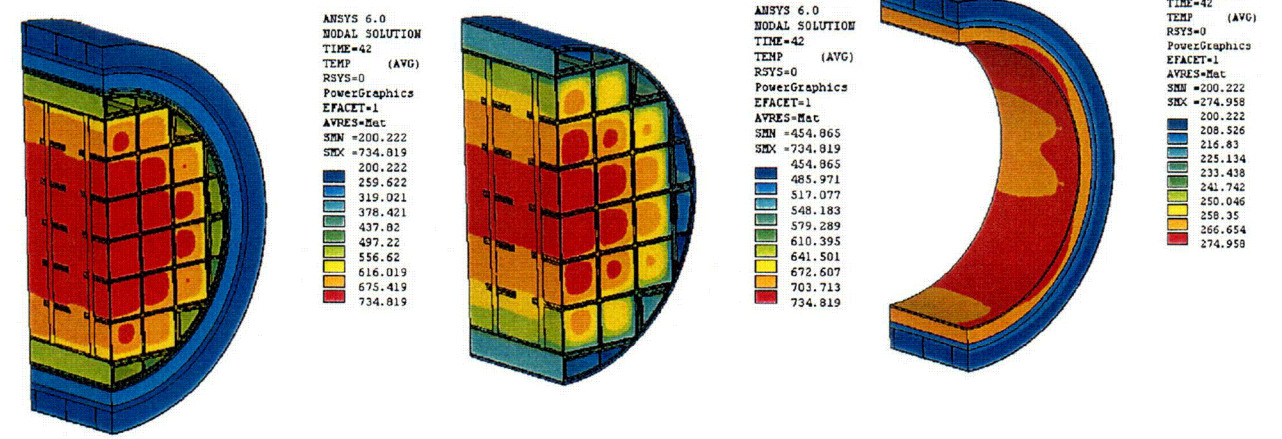

Figure 4-34
Temperature Distribution at the End of Vacuum Drying Process

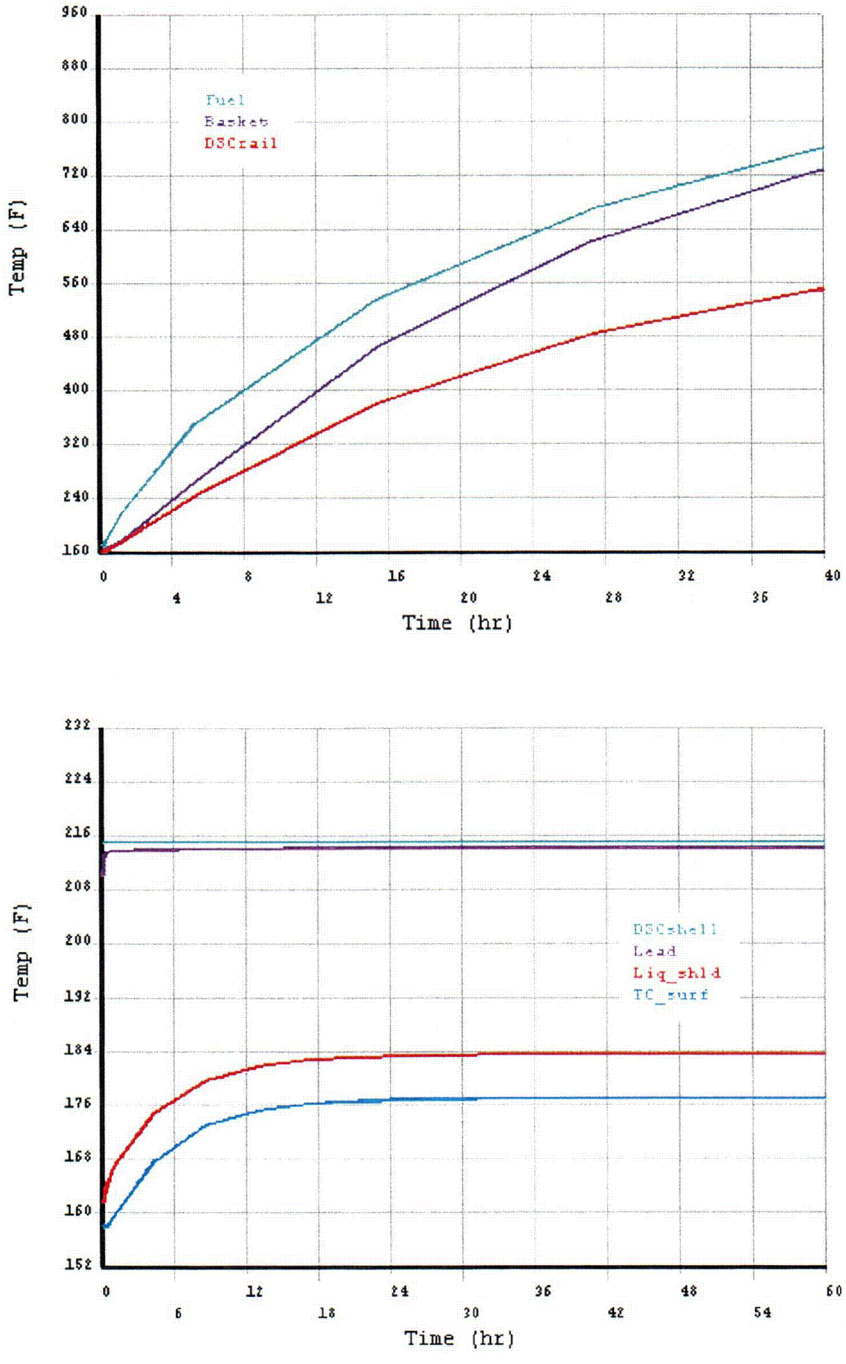

Figure 4-35
Time-Temperature History for Vacuum Drying Procedure A

C 32

Procedure B

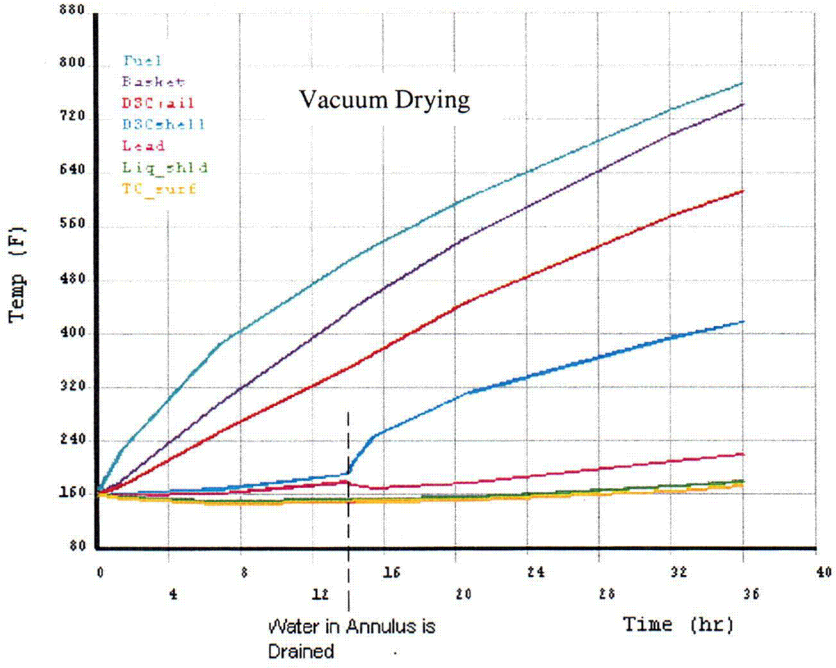

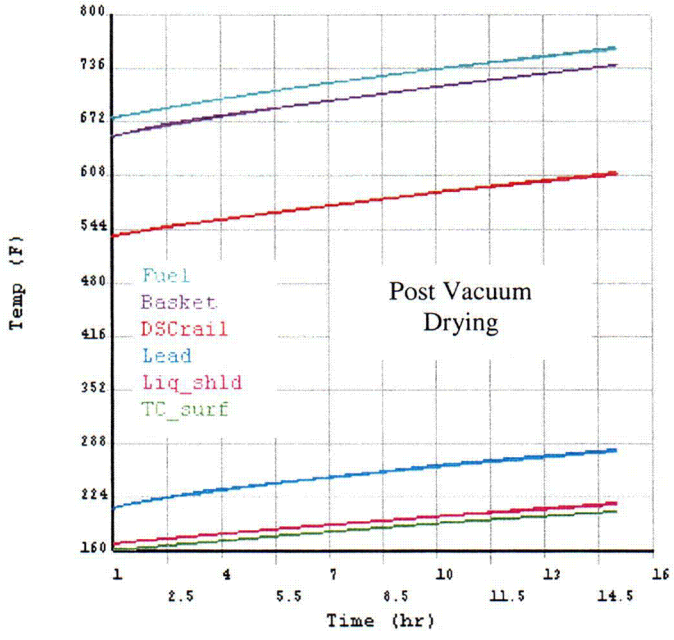

Figure 4-36
Time-Temperature History for Vacuum Drying Procedure B

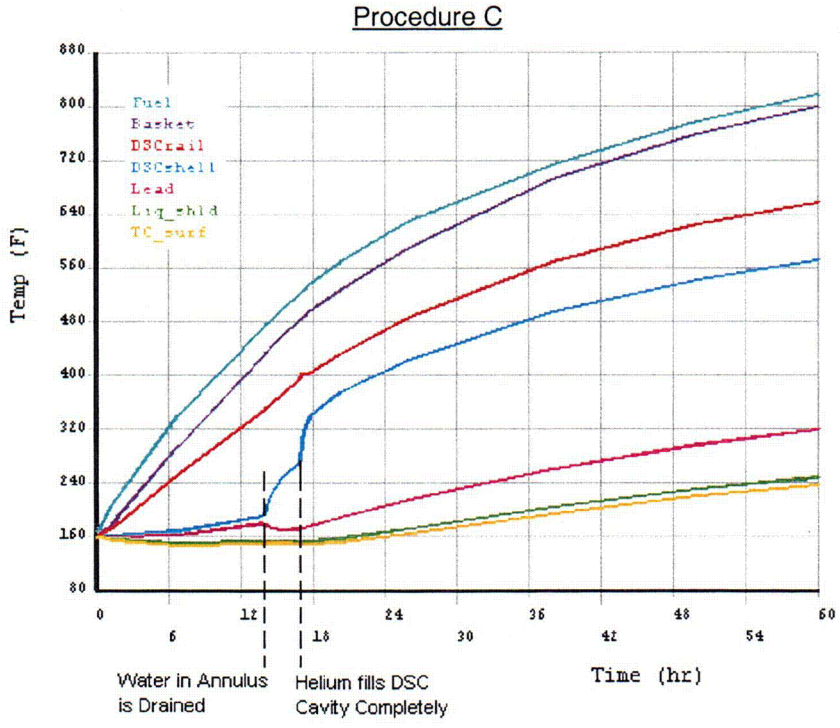

Figure 4-37
Time-Temperature History for Vacuum Drying Procedure C

Burnup rate MWD/MTU	Total Free Gas (cc/fuel rod)
35000	760
45000	939
55000	1073
60000	1123

← extrapolated

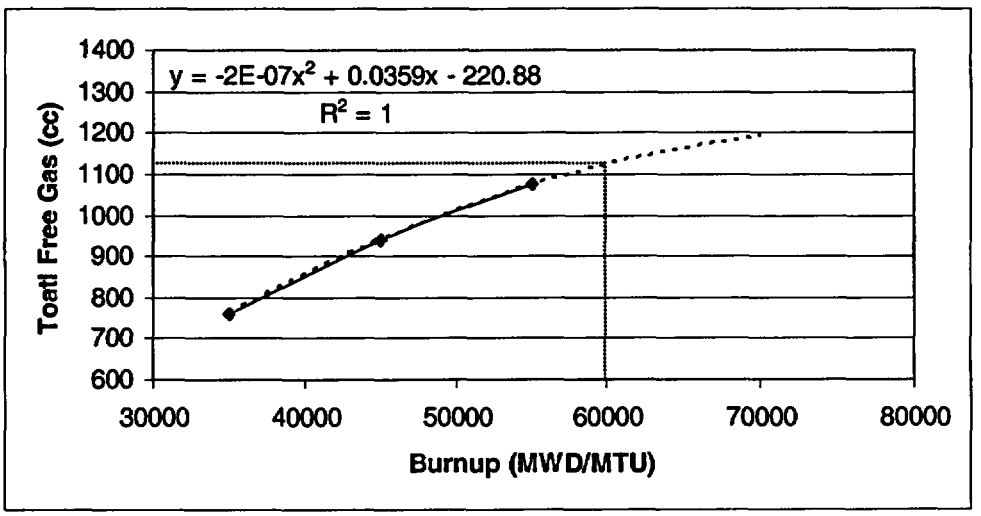

Figure 4-38
Total Free Gas Volume verses Burnup Rate

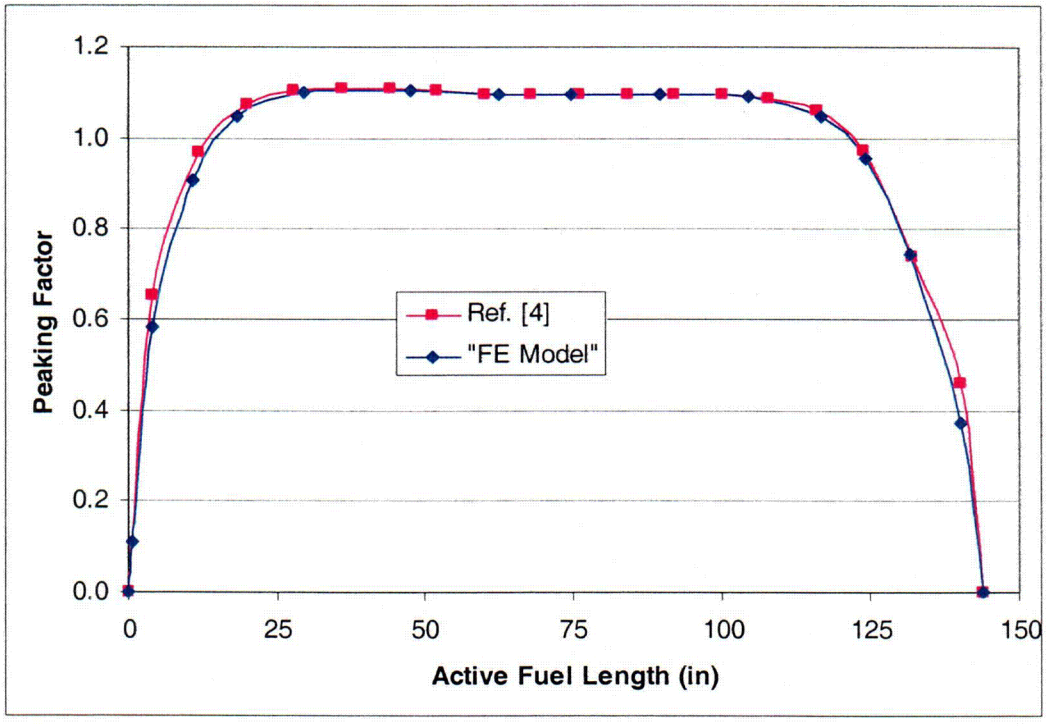

Figure 4-39
Comparison of the Axial Heat Profiles in the FE Model and in Ref. [4]

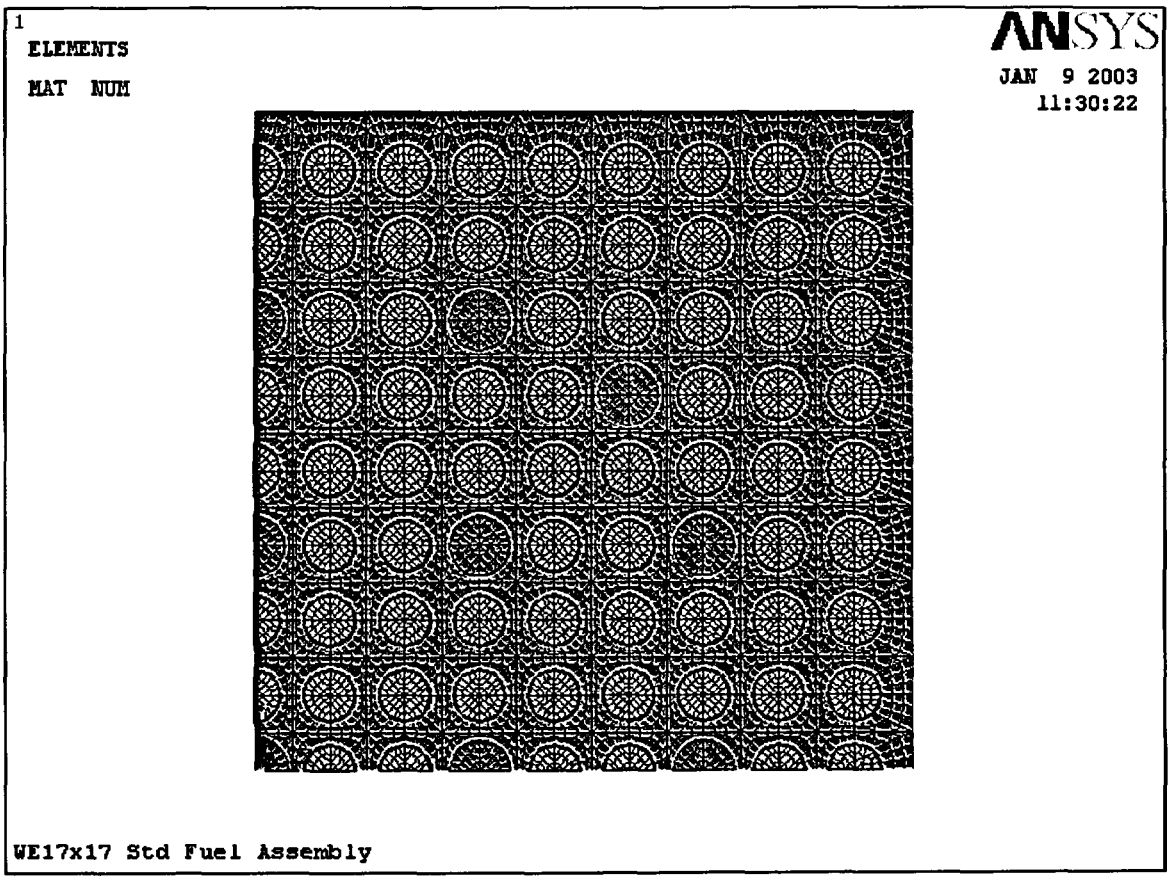

Figure 4-40
Finite Element Model of Fuel Assembly WE17x17 standard

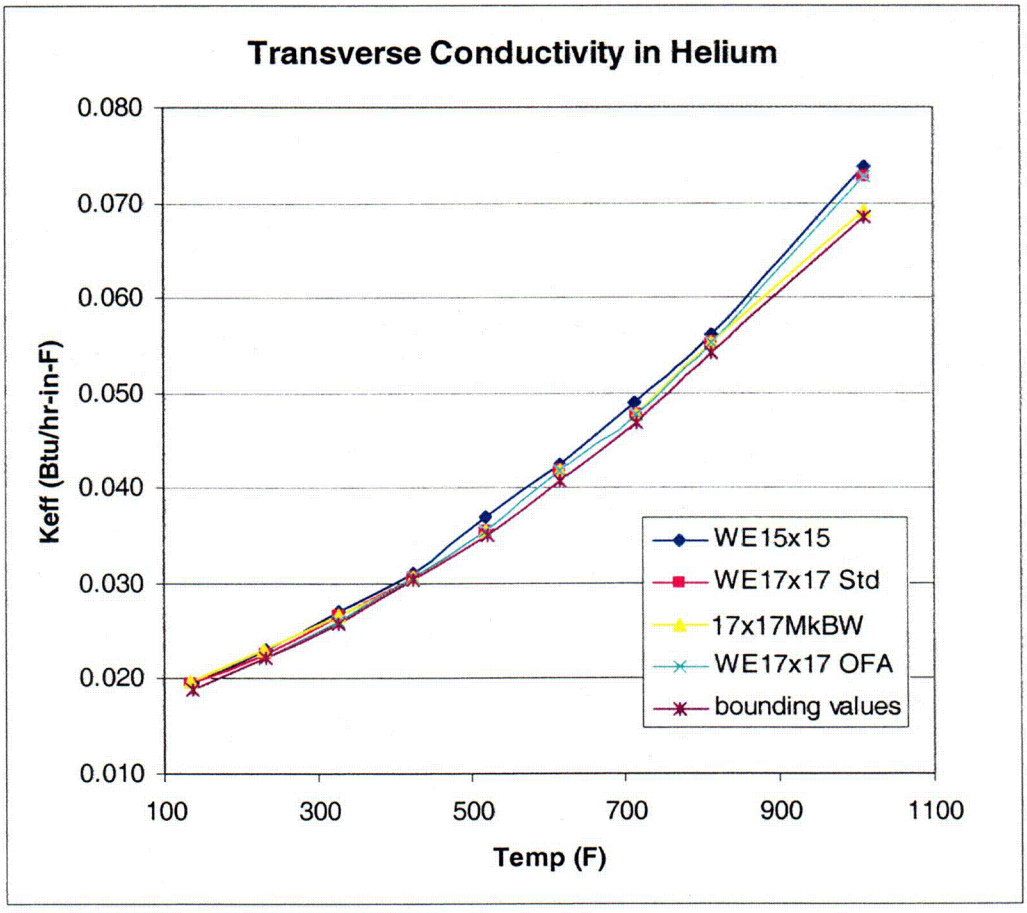

Figure 4-41
Effective Transverse Fuel Conductivity in Helium

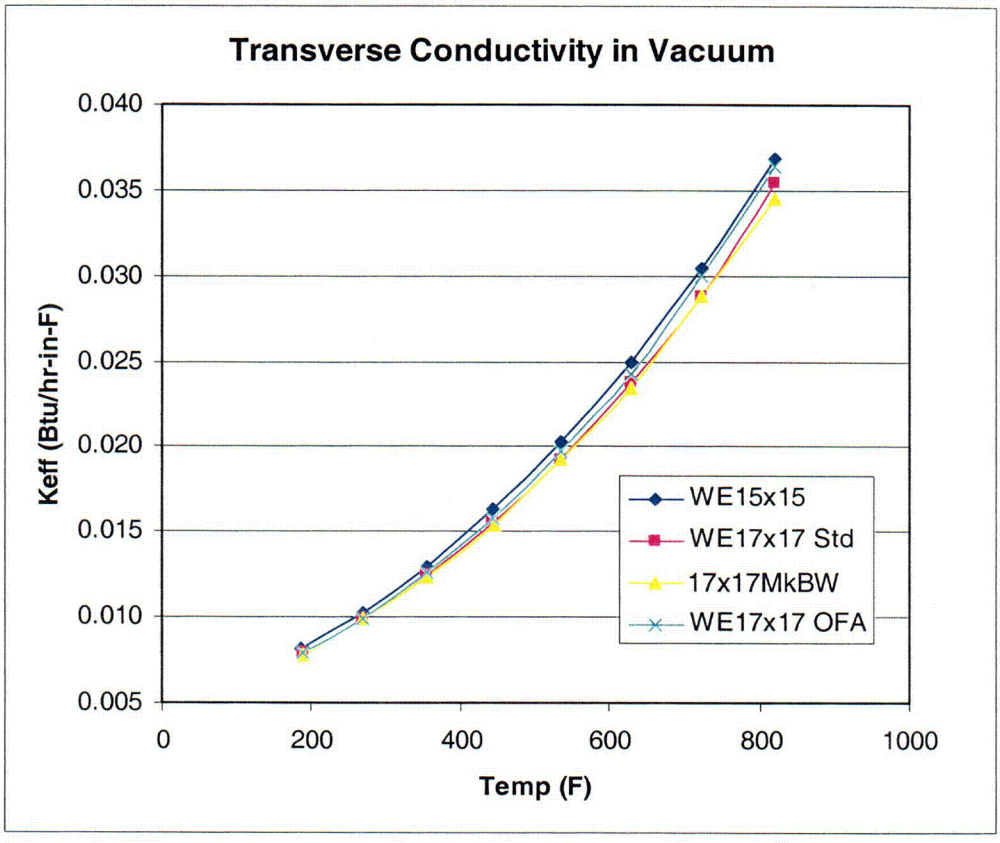

Figure 4-42
Effective Transverse Fuel Conductivity for Vacuum Conditions

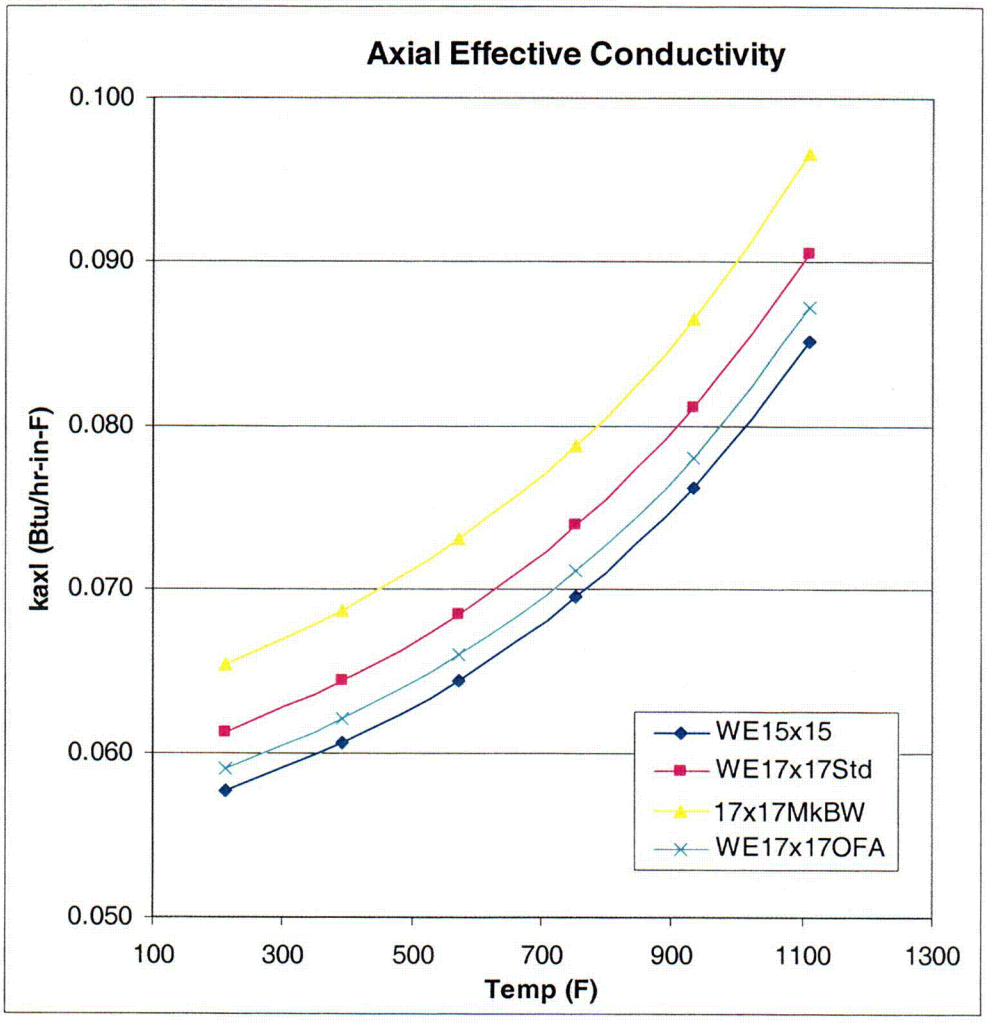

Figure 4-43
Effective Axial Fuel Conductivity

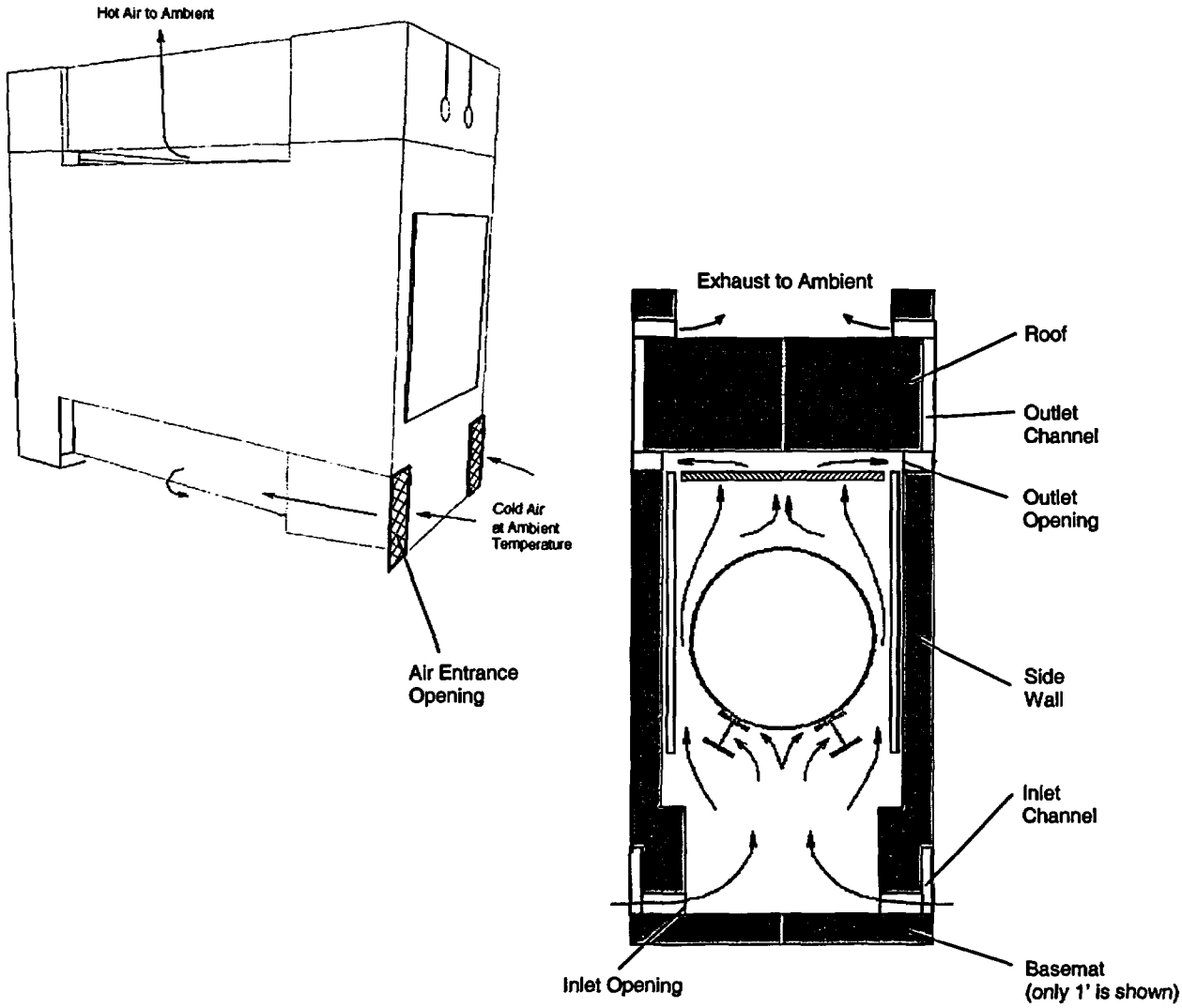

Figure 4-44
Schematic Flow Paths through HSM-H

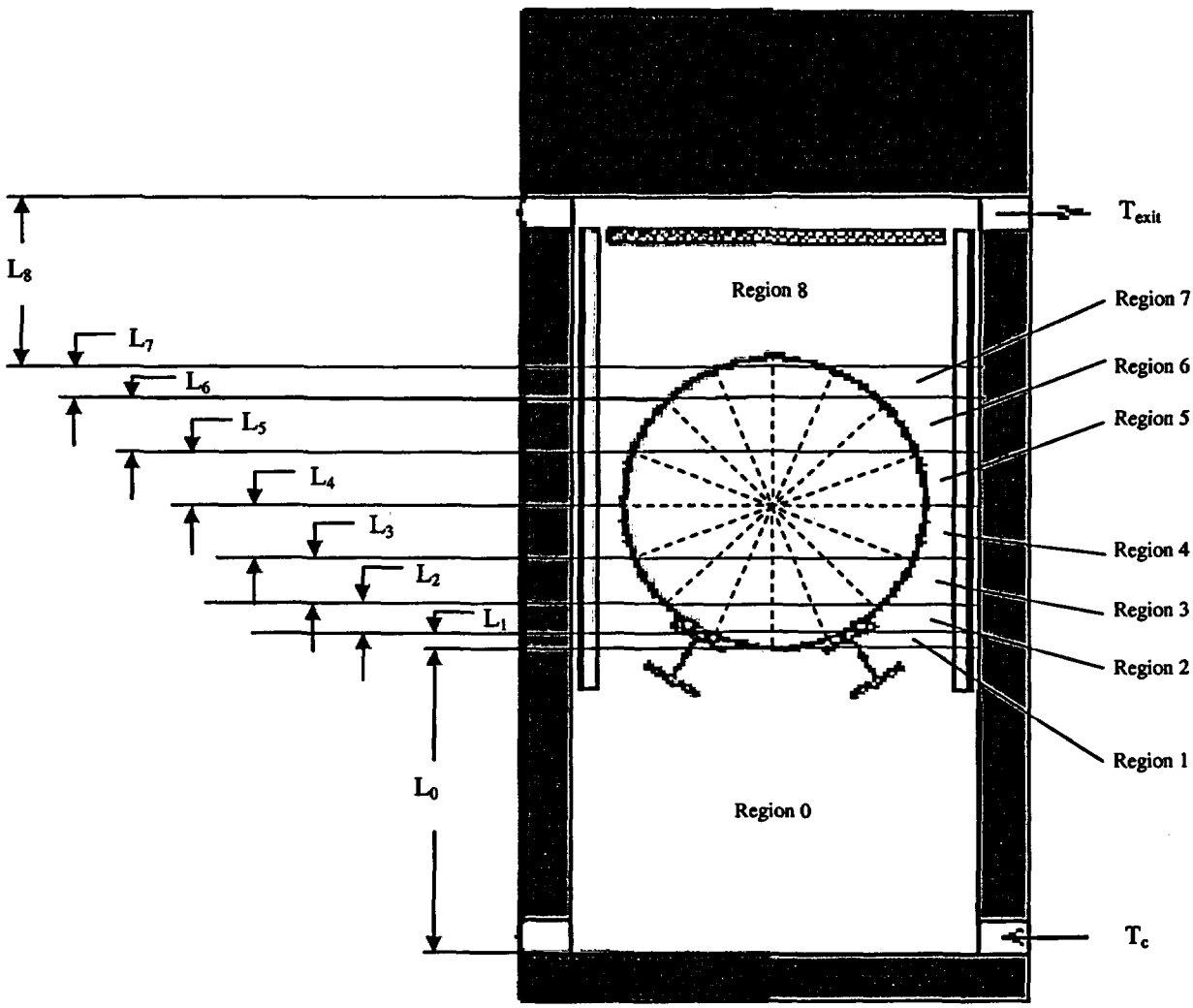

Figure 4-45
Temperature Regions around DSC in the HSM-H Cavity

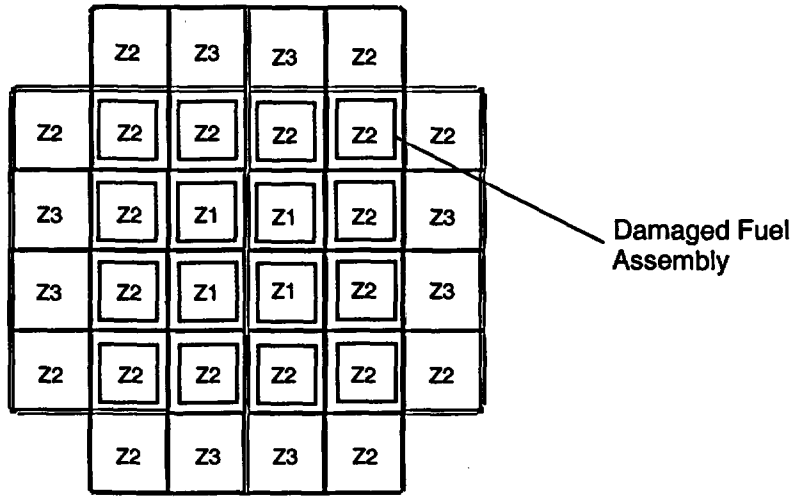

Figure 4-46
Location of the Damaged Fuel Assemblies in the Basket

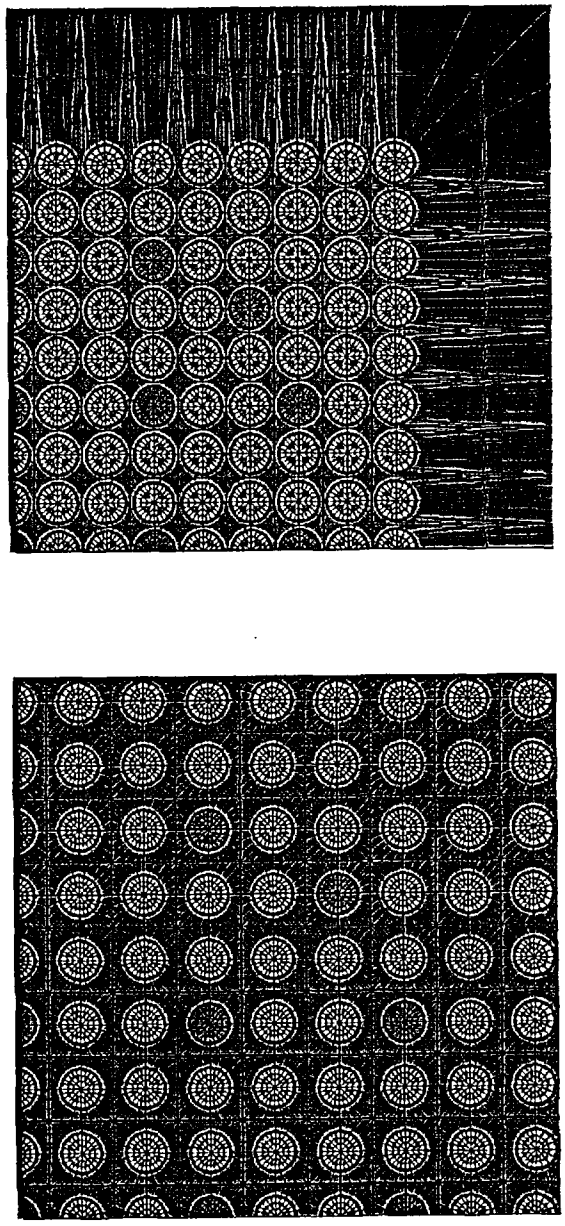

Figure 4-47
Typical FE Models of Damaged (Reconfigured) Fuel WE17x17OFA

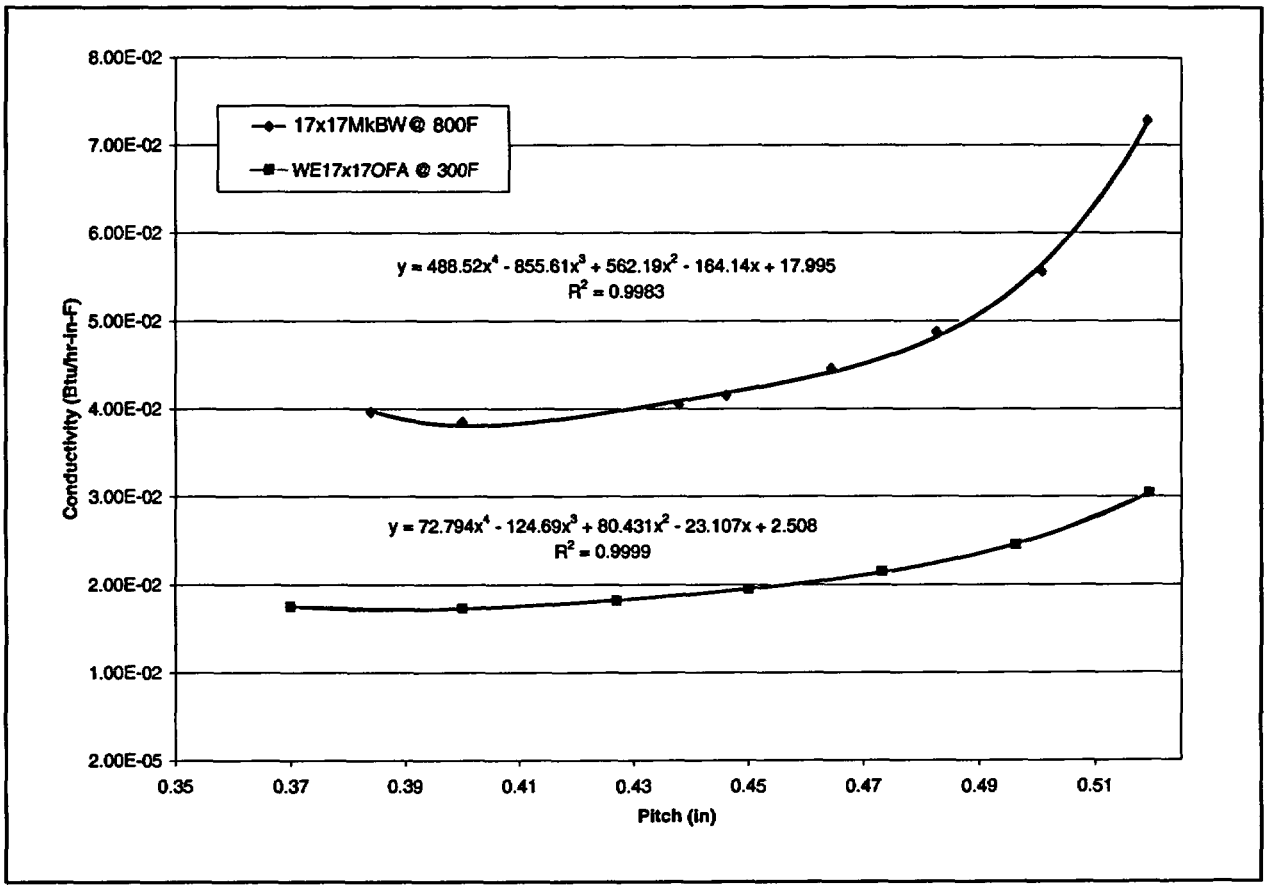

Figure 4-48
Transverse Effective Fuel Conductivity verses Pitch Size

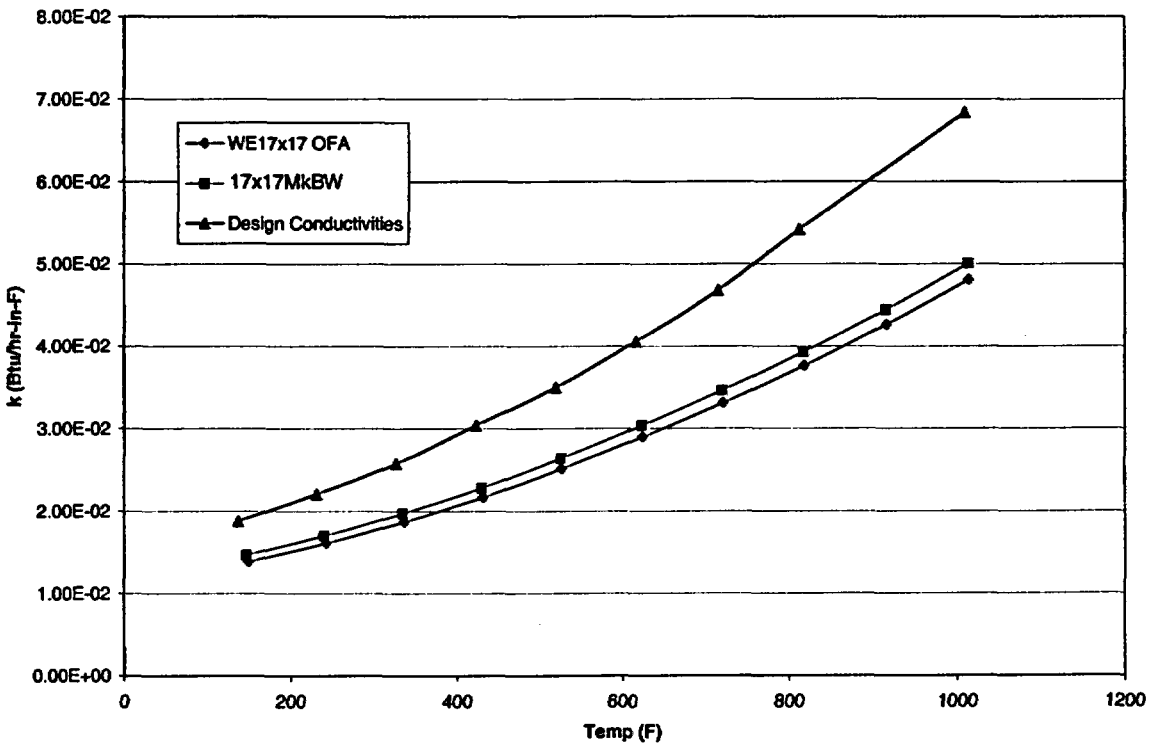

Figure 4-49
Effective Transverse Conductivity of Damaged (Reconfigured) Fuel

DSC Model

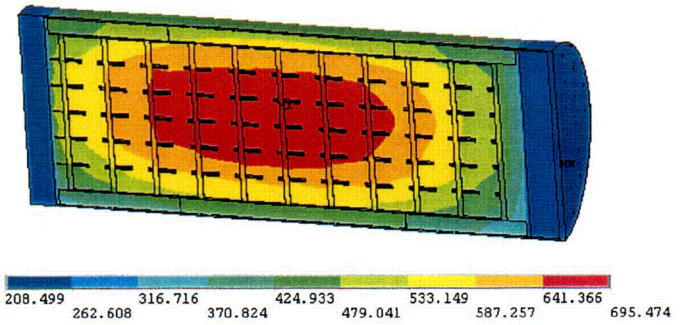

Basket

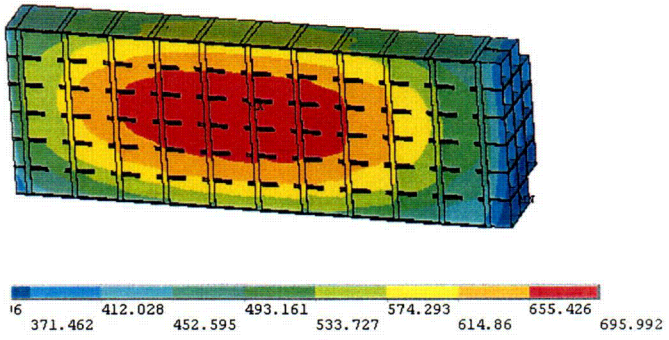

Basket Rails

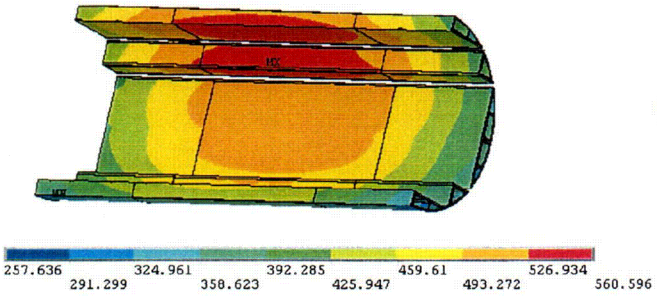

Fuel Assemblies

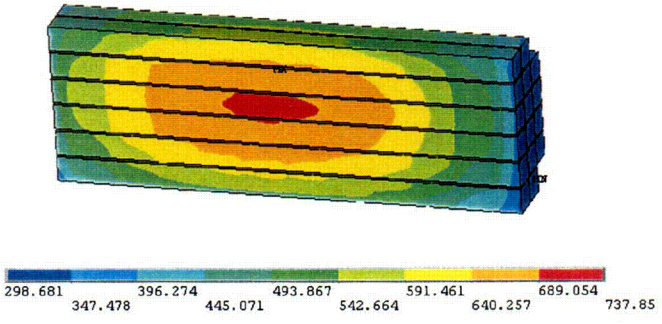

Figure 4-50
Temperature Distributions in the DSC containing 16 Damaged Fuel Assemblies for Normal / Off-Normal Transfer Conditions

TC Model

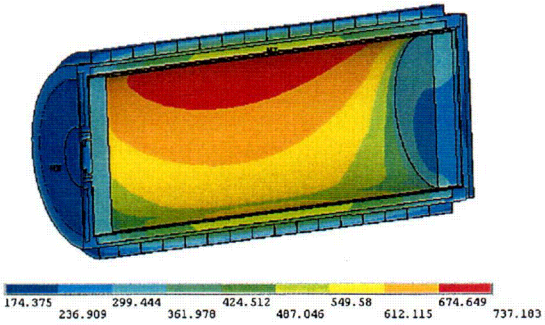

DSC Model

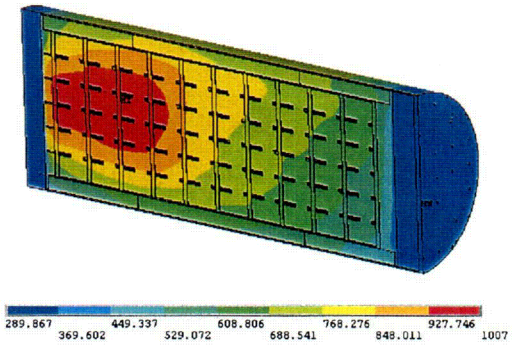

Lead

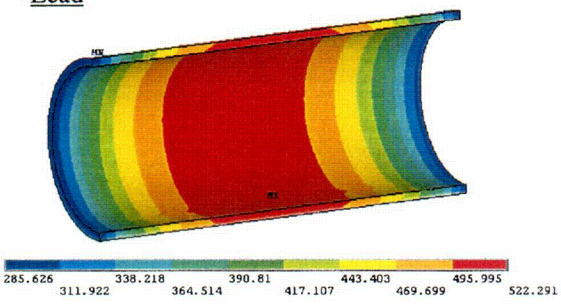

Basket

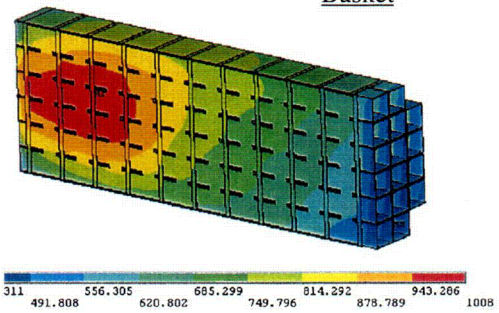

DSC Shell

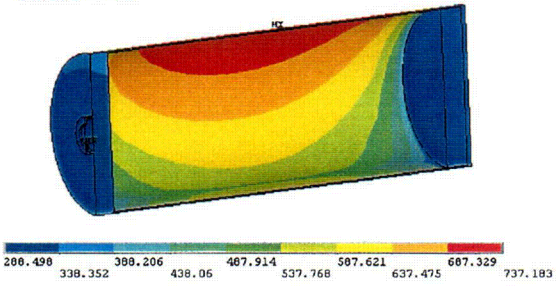

Intact Fuel Assemblies

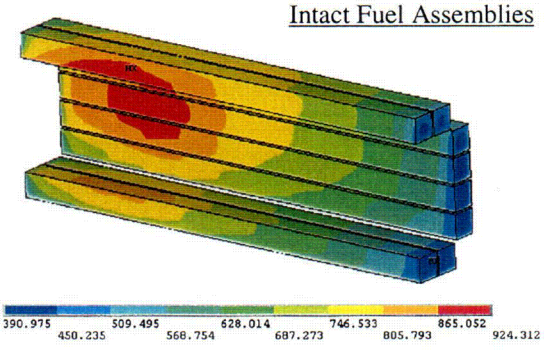

Figure 4-51
Temperature Distributions in the DSC containing 16 Damaged (Rubble) Fuel Assemblies for Accident Conditions

C 40